EES Catalysis



REVIEW ARTICLE

View Article Online



Cite this: EES Catal., 2025, **3**, 1196

main group metals and their tetrahydroborates and tetrahydroaluminates

Advances in catalysing the hydrogen storage in

Melinda Krebsz, D†*ab Tibor Pasinszki, Dc Sooraj Sreenatha and Valeska P. Tingbd

Hydrogen is a promising clean and renewable energy source; however, its efficient storage is one of the key challenges in establishing the sustainable hydrogen economy. The light main group metals and their tetrahydroborates and tetrahydroaluminates show great potential for high hydrogen storage capacity close to ambient conditions; however, their high hydrogenation and dehydrogenation temperatures, sluggish kinetics, and limited reversibility have always been an obstacle for practical applications. Large efforts have been devoted to modifying the thermodynamic and kinetic properties of these systems, and reviewing these efforts and highlighting future directions are the aims of the present review. Based on recent research, the application of multicomponent systems utilizing multiple modification methods, such as catalysis, nanoconfinement, alloying, and structure engineering, is essential for enhancing the storage conditions. The synergistic effect of multiple catalysts is now a key requirement to address various steps of the overall process, including forming/breaking the H-H and metal-H bonds, transporting hydrogen and heat, and suppressing the formation of side products. Compared to pristine systems, tremendous improvement has been achieved. Catalysed AlH₃ decomposition can now operate as a oneway hydrogen source below 100 °C and the Mg/MgH₂ hydrogen storage system exhibits good cyclic performance at elevated temperatures. Metal hydrides, tetrahydroborates, tetrahydroaluminates, and their composite systems face challenges in achieving close to ambient operating conditions and cyclic stability. As the demand for improved hydrogen energy storage is expected to grow, further research for the enhancement of these systems will continue to advance the state of hydrogen storage technology.

Received 30th April 2025, Accepted 18th July 2025

DOI: 10.1039/d5ey00134j

rsc.li/eescatalysis

Broader context

Development of effective storage technologies for the hydrogen industry will support decarbonisation and shifting away from fossil fuels. Mobile applications require safe and robust technologies operating close to ambient conditions. To address this, storage materials capable of delivering and absorbing hydrogen under mild conditions need to be explored. Promising material groups for mobile hydrogen storage are the light main group metals and their tetrahydroborates and tetrahydroaluminates. We demonstrate in our present study the possibility of improving the storage performances of these compounds by tuning their thermodynamic and kinetic properties utilizing multiple modification methods, such as multi-component catalysis, nanoconfinement and alloying. Given the potential of these techniques, findings presented in this review may enable the much-needed improvements in solid-phase hydrogen storage to develop highcapacity storage systems operating close to ambient conditions.

1. Introduction

Three of the most difficult challenges facing mankind today are global warming caused by air pollution, increasing energy demand, and depleting sources of fossil fuels. The three are interconnected as current energy production is heavily based on fossil fuels, the combustion of fossil fuels leads to about three quarters of global greenhouse gas emissions, and depleting fossil fuel sources endanger energy supply.2 76.5% of the global primary energy consumed in 2023 was based on fossil fuels, and the mass of carbon in the atmosphere has increased

^a School of Engineering, STEM College, RMIT University, Bundoora, Victoria 3083, Australia. E-mail: melinda.krebsz@anu.edu.au

^b Research School of Chemistry, College of Science and Medicine, The Australian National University, Canberra, ACT 2601, Australia

^c School of Sciences, College of Engineering and TVET, Fiji National University, Suva, P.O. Box 3722, Fiji

^d Department of Mechanical Engineering, University of Bristol, Bristol, BS8 1TR, UK † Current address: Research School of Chemistry, College of Science and Medicine, The Australian National University, Canberra, ACT 2601, Australia.

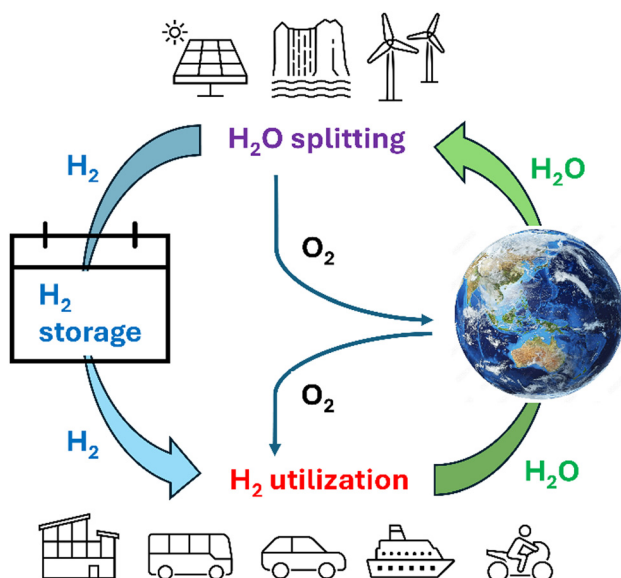


Fig. 1 The carbon-free hydrogen energy cycle

by 48% from eighteenth century pre-industrial levels.3 The world therefore needs an alternative energy source and technology to shift away from fossil fuels. Water is abundant on Earth and splitting water into hydrogen and oxygen and using hydrogen to generate energy if needed would provide a sustainable and carbon-free energy cycle if hydrogen is generated by utilizing renewable energy (Fig. 1). Several governments around the globe have realised the need for technology change and abandoning dependence on fossil fuels and started to build a 'hydrogenpowered economy'. 4-8 Key enabling technologies to realize these plans are needed for the production, storage, distribution, and application of hydrogen. The storage of hydrogen, however, is challenging due to its inherent nature; hydrogen is a low-density gas under ambient conditions (0.0813 kg m⁻³ at 1 bar and 25 °C)⁹ and storage, transport and utilization, especially in mobile applications, require high storage densities. The U.S. Department of Energy (DOE) technical system targets for onboard hydrogen storage for light-duty fuel cell vehicles highlight these challenges and formulate targets for industry and academic research (Table 1). 10 Considering these, a 615-fold increase of the density of hydrogen in the storage system must be achieved compared to that of ambient gas, which is even more demanding for the storage material as the storage vessel also has volume and mass.

The hydrogen storage system needs to fulfill several requirements, including safety, high gravimetric and volumetric storage

capacity, sufficient rate of hydrogen delivery and recharging, close to ambient operating conditions, easy handling, abundant resources, and competitive price. None of the current systems can fulfill all these requirements. There are several research directions reflecting application needs, and hydrogen may be stored in molecular form or in compounds. The current most advanced molecular hydrogen storage methods are storage of hydrogen as a pressurized gas at ambient temperatures (technology readiness level¹¹ (TRL) = 9) and as liquified hydrogen at cryogenic temperatures (TRL = 9). Drawbacks of these methods include the safety issues and cost of compressing hydrogen to pressures up to 700 bar, the low volumetric density of the pressurized gas and the high production cost of high pressure storage containers for high pressure gaseous storage, and the cost of liquefaction, bulky insulation to maintain low temperatures (<33 K) and the control of the boil off for liquid hydrogen storage. 12-15 Large efforts have been devoted to developing hydrogen storage based on molecular hydrogen adsorption on solid materials such as doped carbons, metal organic frameworks (MOFs), covalent organic frameworks (COFs) and porous aromatic frameworks (PAFs). 16-19 However, high storage capacity can only be achieved at cryogenic temperatures (TRL = 5); ambient temperature storage satisfying DOE targets is not yet feasible for storage of hydrogen via adsorption. 16-19 Storing hydrogen in compounds is an alternative to molecular hydrogen storage and has several advantages such as the stability of many hydrogen compounds under ambient conditions, the high gravimetric and volumetric hydrogen capacity (up to about 20 wt% or 150 kg m⁻³), and the relatively easy storage and transport. 20-23 Hydrogen compounds for storage may be classified into three groups, namely (1) molecular hydrides (e.g., ammonia, perhydro-dibenzyltoluene, methylcyclohexane), (2) interstitial hydrides of transition metals and their alloys (e.g., TiFe, Nd2Ni7, high entropy alloys such as V₃₅Ti₃₀Cr₂₅Fe₅Mn₅), or (3) ionic and polymeric hydrides (e.g., LiH, MgH₂). An advantage of currently considered liquid organic molecular hydrides is that they closely resemble conventional fuels and existing infrastructures could be used to store and transport them safely.²⁴⁻²⁷ However, industrial environments are required for the hydrogenation and purification of the hydrogen-lean and hydrogen-rich forms of storage compounds and mobile applications can consider these hydrogen carriers only as "off-board" regenerable materials. None of the currently considered molecular liquid hydrogen carriers fulfill all storage requirements, namely low melting (< -30 °C) and high boiling (> 300 °C) point, high volumetric and gravimetric hydrogen storage capacities, stability for long lifespan, low dehydrogenation temperatures, low

Table 1 DOE technical system targets for onboard hydrogen storage for light-duty fuel cell vehicles¹⁰

	System properties					
	Gravimetric capacity (wt%)	Volumetric capacity (kg m^{-3})	Min/max delivery temperature (°C)	System fill time (min)	Operational cycle life	Dormancy ^a (days)
2025 target Ultimate target	5.5 6.5	40 50	-40/85 -40/85	3-5 3-5	1500 1500	10 14

^a Considering that the vehicle is parked at an ambient temperature of 35 °C; minimum until first release from initial 95% usable capacity.

EES Catalysis Review

production cost, and low toxicity. The toluene/methylcyclohexane system is technologically the most advanced (TRL = 9); a demonstration project has been carried out by hydrogenating toluene in a chemical plant in Brunei, shipping methylcyclohexane to Japan, dehydrogenating methylcyclohexane in Japan, and shipping toluene back to Brunei. 26,28 Storing hydrogen in interstitial, ionic or polymeric metal hydrides solves the problem of volatility of molecular hydrides; however, it introduces new challenges. The hydrogen storage in interstitial hydrides has several advantages such as reversibility, fast kinetics, and the ability of several transition metals and alloys to absorb and desorb hydrogen under ambient and near ambient conditions, as well as the tunability of operating pressure and temperature, including the region in which electrolysers and fuel cells operate (between 1 and 10 bar pressure and below 100 °C) (TRL = 9). ^{22,29,30} Disadvantages, however, are the high cost and low gravimetric storage capacity, well below the DOE targets, which prevent their wide scale use. Nonetheless, interstitial hydrides are successfully applied as hydrogen storage materials in vehicles where the heavy storage material is not a weight penalty, for example in forklifts, submarines, and canal boats. 31-33

Promising groups of hydride compounds for hydrogen storage, that may fulfill storage requirements in the future and bypass the limitations of storage methods mentioned above, are the ionic and polymeric binary hydrides of light main group metals (alkali and alkali earth elements and aluminium) and their tetrahydroborates and tetrahydroaluminates (which can be considered to be complexes of metal hydrides and BH3 and AlH3, respectively), as well as their mixtures (reactive hydride composites, RHCs) due to their high gravimetric and volumetric hydrogen storage capacities (Table 2). These compounds are stable under ambient conditions in an inert atmosphere and several of the relevant metals, e.g. Mg and Al, are cheap, light, and abundant on Earth, which makes them very attractive for both mobile and stationary storage systems. Inherent properties of these compounds, namely the high temperatures and pressures needed for hydrogen uptake and release, the sluggish kinetics, and the partial- or non-reversibility of hydrogen release and uptake, as well as the formation of side products, however, have impeded their wide scale application to date (TRL = 3-5 depending on the compound). Due to their potential in filling the gap in reversible and high-capacity hydrogen storage under close to ambient conditions, large efforts have been devoted during the last few decades to bring operation conditions closer to ambient conditions by improving the kinetics and thermodynamics of the hydrogenation and dehydrogenation reactions using additives and catalysts. Considering this and the increasing demand for effective storage materials, as well as the rapidly changing hydrogen storage industry, the aim of the present work is to review advances in improving hydrogen storage properties of binary hydrides of light main group metals and their tetrahydroborates and tetrahydroaluminates, and to highlight their advantages, limitations, and challenges, as well as to point out future trends in developing storage materials for the hydrogen industry. We consider DOE initiatives and the operation conditions of fuel cells as research targets, namely storage capacities of 6.5 wt% and 50 kg m⁻³ and lower than 10 bar pressure and 100 °C temperature (note that the DOE target is the storage system target and the storage material must perform better, but to keep discussion simple we use these target numbers for the storage material in this article). Additives to hydrides which

Table 2 Gravimetric storage capacity of main group metal hydrides and alkali and alkali earth tetrahydroborates and tetrahydroaluminates^{ab}

Metal hydride	Grav. capacity (wt.%)	Vol. capacity (kg·m ⁻³ H ₂)	Tetrahydro- borate	Grav. capacity (wt.%)	Vol. capacity (kg·m ⁻³ H ₂)	Tetrahydro- aluminate	Grav. capacity (wt.%)	Vol. capacity (kg·m ⁻³ H ₂)
LiH	12.68	98.3	LiBH₄	18.51	122.2	LiAlH ₄	10.62	96.6
NaH	4.20	57.2	NaBH ₄	10.66	114.1	NaAlH ₄	7.47	94.9
КН	2.51	35.9	KBH₄	7.47	87.4	KAIH ₄	5.75	71.6
BeH ₂	18.28	118.8	Be(BH ₄) ₂	20.84	146.3	Be(AlH ₄) ₂	11.35	
MgH ₂	7.66	111.1	Mg(BH ₄) ₂	14.94	147.8	Mg(AlH ₄) ₂	9.34	97.7
CaH ₂	4.79	91.1	Ca(BH ₄) ₂	11.56	126.5	Ca(AlH ₄) ₂	7.90	
AlH ₃	10.08	148.9	AI(BH ₄) ₃	16.92	92.9	AlH ₃ ^c	10.08	148.9

^a Calculated in this work using atomic masses and the density of hydrides. ^{35,39-44} ^b BeH₂, MgH₂, and AlH₃ have a polymeric structure with threecentre M-H-M bonds (M = Be, Mg, or Al). Colour codes: above the DOE target (green and yellow, green is higher than yellow and primary target), below the DOE target (pink), and not considered for hydrogen storage (no colour). Al(AIH₄)₃ = AlH₃

do not contain hydrogen decreases the storage capacity; therefore large amounts of additives used to alter reaction conditions are not considered in this review. Considering gravimetric capacities in Table 2, pristine NaH, KH, CaH₂, and KAlH₄ do not satisfy DOE targets (Table 1), but can be considered as one of the components of RHCs. Heavier I-III group metals are not relevant for hydrogen storage due to their weight, toxicity, and/or low abundance. Although beryllium compounds have exceptionally high hydrogen storage capacity (Table 2), they are not considered for hydrogen storage because beryllium ores are not abundant, beryllium is expensive, and beryllium salts, including the hydride, are extremely toxic.34,35 Al(BH4)3 is a volatile pyrophoric liquid at room temperature, explosive in air, has poor storage stability, and releases also diborane upon heating; therefore, its practical use in hydrogen storage is restricted. 36-38 To discuss the highlighted topic, this review is organised in subchapters according to the

2. Results and discussion

chemical groups of hydrogen compounds.

2.1. General considerations and experimental determination of thermodynamic and kinetic parameters of hydrogen absorption and release

The hydrogen absorption by metals is a multiple-step process, and involves several consecutive steps, namely (a) physisorption of hydrogen, (b) dissociation of hydrogen into atoms on the surface, (c) penetration of hydrogen atoms in the subsurface, (d) hydrogen diffusion in the bulk material, and (e) nucleation and growth of the hydride phase. The reverse process, hydrogen release, follows the opposite multistep process, starting with the dissociation of the metal-hydrogen bond. Each step of both absorption and desorption processes must overcome a range of activation energy barriers, and decreasing these energy barriers. especially that of the rate determining step, is of crucial importance for improving the rate and/or decreasing the reaction temperature of hydrogen absorption and desorption. Covalent and ionic bonds are strong; therefore, dissociation of molecular hydrogen and the metal-hydrogen bond is, in general, rate determining and thermodynamically limiting. The overall thermodynamics and kinetics govern the hydrogen uptake and release and altering these is an effective strategy for improving hydrogen storage properties in metals.

Thermodynamically, the hydrogenation reaction occurs if the Gibbs free energy (ΔG) of the reaction, related to the enthalpy of formation (ΔH), entropy of formation (ΔS), and temperature (T), is negative $(\Delta G = \Delta H - T \cdot \Delta S)$. Since heat is released and entropy is reduced during the hydrogenation reaction (as hydrogen is moving from the gas phase into its bonded solid phase), the enthalpy and entropy both have negative signs; consequently, thermodynamically, and depending on the concrete value of ΔH ,

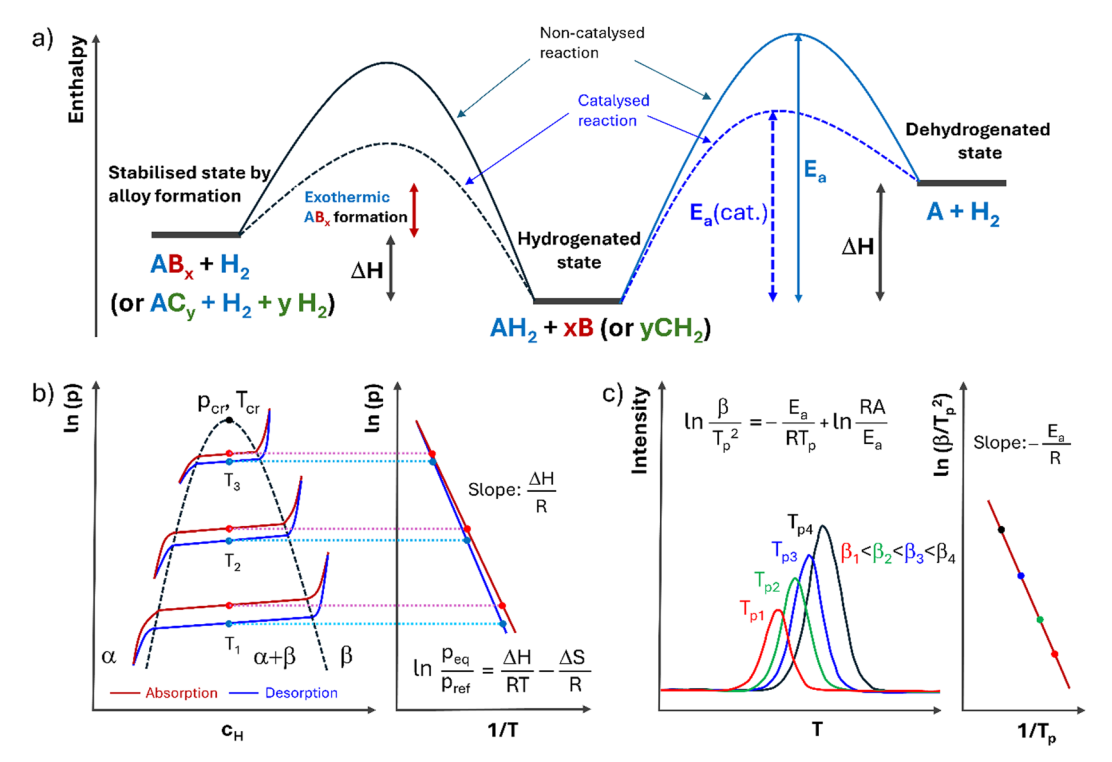


Fig. 2 (a) Generalized enthalpy diagram showing the effect of a catalyst on the kinetics and the effect of alloy formation on the thermodynamics for a hypothetical metal/metal hydride system (A = Li, Na, K, Mg, Ca or Al; B = non-hydriding alloying element; C = hydriding alloying element), (b) schematic PCT phase diagram on the left hand side and the van't Hoff equation and the corresponding van't Hoff lines on the right hand side for hydrogen absorption and desorption on a typical metal (c_H = hydrogen concentration in the solid phase, p = hydrogen pressure, p_{eq} = mid-plateau equilibrium pressure, p_{ref} = reference pressure of 1 bar, p_{cr} = critical pressure, R = universal gas constant, T = absolute temperature, T_{cr} = critical temperature), and (c) schematic representation of a thermal event at various heating rates on the left hand side and the Kissinger line on the right hand side (β = heating rate, T_p = peak temperature, E_a = apparent activation energy, A = pre-exponential factor).

EES Catalysis Review

the hydrogenation is favoured at lower temperatures, but the reverse reaction, dehydrogenation, is favoured at higher temperatures when ΔG becomes positive. Considering an ideal hydrogen storage system using temperature swing, a right balance between ΔH and $T \cdot \Delta S$ must exist where $|\Delta H| > |T \cdot \Delta S|$ at charging (hydrogenation at lower temperature, ideally under ambient conditions) and $|\Delta H| < |T \cdot \Delta S|$ at discharging (hydrogen release at elevated temperature). With very large ΔH , which is related to the strength of the metal-hydrogen bond, hydrogen release requires high temperatures. Considering that the entropy change during hydrogen absorption corresponds mostly to the change from molecular hydrogen gas to bonded hydrogen in solid hydrides, ΔS is approximately equal to the standard entropy of hydrogen for all metal-hydrogen systems, namely -130 J K⁻¹ mol⁻¹H₂. ^{45,46} The thermodynamic properties of metal-hydrogen systems are therefore usually characterized by the reaction enthalpy. (The same principle can be applied to tetrahydroborates and tetrahydroaluminates, too.) One way to alter thermodynamics is the application of additives which form alloys during dehydriding (see Fig. 2a). Non-hydriding additives decrease hydrogen storage capacity, as they dilute the metal; however, hydriding additives can preserve or even increase hydrogen storage capacity (Fig. 2a), which highlights the advantage of RHCs. In this sense, the formation of metal borides and alloys during the dehydrogenation reactions of tetrahydroborates, tetrahydroaluminates, and RHCs (formally the mixtures of two or more binary hydrides) is crucial for the desired thermodynamics of the system; the separation of metallic and boron phases is unfavourable (as will be discussed below). Thermodynamic parameters of hydrogen absorption and desorption are usually determined using the pressure-composition-temperature (PCT) phase diagram and the van't Hoff equation (Fig. 2b). 45-48 Considering a metal-hydrogen system and the Gibbs phase rule, the system has two degrees of freedom (due to the presence of two phases and two components) when hydrogen starts to absorb. Hydrogen first dissolves in the metal lattice and forms a solid solution phase (α phase), which has the same crystal structure as the bare metal and has low hydrogen concentration. In the α-phase region the concentration of hydrogen in the solid phase increases as the hydrogen pressure increases. At a certain point, nucleation of a higher concentration phase (β-phase) occurs. Due to the occurrence of an additional phase and thus the presence of three phases (α, β) and gas), the system's degree of freedom is decreased to one, and the pressure stays constant (equilibrium pressure, $p_{\rm eq}$) until the α - and β -phases coexist. After the disappearance of the α -phase, hydrogen enters the β -phase (solid solution) and the system's degree of freedom is two again and the concentration of hydrogen increases as the pressure is increases. As Fig. 2b shows, there are three phase regions in the PCT diagram, the α , $\alpha + \beta$, and β regions separated by the transition dome curve (dotted line). The two-phase region $(\alpha + \beta)$ ends in a critical point, characterized by the critical temperature (T_{cr}) and pressure (p_{cr}) , above which the transition from the α - to β -phase is continuous. When α and β phases coexist, there is a plateau in the isotherms, the pressure hardly changes during the $\alpha \rightarrow \beta$ phase transition, therefore a significant amount of hydrogen is absorbed with

small pressure increases. The plateau region ($\alpha + \beta$ isotherm), however, is not entirely flat due to the expansion of the lattice and small changes of ΔH as a function of hydrogen concentration. In addition, the absorption pressure is slightly higher than the desorption pressure due to unequal accommodation of elastic and plastic energies, which causes a 'hysteresis'. 48 The hysteresis, in general, decreases with increasing temperature. 49 Typical hysteresis magnitudes $(\Delta p/p_{\rm des},$ where $\Delta p = p_{\rm abs} - p_{\rm des})$ for selected systems as examples are 0.015 (at 401 °C) and 0.007 (at 497 °C) for Mg, 50 0.51 (at 0 °C) and 0.24 (at 80 °C) for LaNi $_5$, 49 and 1.43 (at 25 °C) and 0.97 (at 85 °C) for TiFe.⁵¹ The pressuretemperature-concentration relationship can be expressed for both absorption and desorption by the extended van't Hoff equation; by setting the hydrogen concentration to the value at the middle of the α + β phase region, the equation is simplified and the pressure-temperature relationship can be used to determine ΔH values experimentally (see Fig. 2b).

The rates of the hydrogenation and dehydrogenation reactions are of crucial importance for practical storage applications. They depend on the activation energy barrier of the absorption and desorption processes and on the temperature and hydrogen pressure, as well as on the surface area of the solid. Nanosizing metals and alloys to increase the rate of the heterogeneous hydrogenation reaction is an obvious step to increase the rate. Current research on improving the kinetics of hydrogen absorption/desorption aims to reduce the activation energy barrier using catalysts to allow milder reaction conditions (temperature and pressure) for practical applications. The Kissinger method is currently overwhelmingly popular to estimate the apparent activation energy (E_a) for both hydrogen absorption and desorption due to its simplicity (even if complex processes may not be well represented by a single activation energy). 52,53 The Kissinger equation is shown in Fig. 2c. The method is based on measuring a chemical (or physical) thermal event at several non-isothermal tests conducted at constant heating rates (β), using e.g. DSC, DTG, DTA, or MS, and measuring the peak (or onset) temperature of the event (T_p) . A plot of $\ln(\beta/T_p^2)$ versus $1/T_p$ leads to a straight line with the slope equal to $-E_a/R$ (Fig. 2c). Although this method is simple, it oversimplifies the process by assuming single-step kinetics with first-order reaction. If the reaction model is not first order, its dependence on the heating rate introduces an inaccuracy which increases with decreasing E_a/RT . This error has been shown to be below 5% as long as E_a/RT is larger than 10;^{53,54} therefore the $E_a/RT > 10$ relationship may be considered as a prerequisite for using the Kissinger method.⁵³ In addition, the linear heating rate is an integral part of the Kissinger equation; therefore nonlinear heating programs can be applied only if the extent of conversion of the reactant to products doesn't vary significantly with the heating rate at the event peak. 53 Further drawbacks of the method are its inability to detect complexity of processes (namely multiple steps covered by one event peak) and inapplicability to any data obtained on cooling.⁵³ The appearance of multiple peaks in experimental data requires treating them separately (note that a single peak doesn't necessarily mean a single-step process). If peaks are overlapping, they

gen storage materials.56

Review

need to be deconvoluted and the Kissinger method should be applied separately to each individual peak to estimate activation energies of specific processes. Considering its limitations, the Kissinger method should be used for quick estimation of apparent activation energies in comparative studies of simple transformations, rather than providing details of process kinetics. An alternative, although less frequently used and more time consuming, way to obtain activation energies is based on calculating rate constants at several temperatures using the Johnson-Mehl-Avrami-Kolmogorov (JMAK)55,56 equation ["linearized" form: $\ln[-\ln(1-\alpha)] = \eta \ln(k) + \eta \ln(t)$, where k = rateconstant, α = converted reaction fraction, η = growth dimensionality, t = time by fitting (de)hydrogenation curves and calculating the activation energy using the Arrhenius equation (the slope of ln(k) versus 1/T is equal to $-E_a/R$). The JMAK model includes simultaneous nucleation, growth and impingement and offers a more detailed model of phase transformation kinetics than the Kissinger method. Limitations may arise from model specifics, namely assuming phase transformation by random nucleation and growth, a zero critical nucleus size, requirement of a large number of nuclei for accurate prediction, and nucleation and growth following a predetermined law. 56-59 It is important to note that although the limitations of the Kissinger model have been stretched, its popularity continues;^{53,60} however, this may change in the future by wider application of more sophisticated, currently underutilised kinetic models for hydro-

Macroscopic PCT and thermal analyses are the most widely used methods for obtaining information about the kinetics and thermodynamics of the system due to easy accessibility and cost of the instrumentation, but modern operando tools (e.g., synchrotron radiation X-ray power diffraction (SR-XRPD), neutron scattering (NS), and in situ transmission electron microscopy (TEM)) can allow direct observation of phase evolution and kinetics. The SR-XRPD light source is more intense than those of laboratory XRPD instruments, highly collimated, tuneable in a wide energy spectrum, and has a short pulse time structure; therefore SR-XRPD allows high-resolution and timeresolved studies to investigate microstructures of materials, including crystal structure, crystallite size, phase composition, defect and strain. 61,62 Recording in situ SR-XRPD data throughout the whole hydrogenation/dehydrogenation reaction can provide information on the reaction mechanism, transient phases, and kinetics of phase transitions. Hydrogen has a high scattering cross section with neutrons; therefore, neutron scattering techniques, including neutron diffraction (ND), total neutron scattering (TNS), inelastic neutron scattering (INS), quasi-elastic neutron scattering (QENS) and small-angle neutron scattering (SANS), are valuable tools for studying hydrogen storage materials. 63-68 ND and TNS can locate hydrogen atoms in the crystal structure which is practically impossible with XRD. TNS is also powerful for studying amorphous materials. Using neutrons also has the benefit of being able to put the sample under a greater range of pressures, temperatures and gas environments, compared to X-ray instruments, as the neutrons can pass through thick stainless-steel cells and

instruments. This makes them particularly useful for operando measurements. INS and QENS are conceptually similar to infrared and Raman spectroscopy and provide information on molecular and crystal vibrations as well as diffusion and liberation of hydrogen, but in contrast to IR and Raman all vibrations are visible (no selection rules) and the spectrum is dominated by hydrogen displacements due to the approximately order of magnitude higher scattering cross section of neutrons for hydrogen as compared to other elements. The SANS pattern contains information on atomic positions and shapes of particles and can therefore be used to obtain information on the size, shape, and interaction of nanoparticles. Both SR-XPRD and NS facilities are uncommon and accessing them can be expensive and highly competitive. In situ TEM is a much cheaper and more widely available technique suited to follow phase transformations and kinetics. 69-71 Real-time observations during dehydrogenation can be readily performed in the high vacuum environment of the instrument; however, studying hydrogenation (which requires a high-pressure hydrogen atmosphere) is challenging. The reactant and hydrogen must be sealed within a tiny space of a gas cell equipped with electrontransparent windows, allowing a gas layer only a few micrometres thick and separated from the other parts of the microscope. An advantage of the sealed-gas-cell approach is that normal TEM instruments can be modified to run in situ hydrogen absorption experiments by modifying the sample holder.⁷¹

The hydrogen release from binary hydrides is a one-step chemical reaction, but it is multi-step for tetrahydroborates, tetrahydroaluminates, and RHCs involving the formation and decomposition of alkali and earth alkali hydrides in the last step. Fig. 3 shows a simplified decomposition scheme for hydrogen release from these compounds and a more complex scheme for $Mg(BH_4)_2^{72}$ to illustrate the complexity of the problem. Phase separation of metals or metals and boron is an issue for reversibility, and the formation of alloys or borides is favourable for the overall thermodynamics of the system (see Fig. 2a). In addition, passivation of metal surfaces during hydrogenation influences kinetics negatively. The diffusion of hydrogen in LiH and MgH₂ was found to be much slower than in respective metals (there is a three-five order of magnitude difference in diffusion coefficients);^{73–75} therefore the hydride layer passivates the surface. As a result, for example, only partial hydriding was observed on magnesium particles larger than 50 µm due to fast hydride formation. 75 Downsizing metals and alloys has a positive effect in solving this issue and improves kinetics as mentioned above. Since the hydrogen absorption/desorption leads to nanocrystalline solids, due to volume expansion and contraction, 45 downsizing is a natural phenomenon after one hydrogen absorption/ desorption cycle. Nanosizing and activation by removing the passivating oxide layer is therefore essential before the first hydrogen absorption step. General strategies to activate metal surfaces, in addition to nanosizing, are thermal annealing and surface functionalization and doping. Thermal annealing creates cracks on the passivating oxide film and surface metal vacancies, thereby exposing the metal to hydrogen and reducing the energy barrier of hydrogen dissociation, respectively.⁷⁶ The most widely

EES Catalysis Review

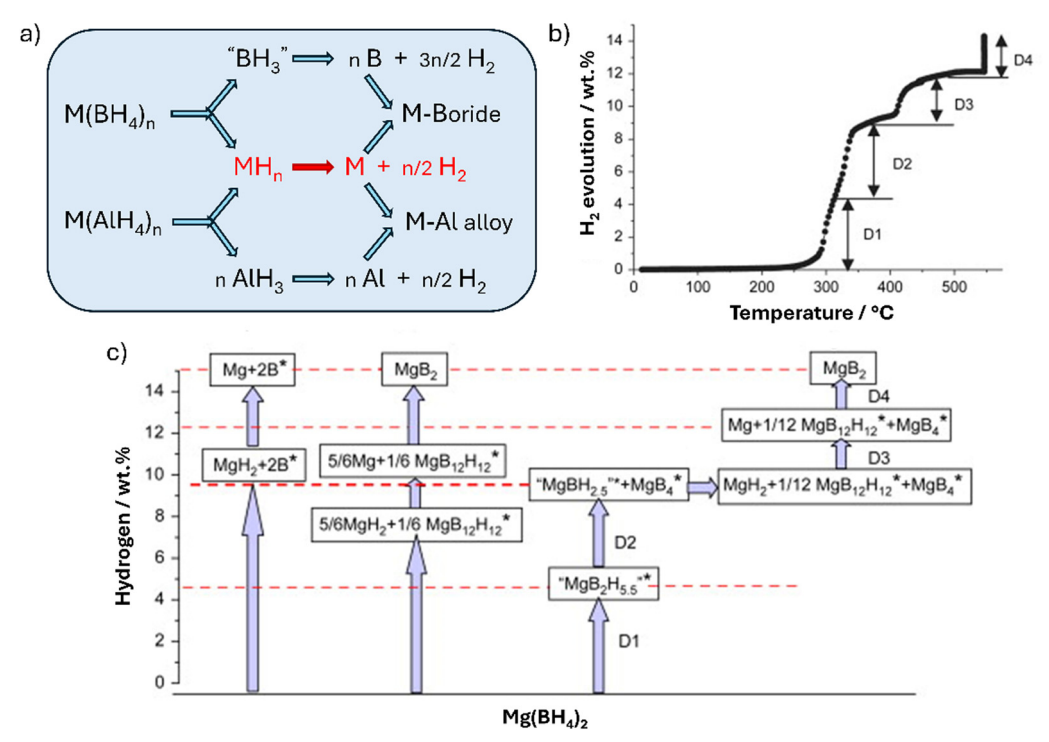


Fig. 3 (a) Simplified decomposition scheme for metal hydrides, tetrahydroborates, and tetrahydroaluminates, (b) volumetric temperature programmed desorption curve of $Mg(BH_4)_2$ and (c) decomposition pathways of $Mg(BH_4)_2$ (observed hydrogen evolution steps, see panel (b), marked by dashed lines; amorphous phases denoted by asterisks). Reproduced from ref. 72 with permission from Elsevier Ltd, copyright 2008.

used method for surface modification and functionalization to create more active sites for molecular hydrogen dissociation and hydrogen atom diffusion on the material surface is currently ball milling with additives and/or catalysts. In general, ball milling introduces mechanical stress and modifies the structure, additives open diffusion channels and catalysts facilitate hydrogen dissociation.^{77–79}

2.2. Tuning the hydrogen storage in lithium, magnesium, and aluminium

Li, Mg, and Al have high hydrogen storage capacities (Table 1, Be is not considered and the capacities of Na, K, and Ca are below the DOE target); however, their practical application faces different challenges. LiH is extremely stable, and the formation enthalpy is -181.2 kJ mol $^{-1}$ H $_2$ (-90.6 kJ mol $^{-1}$ LiH, Table 3); therefore the dehydrogenation of LiH requires very high temperatures (the main desorption peak is observed at 671 °C). Table 3 is addition, there is an activation energy of 52.8 kJ mol $^{-1}$ for the

reaction of H₂ with molten lithium.⁸⁰ Consequently, lithium reacts with hydrogen at high temperatures or pressures (at temperatures above 700 °C under ambient pressure or at 500 bar pressure at room temperature). 73,81,82 LiH therefore cannot be considered as a practical hydrogen storage material as it is economically unviable for cyclic energy storage. Destabilizing the LiH phase and catalysing the hydrogenation and dehydrogenation reactions would be essential to reach milder reaction conditions. To underpin the idea, it is important to note that Wang et al. synthesized LiH nanoparticles with a Ni shell at the surface (composition 85.5 wt% Li, 14.0 wt% Ni and 0.5 wt% Ti, corresponding to an overall hydrogen capacity of 10.8 wt% H₂) and achieved full hydrogen release/uptake in less than 50 min at 350 °C. 73 Extensive cycling, however, could not be achieved at this temperature due to the formation of large particles behaving like bulk LiH and thus not cycling hydrogen at 350 °C; the reversible storage capacity of LiH/nano-Ni remained limited to 2 wt% instead of the potential 10.8 wt% H2. The experiment, however, demonstrated the possibility of tuning the Li/LiH

 $\textbf{Table 3} \quad \text{Comparison of thermodynamic and kinetic properties of AlH}_3\text{, LiH and MgH}_2$

Hydride	$\Delta_{\rm f} H^a$ (s) (kJ mol ⁻¹)	$\Delta_{\mathrm{r}} S^{\circ b}$ (s) (J mol ⁻¹ K ⁻¹)	$\Delta_{\mathrm{f}}G^{c}$ (kJ mol^{-1})	$E_a (\text{des.})^d (\text{kJ mol}^{-1} H_2)$	Cycling properties ^e
AlH ₃	-9.9	-194.3	48.0	102.2	n.a.
LiH	-90.6	-74.1	-68.5	n.a.	n.a.
MgH_2	-76.2	-132.3	-36.7	160	515 (ca. 60%)

^a Enthalpy of formation from elements at 25 °C from ref. 9 and 86. ^b Entropy change of the hydride formation reaction at 25 °C, calculated using *S*° (298 K) values from ref. 9. ^c At 25 °C. ^d Overall activation energy of hydrogen release from ref. 87 and 88. ^e Number of stable cycles and capacity retention (in parenthesis) from ref. 89; n.a. = not available.

system for hydrogen storage. Thermodynamic tuning of the Li/ LiH system was reported earlier, 83-85 but reversible hydrogen cycling at the level of DOE targets could not be achieved. Alloying Li with porous silicon nanowires (molar ratio: 4.4:1), for example, resulted in a reduced hydrogen absorption enthalpy of -118 kJ mol⁻¹ H₂ (-59 kJ mol⁻¹ LiH) and the alloy could reach a maximum observed H2 absorption capacity of 3.95 wt% at 400 $^{\circ}$ C and 40 bar. ⁸³ Hydrogen storage properties of LiH were demonstrated to be size dependent; LiH nanoconfined in high surface area graphite could release 1.9 wt% hydrogen with a peak at 340 °C and could reversibly absorb 1 wt% hydrogen at 300 °C and 60 bar hydrogen pressure.81

AlH₃, in contrast to LiH, is metastable at room temperature; although the formation enthalpy is slightly negative (-9.9 kJ mol^{-1} for α -AlH₃), the Gibbs free energy (ΔG) is positive (+48 kJ mol⁻¹ at 25 °C) (Table 3). AlH₃ fully decomposes in the 100-200 °C temperature region, and the activation energy of decomposition can be decreased by using alkali hydrides and transition metal compounds. 90-92 The hydrogenation of aluminium, however, requires extremely high pressures (above 25 000 bar);90,91,93 therefore AlH₃ can be considered only as a oneway hydrogen storage material and cannot be regenerated onboard a vehicle. 90,93 The findings from recent research to bring the AlH₃ decomposition temperature below 100 °C by doping catalytic amounts of various metal compounds into the AlH₃ matrix through ball milling are summarized in Table 4. Substantial improvement in reaction kinetics was observed compared to pristine AlH₃, promoted by metal hydrides, metals, and solid solutions, formed in situ or by the accordion structure of MXene additives (Table 4). The catalytic effect of these materials is based on lattice distortion, 92 destruction of the aluminium oxide layer by Ti₃C₂, 96 enhanced electron transfer and hydrogen diffusion by in situ formed transition metals or metal compound species, 94,95,97,98 and/or destabilization of AlH₃ through increased Al-H bond length. 98-100 As an example, the multivalent conversion of TiO2 and Pr6O11 promoted the electron transfer of H⁻ in AlH₃, and the newly generated PrH_{2.37} hydrogen diffusion pathway promoted the release of hydrogen (Fig. 4a). It seems that the DOE system targets considering storage capacity and hydrogen release temperature can be met with catalysed AlH₃ decomposition, which makes AlH₃ a

promising one-way hydrogen source medium for mobile applications. Cheap production or regeneration of the hydride, however, is not solved yet.

Considering the extreme stability of LiH and the thermodynamic instability of AlH3, the Mg/MgH2 system seems to be the golden middle road for reversible hydrogen storage. Hydrogen absorption in Mg and especially desorption from MgH2, however, require high temperatures. Considering the van't Hoff equation (Fig. 2b), the enthalpy of MgH2 formation of $-74 \text{ kJ mol}^{-1} \text{ H}_2^{-101}$ and an entropy change of 130 J K⁻¹ mol⁻¹ H₂, the temperature required to reach 1 bar hydrogen equilibrium pressure at MgH₂ desorption is about 300 °C. If MgH₂ could be destabilized to have a desorption enthalpy below 48.5 kJ mol⁻¹ ($T\Delta S$ at 100 °C), hydrogen release would be thermodynamically favoured at 100 °C. Improving both thermodynamics and kinetics of the Mg/MgH2 system is therefore essential for reversible hydrogen storage; however, there is a limit of 15 wt% for the additive concerning the ultimate DOE target of 6.5 wt% and the theoretical MgH₂ storage capacity of 7.66 wt%. Alloying Mg with Al was found to improve both kinetics and thermodynamics of the system; 102,103 however, Al served only as a diluent due to the instability of AlH3 (see above). Despite improvements, the kinetics of hydrogen absorption in the Mg₉₀Al₁₀ alloy (11 wt% Al) was still slow, namely 2.7 wt% and 4.6 wt% hydrogen capacity could be achieved at 260 °C and 380 °C, respectively, at 30 bar hydrogen pressure within 2 hours. 102 The Mg-Zn alloy containing 17 wt% Zn performed better and could absorb 5.0 wt% hydrogen in 20 min at 300 °C and had a hydrogen storage capacity of 6.1 wt% at this temperature (but below the DOE target); the enhanced hydrogen storage properties for this system were attributed to improved kinetics (low hydrogen absorption activation energy of 56.3 kJ mol⁻¹) rather than the change in enthalpy.104 Mg has also been alloyed with Li; however, the hydrogenation of Mg-Li alloys always leads to a mixture of MgH₂ and LiH, from which MgH₂ could be thermally decomposed up to 450 °C, but LiH remained stable. 105 Considering this, Mg-Li alloys are not good candidates for reversible hydrogen storage because their reversibility and stability are very similar to those of pure Mg, but with lower storage capacity.

Early long term hydrogen cycling experiments on Mg in 1984,89 involving 515 cycles and using high purity hydrogen

Table 4 Effect of catalysts on the hydrogen release properties of AlH₃

Catalyst precursor	Active form ^a	Capacity ^b (wt%)	Decomp. temp. conset/peak (°C)	Isothermal H ₂ release wt%/°C/min	$E_{ m a}$ (des.) (kJ mol $^{-1}$ H $_{ m 2}$)	Ref.
TiB ₂ (2.5 wt%)	Al-Ti-B ss	8.7	78/n.a.	5.3/80/200 7.3/110/60	86	92
NbF ₅ (1 mol%)	Nb, AlF ₃	6	60/122		96	94
LaNi ₅ (10 wt%)	Ni	8.6	86/n.a.	6.3/100/60 7.7/120/30	98	95
Ti_3C_2 (4 wt%)	Ti_3C_2	8.1	61/n.a.	6.9/100/20	40	96
CeO ₂ (1 mol%)	CeH_{2+x}	7.8	114/n.a.	6.5/100/100	69	97
$TiO_2 - Pr_6O_{11}$ (1 mol%)	$PrH_{2.37}$	8.3	43/119	5.9/100/60	56	98
Bi@C (5 wt%)	Bi	8.0	80/n.a.	5.4/120/40	87	99
Fe@C (3 wt%)	Fe@C	8.5	94/n.a.	6.2/120/40	78	100

^a Catalytically active component formed during ball milling of precursors; ss = solid solution. ^b Experimentally determined maximum storage capacity. c n.a. = not available.

EES Catalysis

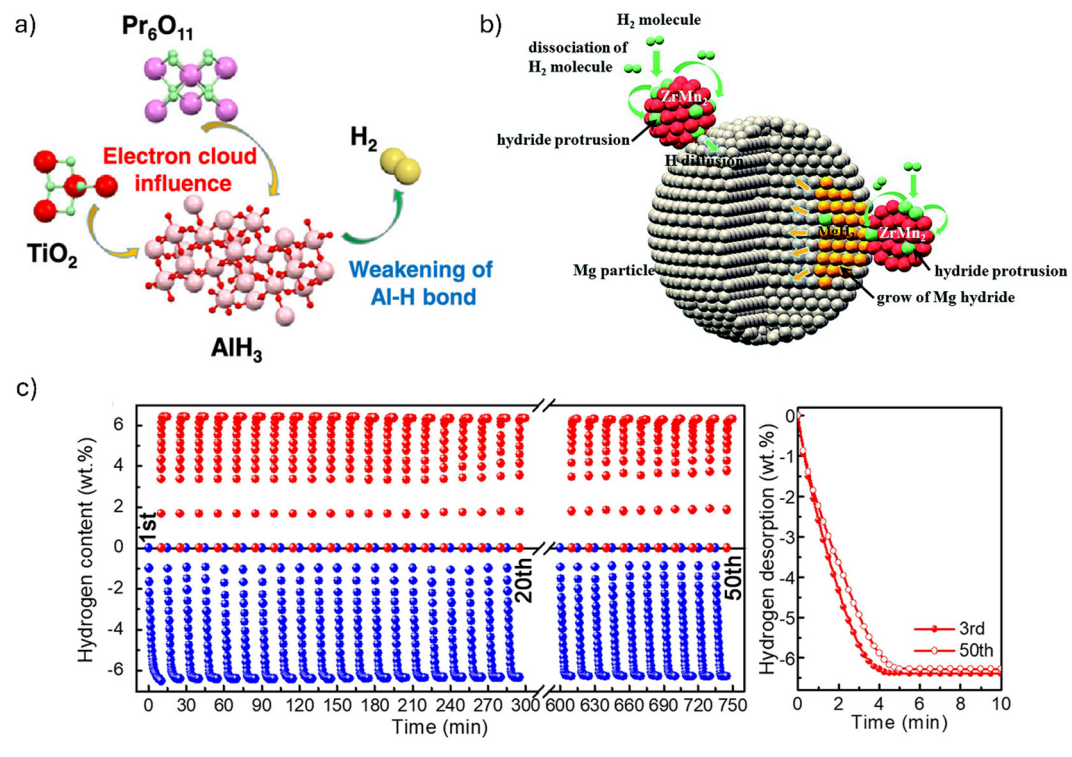


Fig. 4 (a) Mechanism for the catalytic effect of TiO₂ and Pr₆O₁₁ on AlH₃. Reproduced from ref. 98 with permission from the American Chemical Society, copyright 2021, (b) mechanism for the hydrogenation of Mg catalysed by ZrMn₂ nanoparticles. Reproduced from ref. 118 with permission from the Royal Society of Chemistry, copyright 2019, and (c) dehydrogenation/hydrogenation cyclic curves of MgH₂ with 10 wt% TiO₂-ZrO₂-V₂O₅ catalyst at 300 °C. Reproduced from ref. 127 with permission from Elsevier Ltd, copyright 2024.

(99.9997%), an operating temperature of 390 °C, and 30 min charging and discharging time at 32 bar H₂ pressure and vacuum, respectively, highlighted the potential of reversible hydrogen storage in Mg and challenges as well, namely the high operating temperature and pressure, decreasing storage capacity by cycle numbers and the sensitivity of magnesium to oxygen and nitrogen impurities in repeated experiments. 106 The high activity of freshly prepared pure magnesium to oxygen, water and nitrogen was pointed out recently. 107,108 To bring operating conditions closer to ambient conditions and improve hydrogen cycling properties, a very wide range of metal compounds have been screened during the last few decades to find effective catalysts to improve kinetic and cycling properties for magnesium by reducing activation energies; 74,101,109-115 these included transition and rare earth metals, alloys, oxides, halides, carbides, carbonitrides, nitrides, sulphides, hydrides, carbon materials, MXenes, and their mixtures. The catalytic activity of these compounds was based on various mechanisms, 114-144 namely absorbing and delivering hydrogen to Mg thereby acting as a "hydrogen pump", $^{114,116-118,123,129,130,133,135,137,139,142,144}$ providing channels for fast hydrogen diffusion, 114,115,121,125,128,130,131,137,139,142 providing nucleation sites, 115,119,121,125,135 providing abundant oxygen vacancies in oxides, ^{116,127,132} and weakening the Mg-H and/or H-H bond strength. ^{114,120,123,124,136,138,141,143} The addition of carbon nanotubes (CNTs) or carbon was found to be advantageous for preventing the aggregation of Mg/MgH2 particles, thereby preserving stable cycle properties, 122,130,142,143 as well

as aiding hydrogen diffusion and heat transfer. 141 The catalytic mechanism can be structured into three groups: (1) kinetic facilitation of dehydrogenation/hydrogenation processes (e.g., LiCoO₂, 114 TiO_{2-x}, 115 V₂O₅, 116 NiV₂O₆, 117 ZrMn₂, 118 TiFe, 122 Ni₃ZnC_{0.7}, 123 Nb₂CTx MXene, 124 TiO₂@MnCo₂O_{4.5}, 125 TiMn₂, 126 TiO₂-ZrO₂-V₂O₅, ¹²⁷ Ti₂VC₂ MXene, ¹²⁸ shell-like Ni/Mo₂N, ¹²⁹ Ni₃Fe/Ni/NiFe₂O₄@C, ¹³⁰ Nb₂O₅-C/Ti₃C₂Tx MXene, ¹³¹ MoO_{3-x}, ¹³² MXene Ti_3C_2 @NiO, 133 NiSe₂, 135 Ni/TiO₂, 136 Ce_{0.6}Zr_{0.4}O₂, 137 $\text{Co}_3\text{V}_2\text{O}_8$, ¹³⁸ NaNbO_3 , ¹³⁹ Al_3V , ¹⁴⁰ $\text{Ti}_{0.9}\text{Zr}_{0.1}\text{Mn}_{1.5}\text{V}_{0.3}$, ¹⁴¹ NiS@C, ¹⁴² Ni/Mo2C@C, 143 Ni₃Mn 144), (2) structural stabilization of nanoparticles (e.g., V₂O₅, 116 CoFeB/CNT, 121 CNT, 122 carbon 123,142,143), and (3) thermodynamic tuning (e.g., TiH₂¹¹⁹). Most of the materials in catalyst groups 1 and 2 did little to reduce the thermodynamic stability of MgH2. In general, transition metal oxides acted as precursors for in situ formation of catalytically active species (see Table 5).

Each step of the multistep hydrogenation and dehydrogenation processes must be addressed for effective catalysis, including bond dissociation, hydrogen transfer, bond formation, phase transformation, and heat transfer. In addition, uniform distribution and prevention of phase separation of catalysts and controlling the surface area of MgH₂/Mg particles by blocking large particle growth and aggregation are also of key importance. In situ formed hydride/metal or hydride/alloy couples that more easily release and accept hydrogen than MgH₂/Mg in the material matrix can serve as "hydrogen pumps" by removing/ delivering hydrogen to MgH₂/Mg; examples are Mg₂Co/Mg₂CoH₅, 114

Table 5 Effect of catalysts on the hydrogen absorption and desorption kinetics of Mg/MgH $_{
m s}^{
m a}$

	Isother	Isothermal absorption	orption		Non-isoth. des. onset/peak	Isother	Isothermal desorption	orption		Cycles/ca	Cycles/capacity retention	tention		F (abs/des)	
Catalyst (active form)	wt%	\mathbf{O}_{\circ}	bar	min	∂ ₀/ ∂ ∘	wt%	\mathbf{O}_{\circ}	bar	min	wt%	\mathbf{O}_{\circ}	No.	%	$E_{\rm a} ({\rm abs/acs})$ kj mol ⁻¹ H ₂	Ref.
$\overline{\text{(no catalyst)}^b}$	1.3	210	32	10	310/n.a.	1.1	325	0.003	10	n.a.	n.a.	n.a.	n.a.	81/156	114
	6.1	270	32	10		7.1	375	0.003	10						
$LiCoO_2$ (7 wt%)	2.2	125	32	10	180/n.a.	5.5	250	0.003	09	6.2	300	20	94	45/49	114
$(\mathrm{Mg_2Co ext{-}Mg_2CoH_5})$	3.8	150	32	10		9.9	325	0.003	10						
<u> </u>	0 -	007 E	20	01	104/041	1	000	600	6	L	000	6	007	00/	4 7 1
$3\% \text{ K-}110_{2-x}$	4 4	R.I.	080	180	194/24/	0.,	200	0.001	10	0.0	200	90	100	11.a./ 09	CII
(1211203)	6.7	200	30	09											
$10\% \text{ H-V}_2\text{O}_5$	2.4	30	30	09	185/n.a.	4.4	225	0.1	10	5.7	275	100	66	43/85	116
$(VH_2, V)^{\frac{1}{2}}$	4.1	100	30	30		9	275	0.1	2						
$10\% \text{ NiV}_2\text{O}_6$	2.2	75	30	50	n.a.	4.5	250	0.01	75	6.1	325	20	06	25/93	117
$(\mathrm{Mg_2Ni},\mathrm{v_2O_5})$	5.6	150	30	20		5.2	300	0.01	10						
$10\% \text{ ZrMn}_2$	4.3	20	30	40	182/251	6.7	300	I	2	6.5	275	10	85	22/82	118
	5.3	100	30	10											
$10\%~{ m TiH}_2$	41	RT	20	240	180/n.a.	4	240	0.001	20	9	300	80	100	n.a./58	119
	ر د	240	20	., t	000		0	0	,			Ç L	ć		,
5% Fe NS	ه و	200	32	10	182/223	5.4 r	300	0.03	01	٠,	300	20	83	n.a./41	120
10% COFEB/CIVI (CO_3MgC , Fe, COFE) TiFe + CNT (10 + 5 w#%)	0.7 7.7	125	30	07	1//II.a. 210/n a	6.0	275	vac. 0 03	30	6.2	300	10	100	11.a./83.2 61/n a	121
			8	8	710/11:4:	6.2	300	0.03	41	1		21			
Ni ₃ ZnC _{0,7} (a)C (2.5 wt%) (Mg ₂ Ni, MgZn ₂)	5.2	150	50	3	312/360	5.7	400	0.001	5	4.5	400	20	95	42/101	123
Nb_2CT_x-5Na (5 wt%)	4	100	30	1	n.a.	2.6	250	0.01	12	6.2	300	40	06	n.a./70	124
	5.5	125	30	1		6.4	300	0.01	3						
$TiO_2@MnCo_2O_{4.5}$ (6 wt%)	2	30	30	30	n.a./290	2	225	0.01	120	6.2	325	30	79	n.a./76	125
	5.1	150	30	8		6.4	300	0.01	30			:	,		
$\frac{\text{TiMn}_2}{\text{ris}}$ (10 wt%)	5.1	225	10	2	n.a.	5.1	225	0.2	∞	2.8	225	414	100	19/83	126
$110_2 - 2rO_2 - V_2O_5 (10 \text{ wt}\%)$	5.1	50	40	30	220/n.a. 170/m.a	6.5	300	0.001	ი (6.4	300	50	80 0	n.a./66	127
11_2 VC ₂ (10 WC%)	о 1. 1. 1.	25 150	09	10	1/0/n.a.	4.5 C	300	0.1	00 r	7.0	373	100	98	II.a./ / I	178
Ni/Mo. N (6 w#0%)	у г С -	130 135	00	10	186/n a	2. r	300 265		30	7 2	330	10	80	92/ 6 u	100
$(M_{\rm P},N_{\rm I})$	5.5	150	20	15	100/11.4.	6.8	325			\. 0	230	TO	000	11.a./ / 0	671
$N_{13}Fe/Ni/NiFe_2O_4@C$ (10 wt%)	4.2	100	30	10	n.a./290	3.6	250	0.2	09	6.4	300	10	100	n.a./91	130
	5.8	150	30	7		5.8	325	0.2	2						
${ m Nb_2O_5-C/Ti_3C_2}~(10~{ m wt\%})$	5.5	100	40	15	n.a.	5.8	300	0.001	3	6.3	300	20	66	n.a./63	131
$MoO_{3-x} (10 \text{ wt}\%)$	4.6	175	30	8	200/n.a.	5.9	300	0.05	8	6.1	300	20	66	n.a./71	132
${ m Ti_3C_2@NiO}$ (9 wt%) (Mg ₂ Ni, Ti)	4 r	100	30	10	184/n.a.	6.7	300	0.01	10	2.9	300	20	96	n.a./53	133
Cr Mn Fe Co Ni-oxide (10 w#%)	5.5 5.7	150	30	10 20	184/n a	7 9	250	9	7	7.	250	05	80	17/55	134
$NiSe_2$ (5 wt%) (MgSe, Mg ₂ NiH ₄)	5.2	100	30	80	n.a./319	9	300	0.2	20	6.2	360	20	100	n.a./71	135
)	5.7	200	30	4											
$\mathrm{Ni/TiO_2}\ (7\ \mathrm{wt\%})\ (\mathrm{Mg_2Ni})$	5.4	150	25	1	181/n.a.	9	250	0.001	30	5.5	200	20	92	n.a./78	136
					,	6.3	300	0.001	ر د	(į	;		į	!
$Ce_{0.6}Zr_{0.4}O_2$ (7 wt%) ($CeH_{2.73}/CeO_{2-x}$)	4.4	100	50	ი ი	201/n.a.	3.9 6.9	230	0.001	40	2.8	2/0	70	66	n.a./69	137
$C_{O_2}V_2O_2$ (6 wt%) ($C_{O_1}V_2O_2$)	, (RT	30	30	6.0	2. 6	22.5	0.09	120	9	300	30	73	99/ e u	138
(5) 7. (5) (5:3)	3.9	100	30	30		5.9	300	0.09	5)))			0
	5.9	300	30	1		6.4	325	0.09	3						
$NaNbO_3$ (5 wt%) (NbH_x , Nb , $NaMgH_3$)	3.5	30	30	06	n.a.	6.2	260	0.01	12	6.3	300	40	100	n.a./85	139
()07 1) 11 [4	4.7	125	30	ر د د	2,700	L	001	500	,	,	900	S	1	00/	6
Al ₃ V (5 Wt%)	0.3	200	ne	10	291/n.a.	6.5	400	0.001	٥	٥	400	70	/6	n.a./86	140

Table 5 (continued)

	Isothe	rmal abs	Isothermal absorption		Non-isoth. des. onset/peak	Isother	mal des	orption		Cycles/c	apacity re	etention		T (ahe/dae)	Cata
Catalyst (active form)	wt%	wt% °C bar	bar	min	D₀/D₀	wt%	၁့	bar	min	wt%	၁	No.	%	$E_a (abs/acs)$ kj mol ⁻¹ H ₂	Ref.
$\overline{{ m Ti}_{0.9}{ m Zr}_{0.1}{ m Mn}_{1.5}{ m V}_{0.3}/{ m CNT}\left(10+1~{ m wt}\% ight)}$	2.4	25	30	09	195/n.a.	6.1	300	0.001	2	6.2	325	100	97	n.a./86	141
	4.8	150	30	10											
NiS/C (5 wt%) (Mg_2Ni , MgS)	3	180	20	09	235/n.a.	3.5	300	0	09	6.5	400	20	26	24/67	142
$Ni/Mo_2C@C$ (7.5 wt%) (Mg_2Ni)	n.a.	n.a.	35	n.a.	240/318	6.4	300	0.001	20	6.5	300	20	86	n.a./97	143
Ni_3Mn (9 wt%) (Mg_2Ni)	3.5	75	30	09	190/n.a.	4.4	235	0.03	09	9.9	295	20	94	39/87	144
	6.1	150	30	10		9.9	295	0.03	2						
CuNi (10 wt%) c (Mg ₂ Ni(Cu))	6.1	265	10	10	n.a./245	6.1	277	n.a.	15	6.1	277	15	92	n.a./81	146

RT = room temperature, NS = nanosheet, CNT = carbon nanotube, n.a. = not available. b As-prepared MgH₂. c Solar heating under a light density of 3.5 W cm⁻².

 VH_2/V_1^{116} Mg_2Ni/Mg_2NiH_4 , $^{117,123,129,130,133,135,136,142-144}$ and $ZrMn_2/NiH_4$ Zr₄Mn₈H_{10.99} (Fig. 4b).¹¹⁸ Another "hydrogen pump" mechanism is found to be the facilitation of electron transfer between Mg²⁺ and H by transition metal compounds, which promotes the dissociation and recombination of H2, observed e.g. for TiFe, 122 and multivalent transition-metal related species formed during hydrogen cycling from Nb₂CTx MXene, ¹²⁴ TiO₂@MnCo₂O_{4.5}, ¹²⁵ Nb₂O₅-C/Ti₃C₂Tx MXene, ¹³¹ Ni/TiO₂, ¹³⁶ Ce_{0.6}Zr_{0.4}O₂, ¹³⁷ or NaNbO₃. ¹³⁹ In addition, transition metals promote the dissociation of H₂ molecules¹²¹ and rupture of the Mg-H bond by weakening the interaction and elongating the bond length (see e.g., the ZrMn2- MgH_{2} , ¹¹⁸ Fe- MgH_{2} , ¹²⁰ Co- H_{2} , ¹³⁸ $V_{2}O_{3}$ - MgH_{2} , ¹³⁸ $Ti_{0.9}Zr_{0.1}Mn_{1.5}V_{0.3}$ -MgH₂ interactions¹⁴¹). Oxygen vacancies of transition metal oxide catalysts have been found to have a promoting effect on dehydrogenation/rehydrogenation by accelerating electron transfer and creating a "hydrogen pump" (e.g. V₂O₅)¹¹⁶ or by enhancing the hydrogen adsorption ability of the oxide (e.g. MoO_{3-x}). There are multiple effects and processes during hydrogenation and dehydrogenation of magnesium, and to utilise all of these, synergistic use of multiple catalytic phases is required. The in situ generated phases can collectively constitute an efficient catalytic system. For example the coexistence of Mg₆MnO₈, Mn, Ti₂O₃, and CoO phases generated in situ from $TiO_2@MnCo_2O_{4.5}^{125}$ exhibits abundant diffusion pathways and nucleation sites for hydrogen absorption and desorption reactions. 125 Another example is the Ni₃Fe/Ni/NiFe₂O₄@C catalyst system where the in situ formed Mg2Ni/Mg2NiH4 acts as a "hydrogen pump", Fe⁰ facilitates electron transfer and creates hydrogen diffusion channels, and carbon effectively prevents particle agglomeration. 130 The catalyst Mg/MgH2 interfaces play a key role in hydrogen transfer. Catalysts can cause morphological defects and could boost the nucleation by reducing the nucleation energy of Mg/MgH2 and thereby improve the hydrogen diffusion rate. 115 2D nanomaterial sheets and layered materials, e.g. MXenes, are effective in creating abundant active sites and enabling faster hydrogen boundaries diffusion along the interfaces. 120,128 They are also effective in hindering powder agglomeration. 134

It is becoming clearer that effective hydrogen storage in magnesium requires both addressing each step of the multistep hydrogenation/dehydrogenation processes by benefiting from the synergistic catalytic effect of multiple phases of multiple compounds and limiting the growth of Mg and MgH2 particles. Developing composite materials seems to be the best strategy to achieve long term cyclic goals. Significant, 50-70%, reduction of the overall activation energies could be achieved in dehydrogenation/rehydrogenation considering recent efforts; good performers, also tested for cycling, are provided in Table 5. It is now possible to recharge Mg below 100 °C; however, hydrogen release requires much higher temperatures (Table 5). Although the reduction of operation temperatures is a fundamental aim of research efforts, the excellent cycling stability is also crucial for practical applications; therefore, recent research is increasingly focusing on cycling stability (Table 5, Fig. 4c). To date, cycling tests have been conducted at relatively high temperatures between 275 and 400 °C due to slow hydrogen release at lower temperatures. Capacity retention close to 100% could be achieved

for cycles ranging from 10 up to 414 (Table 5), but long-term cyclic stability evaluation as per DOE requirements is yet to be conducted. The high temperature of the hydrogen release of MgH₂, however, remains problematic for practical applications; therefore the Mg/MgH2 hydrogen storage system still cannot work in the operational range of PEM fuel cells. Its application is currently limited to high-temperature fuel cells or stationary applications, or the released hydrogen must be cooled for PEM fuel cells. An example for high-temperature MgH₂-based storage is the application of the 0.9MgH₂-0.1TiH₂-5 wt% C nanocomposite in a storage tank which could deliver 185 normal litre hydrogen in temperature swing operation involving charging at 150 °C and discharging at 370 °C. 145

It is important to note the recent novel concept of solardriven reversible hydrogen storage for magnesium, which integrates the photothermal localized heat and catalytic action by a single-component phase that simultaneously exhibits photothermal and catalytic effects. 146 Incorporating 10 wt% NiCu into Mg resulted in the formation of Mg2Ni(Cu) which acted as a Mg₂Ni(Cu)/Mg₂Ni(Cu)H₄ hydrogen pump in cycling and also weakened the Mg-H bond. Reversible hydrogen storage was achieved with 6.1 wt% capacity and 95% retention. 146 The photodecomposition and rehydrogenation of the LiH surface under illumination at ambient temperature was also observed recently (dehydrogenated LiH could uptake 0.08 wt% hydrogen at 1 bar hydrogen pressure), 147 highlighting a new path for the development of hydrogen storage methods.

Among Li, Mg, and Al, which exhibit hydrogen storage properties, currently, only magnesium has the potential to become a reversible hydrogen storage material. Although it is still not satisfying all DOE targets, it seems to be on track to meet longterm cycling goals under close to ambient conditions. Strategies that might enable this are expected to use multielement and multiphase systems which can address kinetics of all steps of the multistep hydrogenation and dehydrogenation process and can control phase transfer and growth. A key advantage of magnesium is that it is abundant, non-poisonous, recyclable and a relatively cheap material. Mg is produced on a large scale in the smelting industry (1 million tonnes in 2024)148 and can be hydrogenated directly in a rotary autoclave at 300-400 °C and 100-150 bar hydrogen pressure, or in THF solvent at 60-70 °C and 80 bar in the presence of catalysts. 149 A major disadvantage is its sensitivity to oxygen and water, with Mg nanopowders reacting violently with air and presenting the hazard of dust explosions. 150 Pure and finely divided MgH2 is also pyrophoric. 149 The application of Li as a hydrogen storage material is not practical due to the high temperatures required for hydrogen absorption and release and competing demand for Li for batteries. LiH is produced in the industry by reacting molten lithium with hydrogen at temperatures above 700 °C.149 Although Al is highly abundant and AlH3 releases hydrogen upon moderate heating (temperatures below 100 °C if catalysed), regeneration of AlH₃ is not feasible by the direct Al + H₂ reaction due to thermodynamic instability. AlH₃ is currently not produced in industry; the main small scale laboratory production methods are based on the reaction of LiAlH₄ with AlCl₃ in a diethylether solvent (Scheme 1).149,151 The energy intensive

$$2 \text{ Li} + \text{H}_{2} \xrightarrow{>700 \, ^{\circ}\text{C}, \, 10 \, \text{bar}} 2 \, \text{LiH}$$

$$4 \text{ LiH} + \text{AlCl}_{3} \xrightarrow{35 \, ^{\circ}\text{C}, \, 1 \, \text{bar}} 2 \, \text{LiAlH}_{4} + 3 \, \text{LiCl}$$

$$3 \text{ LiAlH}_{4} + \text{AlCl}_{3} \xrightarrow{35 \, ^{\circ}\text{C}, \, 1 \, \text{bar}} 4 \, \text{AlH}_{3} + 3 \, \text{LiCl}$$

$$AlEt_{3} \xrightarrow{180 \, ^{\circ}\text{C}, \, 100 \, \text{bar}} 4 \, \text{AlH}_{3} + 3 \, \text{C}_{2}\text{H}_{4}$$

$$2 \, \text{Al} + 6 \, \text{C}_{2}\text{H}_{4} + 3 \, \text{H}_{2} \xrightarrow{1.) \, 132 \, ^{\circ}\text{C}, \, 100 \, \text{bar}} 2 \, \text{AlEt}_{3}$$

Scheme 1 Synthesis of AlH₃ and LiH (industrial processes are indicated by the boxes).149-153

nature of the desolvation process and conversion of the LiCl byproduct to lithium limits the potential of this method for large scale production. An alternative to this synthetic route could be the thermal decomposition of Al(Et)₃ (triethylaluminium), produced on an industrial scale from Al, H2 and ethylene in a two-step process; 152 however, the current synthesis at the laboratory scale is still suffering from low yields (19%). Due to the lack of convenient synthesis/regeneration of AlH3, currently, AlH3 cannot compete with other potential one-way storage systems such as ammonia and LOHCs. In addition, the handling of Al and AlH3 nanopowders is more problematic compared to that of LOHCs, as these nanopowders present the same dust explosion hazards as finely divided/powdered magnesium.

2.3. Alkali and alkali earth metal tetrahydroborates

Tetrahydrobotates exhibit higher hydrogen storage capacity than metal hydrides due to the light boron atom constituent but have high decomposition temperatures (above 400 °C), the kinetics of hydrogen desorption are sluggish, and the multi-step decomposition reaction is not or only partially reversible and only at high hydrogen pressures. 72,154-167 In addition, the tetrahydroborate decomposition may generate stable intermediates, such as borate cluster anions, or volatile by-products, like diborane, 72,167 and the evaporation of volatile alkali metals, namely Na and K, is an issue for practical applications. The latter issue might explain the paucity of experimental work on the thermal decomposition of sodium and potassium tetrahydroborates. Alkali and alkali earth tetrahydroborates, therefore, are not suited for reversible hydrogen storage without modifying the thermodynamics and kinetics of hydrogen absorption/desorption and establishing lower operating temperatures and reversibility for these reactions. It is, however, an advantage of tetrahydroborates compared to metal hydrides that they can tolerate larger amounts of additives/ catalysts to satisfy DOE targets due to larger hydrogen storage capacities; the amount of additive in an additive + LiBH₄ mixture can be as high as 75 wt% to satisfy the DOE target of 6.5 wt% hydrogen storage capacity, but it is only 13 wt% for KBH₄ (see Tables 1 and 2). The possible higher additive load and storage capacity therefore opens the door for storage techniques that are not feasible for the Mg/MgH2 system considering the DOE target,

EES Catalysis Review

such as combining (nano)confinement and catalysis or applying only partial dehydrogenation by limiting the temperature and stopping before full decomposition, typically neglecting the final high temperature hydrogen release. An example is LiBH₄ decomposition due to the formation of thermally stable LiH whose hydrogen release proceeds only at very high temperatures (LiBH₄ \rightarrow LiH + B + 3/2H₂).

The role of additives/catalysts is multiple in the tetrahydroborate systems as they should decrease the overall activation energy barrier of decomposition and hydrogen absorption, alter thermodynamics, and prevent the formation of stable intermediates and the separation of elemental boron by establishing an alternative lower energy pathway to metal borides (which are thermodynamically more stable reaction products than elemental boron). Considerable work has been dedicated to date to tailor the hydrogen absorption and desorption properties of tetrahydroborates using transition metal oxides, halides, and carbides, transition, rare earth and main group metals, and carbon-based materials. 46,167-210 Achieving reversible cycling is seemingly the most challenging (Table 6). The formation and accumulation of stable intermediates, for example Li₂B₁₂H₁₂, loss of nanoconfinement effects due to increasing particle size, and segregation of B and metal hydride phases are possibly the main reasons for the decrease in cyclic hydrogen capacity. 185,186,189 The mechanism of catalytic action of various additives may involve weakening B-H bonds, 181,186,188,191,193 facilitating hydrogen diffusion, 181,187,194,200,201,204-206 inhibiting $B_{12}H_{12}^{2-}$ formation, 185,188,191,192,194,198 suppressing the formation of B₂H₆, ^{192,203} enhancing the effect of nanoconfinement, 185,186 providing nucleation sites, 189,204 establishing B reservoirs by boride formation, 197 and limiting particle size growth. 191 Carbonaceous materials, e.g. CNTs, can facilitate heat management as they effectively increase the thermal conductivity of the confined system. 187 As a new approach, the light-driven dehydrogenation of LiBH4, without thermal heating, was achieved recently by incorporating TiO2 for the photocatalytic effect and TiF3 for enhanced dehydrogenation; the LiBH4-8TiF3-2TiO2 composite could release about 3.12 wt% hydrogen in 30 min under a light intensity of 0.76 W cm⁻². ²⁰⁹ LiBH₄ nanoconfined in ultralow-content Ni-doped structured mesoporous carbon could release 11.02 wt% hydrogen of LiBH₄ (not considering the template matrix) in 150 min under 3.5 W cm⁻² light irradiation and maintain a capacity retention of 85% after 5 cycles due to the nanoconfinement effect, trace amounts of Ni, and photogenerated vacancies in the LiH product which thermodynamically destabilize B-H bonds.210 Transition metals and alloys, such as Ti, 201,204,209 Ni, 192,205 and CoNi, 193 and transition metal compounds, such as NbB₂, 186,202 LiTiO₂ and TiB₂, 187 FeB and Fe_2B , 188,190 Ni_2B , 191 Li_3BO_3 and NbH, 194 Co_2B/Ni_2B , 197 V_xB_y and Ni_xB_y , 198 $VH_{2.01}$, 201 TiH_{2} , 203 $TiH_{1.924}$, TiB, and TiB_2 , 204 and NbVH,206 generated in situ from oxide, carbide and halide precursors, as well as additives, such as MXenes (Ti₃C₂, Ti₂C, Nb₂C), ¹⁸¹ were found to destabilize the BH₄ anion by weakening the B-H bond and decreasing thereby hydrogen dissociation energy for hydrogen desorption due to electronic interactions/ electron transfer. NbVH nanoparticles, for example, operated as "bidirectional hydrogen pumps" combining both hydrogen spillover and hydrogen diffusion.206 The bidirectional chargetransfer catalytic mechanisms of FeB and Fe2B were revealed wherein they act as electron acceptors accepting electrons from BH₄ and electron donors donating electrons to boron, which enhances their reactivity for dehydrogenation and hydrogenation, respectively. 188,190 In addition to kinetic facilitation of dehydrogenation/hydrogenation processes, in situ formed borides contribute to thermodynamic tuning of the system. An example is the reversible transformation between NiB/CoB and Ni₂B/Co₂B, acting as boron reservoirs, in the dehydrogenation and hydrogenation reactions of NaBH₄. 197 A problematic side product of tetrahydroborate decomposition is B₂H₆, a poisonous and flammable gas, which results in boron loss and/or in the formation of a stable $B_{12}H_{12}^-$ dodecaborate anion via the B_2H_6 + BH₄ reaction at elevated temperatures. 192 The accumulation of B₁₂H₁₂²⁻ or boron loss during cycling gradually decreases storage capacity. Strategies to prevent these reactions include lowering the temperature below the temperature required to generate B_2H_6 (below 300 °C)¹⁹² or catalytically decomposing $B_{12}H_{12}^{-}$. The nanoconfinement effect has also been found to suppress the release of B₂H₆ and inhibit B₁₂H₁₂ formation during the dehydrogenation process. 185,210 Concerning the stable dodecaborate anion, reactive lithium ferrites and catalysis from iron borides were shown to effectively promote the decomposition of Li₂B₁₂H₁₂. ¹⁸⁸ In situ formed Ni_xB or the synergistic action of Li₃BO₃ and NbH were also found to inhibit the formation of Li₂B₁₂H₁₂ during hydrogenation. 194,210 Carbonaceous materials (e.g., graphene, CNTs) and MXenes have multiple roles, as they provide structural support, interfaces for electron conduction and hydrogen diffusion, and also have a catalytic effect on hydrogenation and dehydrogenation processes. 181,201 The decomposition of LiBH₄, for example, is believed to preferably occur at the graphene-LiBH4 interface, than within bulk LiBH₄, as an interface reaction. 185 Graphene was also shown to weaken both the Mg-H and B-B bonds of MgH2 and B2H6, respectively.200 Nanoconfinement shortens the hydrogen diffusion pathway, and this effect is believed to be responsible for the decrease of activation energy. 185 Table 6 lists recent examples, focusing on those where hydrogen cycling has also been investigated, and highlights challenges for the application of alkali and alkali earth tatrahydroborates in hydrogen storage, namely the high temperature for hydrogen absorption/desorption and poor cycling stability. Obviously, the utilization of the synergistic effects of catalysts, nanoconfinement, improved surface interaction between various phases in the systems, and enhanced thermal transfer has already resulted in marked improvement of hydrogen storage properties. Fig. 5 shows, as an example, the fabrication of a multi-metal catalyst system for enhancing hydrogen release from NaBH4 and the energy diagram illustrating altered thermodynamics and kinetics compared to pristine NaBH₄. There is a large variability for combining catalyst, confinement, and support; the most promising results, in terms of cycle number and capacity retention, are obtained by the nanosynergy of carbon materials and transition metal compounds, such as nitrogen-doped carbon nanocages/NbF₅, 186 few-layer

This article is licensed under a Creative Commons Attribution-NonCommercial 3.0 Unported Licence. Open Access Article. Published on 23 2025. Downloaded on 15-11-2025 3:35:14.

 Table 6
 Effect of catalysts on the hydrogen absorption and desorption kinetics of tetrahydroborates^a

	Isothe	Isothermal absor	orption		Non-isoth. des. onset/peak	Isothe	Isothermal desorption	orption		Cycles/	apacity 1	Cycles/capacity retention		$E_{ m a} ({ m des})$	
Catalyst (active form)	wt%	၁့	bar	min	J _o /J _o	wt%	၁့	bar	min	wt%	၁့	No.	%	$k_1 \text{ mol}^{-1} \text{ H}_2$	Ref.
LiBH ₄ GMF (30 wt%)	5.8	400	100	55	n.a./327	8.0	320	vac	100	8.0	p	10	54	107	185
$NC-NbF_5$ (50 wt%) (NbB_2)	6.3	300	120	96	141/311	5.9	280	vac	159	6.3	300	20	93	83	186
(CNT@C@TiO ₂) (40%) (LiTiO ₂ , TiB ₂)	6.8	400	100	300	224/318	7.3	320 320	vac	99 60	8.4	q	20	61	96	187
Fe_3O_4 (30 wt%) (FeB, Fe_2B)	6.4	450	100	40	183/n.a.	7.9	375	vac	100	6.4	c	10	20	83	188
	ı	i i	4	•		8.3	400	vac	50	,	i.	,	4	,	,
FL-GR (30 Wt%)	_	350	100	400	230/359	5.5	300	vac	400	7.1	320	10	100	116	189
(d 5d Od ; 1 d5d) (70+11 d50 O5d) d5d	-	907	007	7	100/31	7.5	350	vac	09		c	9	C L	G	007
FeF2/FeOx@ork (50 Wt%) (FeB, Li3BO3, Fe2B) Ni/C (20 wrt%) (Ni.B)	4.v	400	100	001	200/3/0	7.0	320	vac 0.01	180	γ. α 4. ο	320	10	5 C C	66	190
Ni@GR (10 + 20 wt%)	9.2	300	100	200	130/285	7.5	200	vac	009	9.2	300	100	92	106	192
	!					9.5	300	vac	175	!	I I		l I	1	
CoNi/C (40 wt%)	11.9	370	100	20	130/355	11.9	350	vac	100	9.4	р	10	82	95	193
Nb(OEt) ₅ (4 mol%) (Li ₃ BO ₃ , NbH)	6.3	350	20	09	190/340	4.5	350	vac	20	7.9	в	30	91	127	194
	7.9	200	20	20		7.0	350	vac	09		4				
Ni/GR (20 wt%)	n.a.	n.a.	n.a.	n.a.	180/275, 465	12.8	450	7	45	15.2	J	30	64	n.a.	195
NaBH ₄	,		;	1									,	į	,
GdF ₃ (25 mol%) NiCo/C (50 wt%) (Ni,B. Co.B)	3.5 5.5	400 350	40 60	069	$\frac{112}{416}$ $308/356$	n.a. 4.2	n.a. 440	n.a. vac	n.a. 60	3.5 5.5	400 400	4 13	100	1/6 37	196 197
V, Ni (V_xB_y, Ni_xB_y)	9.0	350	80	200	50/355	n.a.	n.a.	n.a.	n.a.	9.0	350	2 0	9	n.a.	198
${ m KBH_4} \ { m ZrCl_4} \left(10~{ m wt\%} ight)$	n.a.	n.a.	n.a.	n.a.	350/500	n.a.	n.a.	n.a.	n.a.	n.a.	n.a.	n.a.	n.a.	162	199
$Mg(BH_4)_2$ GR (40 wt%)	n.a.	n.a.	n.a.	n.a.	154/199	5.7	175	n.a.	80	0.6	250	9	36	29	200
						0.6	250		20						
$\mathrm{Ti}_2\mathrm{C}\left(30\ \mathrm{wt}\%\right)\left(\mathrm{Ti}\right)$	10.2	300	100	480	132/281	10.2	260	n.a.	360	10.2	260	ω ₄	32	42	181
VF4@113C2 (20 WU%) (VH2.01, 11)	7.7	6/7	90	360	90/II.a.	3 8.2	275	n.a. n.a.	300	7:7	6/7	4	co	7/7	707
$NaCl + NbF_5 (48 + 10 wt\%) (NbB_2)$	n.a.	n.a.	n.a.	n.a.	135/n.a.	5.6	200	n.a.	250	5.6	200	3	71	n.a.	202
$K_2 TiF_6$ (3 mol%) (KBH ₄ , TiH ₂)	n.a.	n.a.	n.a.	n.a.	105/n.a.	6.4	280	n.a.	200	6.4	280	2	36	n.a.	203
K_2NbF_7 (3 mol%) (KBH ₄ , TiH ₂)	n.a.	n.a.	n.a.	n.a.	118/n.a.	9.9	280	n.a.	200	9.9	280	2	41	n.a.	203
$\operatorname{Ti}\left(\operatorname{TiH}_{1.924},\operatorname{TiB},\operatorname{TiB}_{2}\right)$	n.a.	n.a.	n.a.	n.a.	n.a.	7.9	290	n.a.	2000	6.2	270	4	48	57	204
Ni/CNT (5 wt%)	n.a.	n.a.	n.a.	n.a.	93/n.a.	6.7	300	4	09	n.a.	n.a.	n.a.	n.a.	120	205
$NbVH/Ti_3C_2$ (30 wt%)	n.a.	n.a.	n.a.	n.a.	106/n.a.	9.4	230	vac	1800	0.9	250	10	20	104,125	206
						7.4	270	vac	09						
Ca(BH ₄) ₂	!	6	6		9	!	1							,	
$Ti(OEt)_4 (10 \text{ mol}\%) (TiO_2)$ $TiCl_{(24 \text{ mol}\%)} (Ti)$	4.7	320	06	1400	n.a./318	4.7	270	n.a.	400	n.a.	n.a.	n.a.	n.a.	118 n 3	207
11013 (24 1110170) (1.1)	7:/	one	λ	one	700/700	п.а.	11.4.	II.a.	п.а.	п.а.	11.ä.	11.ä.	11.4.	II.a.	700

^a RT = room temperature, GMF = wrinkled graphene microflowers, FL-GR = few-layer graphene, GR = graphene, NS = nanosheet, CNT = carbon nanotube, NC = nitrogen-doped carbon nanocages, vac = vacuum, n.a. = not available. ^b Desorption at 320 and 400 °C, respectively. ^c Desorption at 350 and 400 °C, respectively. ^c Desorption at 400 and absorption at 400 and 500 °C, respectively. ^f Dehydrogenation at 550 and 400 °C, respectively.

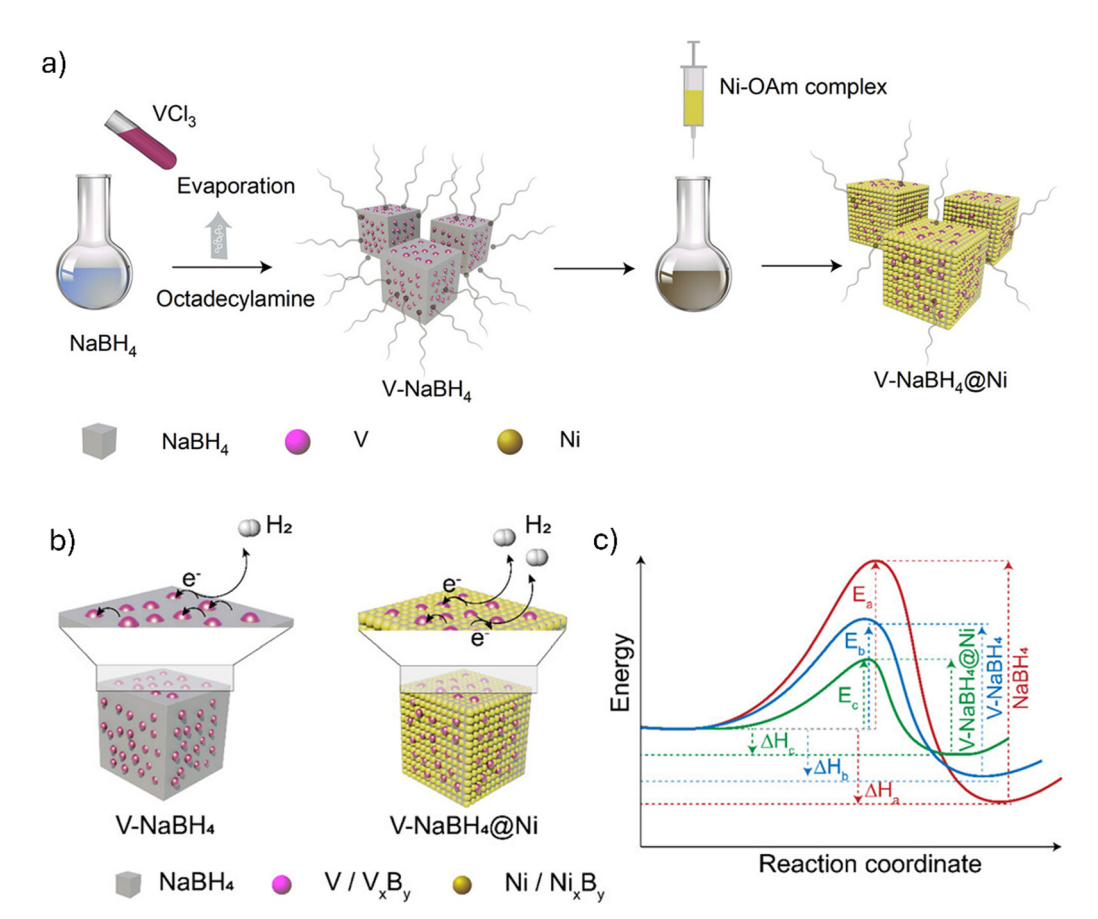


Fig. 5 (a) Illustration of the synthesis of vanadium-doped cube-like NaBH₄ with nickel shells, (b) the hydrogen release *via* the electron transfer process, and (c) the energy diagram showing altered thermodynamics and kinetics compared to pristine NaBH₄. Reproduced from ref. 198 with permission from the American Chemical Society, copyright 2023.

graphene, 189 Ni nanocrystal decorated graphene (which has been reported to have the best performance in terms of cycle number), 192 and bimetallic (NiCo) nanoporous carbon nanosheets. 197 Nanocarbon provides a platform for heat and electron transport, structural support, and interface for catalysts and $\rm BH_4^-$ ions. Transition metals and $in\ situ$ formed transition metal borides catalyse the hydrogen uptake and release.

Currently, in general, tetrahydroborates underperform compared to the Mg/MgH2 system in hydrogen storage due to factors like higher temperature and hydrogen pressure needed for recharging, slower kinetics (longer charging and discharging time) and poor hydrogen cycling stability (fewer cycles and lower capacity retention) (compare Table 5 with Table 6 and see Fig. 6 for selected data). Further improvements to establish reversible long-term cycling at lower than the current operating temperatures are necessary for practical applications. The advantages of the use of tetrahydroborates, compared to the Mg/MgH₂ system, are the higher hydrogen storage capacity per unit weight, larger additive tolerance concerning DOE targets, tunability through chemical design, and safety. Their stability in air increases as the ionic character of the salt increases, namely increasing stability from Li toward K and from Mg to Ca. 149 KBH₄ is stable in dry air and not hygroscopic. NaBH₄ is stable in dry air and can be stored in an airtight container for a

long time. It absorbs water from moist air and decomposes slowly with the liberation of hydrogen. LiBH $_4$ is extremely hygroscopic and decomposes rapidly in moist air. 149 Mg(BH $_4$) $_2$ is hygroscopic and hydrolyses in moist air. 211 Ca(BH $_4$) $_2$ is stable in dry air and slowly hydrolyses in water. An application advantage of NaBH $_4$ is that it is produced on a large scale in the industry (global production reached around 826 000 tons in 2023), 212 e.g., from NaH and B(OCH $_3$) $_3$. 149 All other tetrahydroborates can be synthesized by metathesis reaction from NaBH $_4$ (Scheme 2). 149 , $^{211-215}$

2.4. Alkali and alkali earth metal tetrahydroaluminates

Tetrahydroaluminates and tetrahydroborates are structural analogues, but tetrahydroaluminates have lower gravimetric hydrogen storage capacity due to the replacement of the light boron atom with the heavier aluminium. LiAlH₄ can tolerate a maximum 39 wt% of additive to fulfill DOE target requirements considering that all hydrogen is released from the storage material; these values are 13, 30, and 18 wt% for Na, Mg, and Ca-tetrahydroaluminates, respectively (see Tables 1 and 2). In general, tetrahydroaluminates decompose and release hydrogen at lower temperature than tetrahydroborates and the only volatile decomposition product is hydrogen, and the solid residue consists of metals and/or alloys. The last step of the multi-step hydrogen release is the decomposition of alkali or

Review **EES Catalysis**

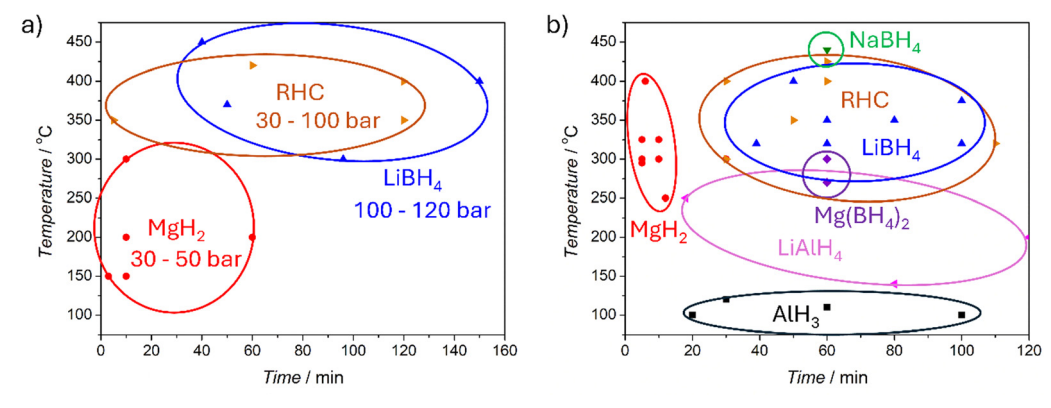
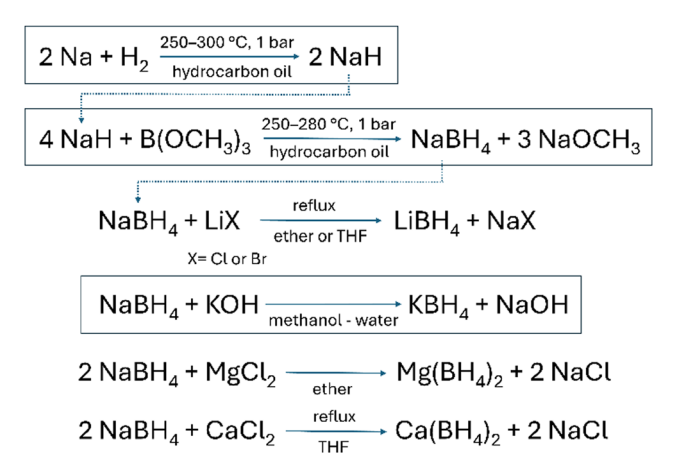


Fig. 6 Relationship between temperature and time for (a) hydrogen uptake of dehydrogenated systems, where uptake is higher than 6.0 wt% within 160 min, and (b) hydrogen release from investigated systems, where the amount of released hydrogen is above 6.5 wt% and release time is within 120 min.



Scheme 2 Synthesis of tetrahydroborates (industrial processes are indicated by boxes). 149,211-215

alkali earth binary hydrides, which is practically not accessible due to the high temperatures required. If hydrogen discharge is conducted below their decomposition temperatures, the maximum hydrogen release from Li, Na, Mg, and Ca-tetrahydroaluminates would be 8.0, 5.6, 7.0, and 5.9 wt%, respectively. This places NaAlH₄ and Ca(AlH₄)₂ on the list of unsatisfactory compounds for hydrogen storage, while LiAlH₄ and Mg(AlH₄)₂ can tolerate only 9% and 7% additive, respectively. One of the major challenges of practical application of tetrahydroaluminates in hydrogen storage is that regenerating dehydrogenated tetrahydroaluminates requires high temperatures and hydrogen pressures. 46,171,173,178 LiAlH₄, Mg(AlH₄)₂ and Ca(AlH₄)₂ are metastable and their rehydrogenation is thermodynamically not favoured.216,217 The reason for the thermodynamic instability of LiAlH₄ and Ca(AlH₄)₂ is the formation of stable intermediates, namely Li₃AlH₆ and CaAlH₅, respectively. ^{218,219} According to thermodynamic calculations, more than 1000 bar hydrogen partial pressure is required for the hydrogen absorption reaction of Li₃AlH₆ → LiAlH₄ and $CaAlH_5 \rightarrow Ca(AlH_4)_2$ above room temperature. ^{218,219} Practical reversible hydrogen storage with LiAlH4 and Ca(AlH4)2 is therefore not possible without thermodynamically stabilizing these materials (and/or destabilizing intermediates). As an attempt to

achieve this, the thermodynamic stabilization of LiAlH₄ within the nanopores of N-doped ordered mesoporous carbon by lithium coordination to nitrogen binding sites was demonstrated recently.216 The decomposition of LiAlH4 bypassed the Li3AlH6 intermediate and more than 80% of LiAlH4 could be regenerated under 1000 bar hydrogen pressure. Mg(AlH₄)₂ decomposes without the formation of a complex hydride intermediate; the first dehydrogenation step to MgH2 and Al is exothermic, which makes the reverse process infeasible.²²⁰ It appears likely that this first dehydrogenation step consists of two events, the endothermic decomposition of Mg(AlH₄)₂ and a consecutive exothermic event which could be the re-crystallization of non-crystalline MgH2. The second dehydrogenation step has a relatively low temperature of 282 °C due to the formation of the intermetallic phase Mg₂Al₃.²²⁰ Considering thermodynamic instability, LiAlH₄, Mg(AlH₄)₂ and Ca(AlH₄)₂ may be best applied as one-way hydrogen storage materials, similarly to AlH3 discussed above (Table 7). This consideration leaves NaAlH4 as the only realistic target for reversible hydrogen storage but only if full dehydrogenation/rehydrogenation can be realized (Table 8). This material has the advantage of consisting only abundant elements, namely Na and Al. To address challenges, a wide range of transition and rare earth metal compounds and carbon-based materials, including oxides, chlorides, fluorides, nitrides, and borides, have been investigated to promote lower reaction temperatures and improved kinetics for tetrahydroaluminates. 221-255 General methods are like those used for main group binary hydrides and tetrahydroborates, discussed above, namely nanoconfinement and using additives and catalysts. Catalyst precursors (see examples in Tables 7 and 8) play a critical role as in situ formed transition metals, e.g. Ti, Zn, and Ni,224,244,248 transition metal oxides, e.g. Ti₂O₃, NaFeO₂, and NiO, 233,244,251 and Al-alloys, e.g. Al_3Zr , Al_3Ti , Al_3 Al₁₃Co₄ and Al_{0.9}Ni_{4.22}, ²⁴⁷ as well as synergic multivalent Tispecies (Ti⁰, Ti³⁺)^{252,253} or Ni and Ti species (Ni, NiO, Ti, Ti₂O₃)²⁵¹ are believed to catalyse the hydrogen uptake and release. The mechanism of catalytic action involved weakening the Al-H bonds, e.g. NiTiO₃ and Ni, 251,255 enhancing hydrogen transfer by shortening the diffusion path, 244,247,254,255 e.g. Ti shell, 255 and/or

Table 7 Effect of catalysts on the hydrogen release properties of LiAlH₄, Mg(AlH₄)₂, and Ca(AlH₄)₂

Catalyst precursor	Active form ^a	Capacity ^b (wt%)	Decomp. temp. ^c onset/peak (°C)	Isothermal H_2 release wt%/ $^{\circ}$ C min $^{-1}$	$E_{\mathrm{a}}^{\ c}$ (des.) (kJ mol ⁻¹ H ₂)	Ref.
LiAlH ₄						
ZrF ₄ (10 wt%)	Al ₃ Zr, LiF	n.a.	80, 130/219, 258	5.6/100/120	60, 80	223
Ti_3C_2 (5 wt%)	Ti, Ti ³⁺	6.5	59/n.a.	4.2/150/10 5.5/200/35	80, 100	224
TiF ₃ (2 mol%)	$\mathrm{Al}_3\mathrm{Ti}$	7.3	35/108	7.0/140/80 7.3/250/18	67, 88	225
Ni _{0.6} Zn _{0.4} O (10 wt%)	NiO, Zn	5.6	124, 170/n.a.	3.1/90/120	73, 85	244
Ni-C@TiO ₂ (7 wt%)	NiAl, Al ₃ Ti, Ni ₂ Al ₃	7.2	56, 131/n.a.	6.3/200/20	59, 68	245
Co-B (5 wt%)	AlCo	7.7	n.a./135, 167	7.7/200/120	83	246
Co ₃ O ₄ @CoNi (7 wt%)	$Al_{13}Co_4$, $Al_{0.9}Ni_{4.22}$	6.9	n.a./85, 177	6.3/200/120	80, 90	247
$Mg(AlH_4)_2$						
TiCl ₃ (1 mol%)	Ti	9	60/n.a	1.5/90/150	n.a.	248
				6/150/n.a.		
No catalyst	_	9.0	125/300, 415	5.5/135/125	123	249
Ca(AlH ₄) ₂						
TiCl ₃ (1 mol%)	n.a.	n.a.	n.a./231, 295	n.a.	n.a.	242
TiF_3 (10 wt.) ^d	Ti	n.a.	n.a./116, 218	n.a.	57	243

^a Catalytically active component formed during ball milling of precursors; ss = solid solution. ^b Experimentally determined maximum storage capacity. ^c Consecutive two dehydrogenation stages, n.a. = not available. ^d Ca(AlH₄)₂·2NaCl, synthesized by ball milling NaAlH₄ and CaCl₂.

providing active sites to promote the nucleation and growth of dehydrogenation products, *e.g.* NiAl, Al₃Ti, Ni₂Al₃,²⁴⁵ and AlCo.²⁴⁶ Ti₃C₂ was found to effectively interact with tetrahydroaluminates and destabilize the Al–H bond through interfacial charge transfer.²²⁴ Nanosizing and nanoconfinement are mainly used to control the hydride particle size, and their effect is kinetic rather than thermodynamic by creating nucleation sites and shortening diffusion paths. N-doped carbon, however, was shown to alter thermodynamics by Li adatom formation and charge redistribution between the metal hydride and the host.²¹⁶ As a new strategy of research, the concept of light-driven reversible hydrogen storage was validated recently on NaAlH₄, using the catalytic effect of TiO₂ and the photothermal effect of nanolayered carbon.²⁵⁶

Handling tetrahydroaluminates requires more caution than handling tetrahydroborates due to the flammability of tetrahydroaluminates when exposed to oxygen and humidity. Tetrahydroaluminates hydrolyse in moist air and react violently with liquid water. Although they are stable and not pyrophoric in the absence of moisture under ambient conditions, they are considered highly explosive in air when finely divided. Considering the one-way hydrogen delivery of LiAlH₄, its performance is approaching that of AlH₃, although the kinetics of LiAlH₄ dehydrogenation are a little slower (compare Table 4 and Table 7 and see Fig. 6); production cost and sustainability are expected to be decisive in their application. LiAlH₄ is produced in the industry, which is not the case for AlH₃. In addition, producing AlH₃ from LiAlH₄ makes AlH₃ more expensive than

Table 8 Effect of catalysts on the hydrogen absorption and desorption kinetics of NaAlH₄^a

	Isothe	ermal	absorp	tion	Non-isoth. des. ^b onset/peak	Isothe	ermal	desorp	tion	Cycles	/capaci	ty reter	ntion	E_a^b (abs/des)	
Catalyst (active form)	wt%	$^{\circ}\mathbf{C}$	bar	min	$^{\circ}\mathrm{C}/^{\circ}\mathrm{C}$	wt%	$^{\circ}\mathbf{C}$	bar	min	wt%	$^{\circ}\mathbf{C}$	No.	%	${\rm kJ~mol}^{-1}~{\rm H}_2$	Ref.
NiFe ₂ O ₄ (3 mol%) (NaFeO ₂ , Al ₃ Ni)	3.7	150	50	30	93, 147, 316/n.a.	4.6	150	vac	60	3.5	150	5	95	—/54 , 73 , 113	233
CNT (8 mol%)	4.2	150	140	600	n.a.	3.3	160	vac	120	3.7	150	8	n.a.	n.a.	237
CeB ₆ (2 mol%)	4.9	120	120	20	n.a.	4.9	160	0.1	120	4.9	С	15	92	— /69, 99	250
NiTiO ₃ (10 wt%)	3.7	60	100	90	89/139, 173	3.3	110	0.01	120	4.6	d	5	95	12/104, 74	251
(Ni, NiO, Ti, Ti ₂ O ₃)						4.7	170	0.01	30						
C@TiO ₂ /Ti ₃ C ₂ (10 wt%)	n.a.	n.a.	n.a.	n.a.	85/120, 160	4.0	140	vac	13	5.0	200	10	93	/72, 64	252
Ti_3C_2 (7 wt%) (Ti, Ti^{3+})	4.3	80	100	180	100/140	3.2	100	vac	180	4.8	200	10	97	—/87 . 88	253
	4.6	120	100	60		4.7	140	vac	100						
$CoTiO_3$ (10 wt%)	n.a.	n.a.	n.a.	n.a.	n.a./135, 185	3.5	150	vac	30	n.a.	n.a.	n.a.	n.a.	 /86. 92	254
$(AlTi_3, Al_xCo)$															
TiCl ₃ (Ti)	4.0	180	130	75	155/180, 250	4.0	180	0.1	150	4.0	180	3	100	n.a.	255
TiO_2/C (10 wt%) ^e	4	202	80	60	n.a.	4	202	vac.	7	4	202	10	85	n.a./56	256
CeCl ₃ (2 mol%)	4	120	100	10	n.a.	3.9	180	1.3	n.a.	3.9	180	36	100	n.a.	261

^a RT = room temperature, CNT = carbon nanotube, vac = vacuum, n.a. = not available. ^b Values for the first, second and third decomposition step are separated by comma. ^c Desorption at 160 °C and absorption at 120 °C. ^d Desorption at 170 °C and absorption at 120 °C. ^e Under the light intensity of 5 and 10 sun during absorption and desorption, respectively (1 sun = 100 mW cm⁻²).

electrolysis >700 °C, 10 bar recycling 4 LiH + AlCl₃ 2 LiAlH₄ + 3 LiCl LiAlH_₄ decomposition RT, 13 bar LiAlH₄·4THF 100 - 200 °C, 100 - 200 bar NaAlH₄ $Na + Al + 2 H_2$ hvdrocarbon $2 \text{ NaAlH}_4 + \text{MCl}_2 \xrightarrow[2.) 100 \,^{\circ}\text{C, vacuum}$ M(AlH₄)₂ + 2 NaCl

Scheme 3 Synthesis of tetrahydroaluminates (industrial processes are indicated by a box. RT = room temperature). 149,217,242,258

M= Mg or Ca

LiAlH₄ (Scheme 1). Considering the economics, LiAlH₄ production can be improved by recycling the LiCl by-product as only 25% of Li is converted to LiAlH₄ (Scheme 3). 149 Although dehydrogenated LiAlH₄ cannot be re-hydrogenated in the solid phase, it can be hydrogenated in THF slurry to form an LiAlH₄· 4THF adduct ($\Delta G = -1.65 \text{ kJ mol}^{-1} \text{ LiAlH}_4$); ²⁵⁸ the latter can be

desolvated in vacuum at a low temperature of 60 °C. 258-260 Dimethyl ether can be used at sub-ambient temperature for this conversion and vents naturally with the excess hydrogen. 259,260 Detailed studies for the hydrogen delivery of magnesium and calcium tetrahydroaluminates are yet to be undertaken. NaAlH4 can reversibly deliver hydrogen in catalysed reactions (Fig. 7a, b and Table 8); however, the limited storage capacity, below the 6.5 wt% DOE target, and the cyclic instability are drawbacks for its application as a hydrogen storage material. It is worth noting that prototypes of hydrogen storage tanks using 0.087 kg,²⁶¹ 8 kg,²⁶² and 20 kg²⁵⁷ NaAlH₄ have been developed and material gravimetric capacity of 3.9 wt% (36 cycles) and 3.6 wt% (18 cycles), and system gravimetric capacity of 2 wt% (25 cycles) could be achieved, respectively. Industry, currently, is not producing NaAlH₄, Mg(AlH₄)₂ and Ca(AlH₄)₂ on a large scale; these materials can be synthesized using various laboratory techniques from elements, hydrides and aluminium halides.217 Selected frequently used methods are summarized in Scheme 3.

2.5. Reactive hydride composites

There is a vast possibility to combine metal hydrides, tetrahydroborates, and tetrahydroaluminates to create RHCs, especially as not only two but several components in various ratios could be mixed (Table 9). The concept of RHCs is that components of this system mutually destabilize each other and enhance the hydrogen desorption/adsorption kinetics, but without losing hydrogen

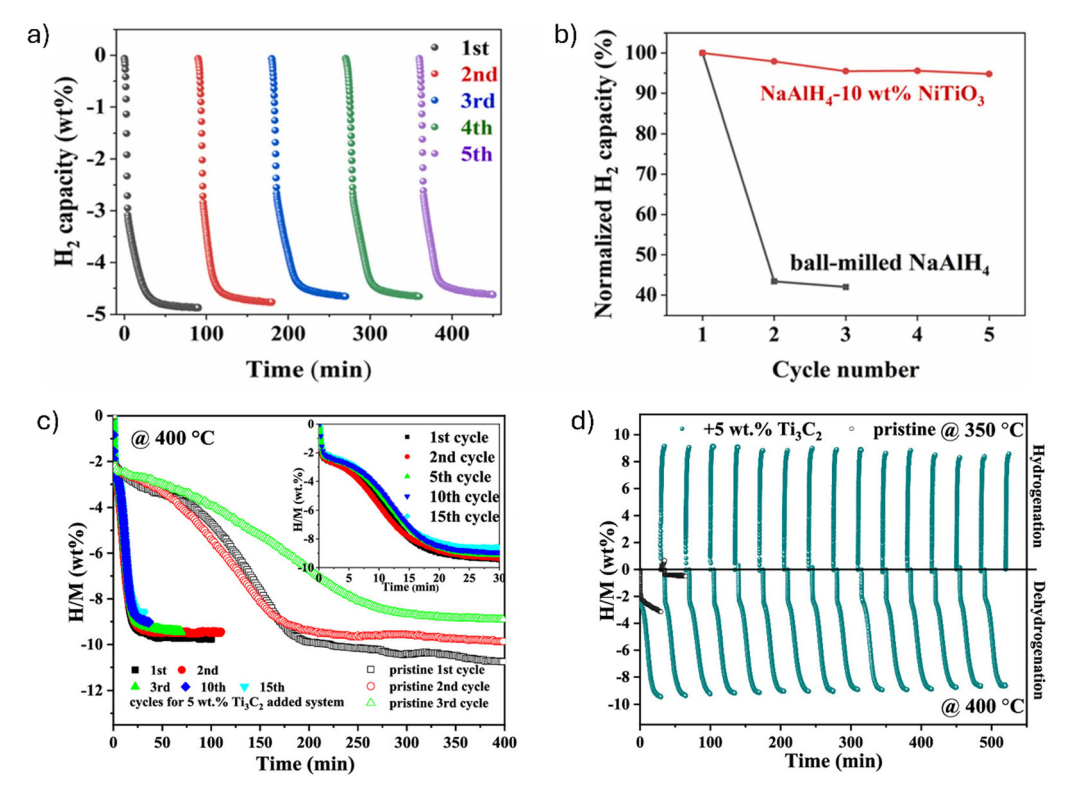


Fig. 7 (a) Isothermal dehydrogenation cyclic curves of NiTiO₃ nanorod-doped NaAlH₄ and (b) cyclic capacity retention of undoped and NiTiO₃ nanorod-doped NaAlH₄. Reproduced from ref. 251 with permission from Elsevier B. V., copyright 2023. (c) and (d) Cyclic performance of the 2LiBH₄ + MgH₂/2LiH + MgB₂ system with and without Ti₃C₂ catalysts: (c) dehydrogenation curves and (d) cyclic curves. Reproduced from ref. 280 with permission from the American Chemical Society, copyright 2019

EES Catalysis Review

storage capacity as the additive/destabilizing agent is also a hydrogen storage material. The presence of a secondary phase introduces new phase boundaries where dehydrogenation can be preferential, compared to the pristine material, may initiate metathesis reaction between components or react to form intermediate phases altering thereby the reaction path, and modify the overall thermodynamics by alloy or metal boride formation. Experiments have confirmed lower onset decomposition temperature, faster dehydrogenation/rehydrogenation rate, and improved hydrogen yield for composites of tetrahydroborates, tetrahydroaluminates and metal hydrides compared to their pristine constituents. 263-289 In addition, nano-sizing, nanoconfinement, and catalysis have further improved hydrogen storage performances.^{273–287} There are also challenges for RHC systems, such as the formation of stable intermediates, which block the reversibility of the dehydrogenation, phase separation of components during hydrogenation or rehydrogenation, or increased interdiffusion barriers, which must be prevented by using additives and catalysts. A simplified view of RHC hydrogen release considers RHC components confined in each other and consecutive decomposition steps; the first step is the decomposition of one of the components, forming fine and well dispersed reagent particles on the surface of the second component, and the second step is the dehydrogenation of the second component. The formation of alloys and borides can thermodynamically reduce the dehydrogenation enthalpy. An example is the 6LiBH₄ + Mg(AlH₄)₂ system, where Mg(AlH₄)₂ decomposes to MgH₂ and Al in the initiating step, MgH2 and Al react further to form Mg₂Al₃, and Mg₂Al₃ and Al particles enhance the subsequent dehydrogenation of LiBH₄ to form MgAlB₄, AlB₂ and LiH. ²⁷⁹ The products of this RHC decomposition, however, could be rehydrogenated only to LiBH₄ + MgH₂ + Al (due to the thermodynamic instability of Mg(AlH₄)₂ discussed above). The 2LiBH₄ + MgH₂ system, the second example, is a typical RHC system exhibiting a high storage capacity of 11.5 wt%. 284 The RHC releases hydrogen in two steps, the first is the MgH2 decomposition to Mg and H2, and the second is the reaction of Mg with LiBH₄ to produce MgB₂ and LiH. The formation of MgB₂ provides thermodynamic stabilization for the system and is essential for the reversibility of hydrogen release. There is however a very long incubation period after the first step (more than 10 hours) which is attributed to the sluggish nucleation process of MgB₂. ^{284,290} Catalysing the nucleation by VB₂ nanoparticles (having a lattice constant close to that of MgB₂) resulted in an excellent cycling performance of 9.3 wt% over 10 cycles with 100% retention, and without the nucleation period.²⁸⁴ It was observed in a similar system that the formation of MgB2 crystallites preferentially occurs on TiB2 nanoparticle surfaces, generated in situ from a 3TiCl₃·AlCl₃ additive, due to reduced elastic strain energy density compared to that of the MgB₂/Mg interface.²⁹⁰ A similar action of NbB₂, ²⁷⁵ MgNi₃B₂ and CoB²⁸¹ nanoparticles has also been confirmed, highlighting an important catalytic role of transition metal borides. In general, catalysts and additives have been confirmed to act as active "hydrogen pumps", 274 preventing aggregation of nanoparticles, 273,277 providing nucleation sites, 274,275,280-284 enhancing diffusion, 283 and destabilizing the

BH₄⁻ anion by elongating the B-H bond. 283 Nanoconfinement was found to inhibit the formation of $B_{12}H_{12}^{2-}$ clusters.²⁷³ As an example, in situ generated Ni₂B nanoparticles were found to act as bidirectional electron transfer catalysts in tetrahydroborate systems, destabilize the tetrahydroborate anion and reduce the kinetic barrier for its formation.²⁷³ VH_{2.01}, formed from V₂C, exhibited multiple roles; it enhanced H2 diffusion due to its open crystal structure, increased the hydrogen atom diffusion rate by providing pathways, and effectively weakened the B-H bonds and catalysed hydrogen release/absorption through a "hydrogen pump" effect.²⁷⁴ The effect of Ti₂C, V₂C and Ti₃CN MXenes was also found to be multiple as they prevented the aggregation of hydrides and generated active metal, e.g. Ti, 277 metal hydride, e.g. $VH_{2.01}$, 274 or metal boride, e.g. TiB_2 , 282 species. The traditional focus of catalytic tuning of hydrogenation kinetics is on transition metal cations; however, the perspective of additional anion tuning was proposed recently by highlighting the role of S²⁻ anions in Li⁺ ion migration and destabilization of B-H bonds using TiS₂, MoS₂, or ZrS₂ for catalysing the dehydrogenation/ hydrogenation of 2LiBH₄ + MgH₂.²⁸³

The concept of forming RHCs by combining two or more hydrides has been proven to work in practice and combining hydrides has significantly improved the hydrogen storage performance of these composites, compared to their pristine constituents (Fig. 7c, d and Table 9). Challenges, however, remain the same for practical applications as for their constituents, namely further reduction of the operating temperature, enhancement of the kinetics, and especially improving reversibility of the hydrogen release and cyclic stability (Fig. 6). The VB2 catalysed 2LiBH₄ + MgH₂ system exhibits currently the best performance in terms of storage capacity and capacity retention during cycling (Table 9), which is the result of combining the relatively low decomposition temperature of MgH2, the reactivity of Mg with LiBH₄, the thermodynamic stabilization by MgB₂ formation, and the catalytic activity of VB₂ nanoparticles on MgB₂ nucleation.²⁸⁴

Conclusion

Developing solid-phase hydrogen storage materials for practical applications is of high importance for boosting the hydrogen industry. Light main group metal hydrides (LiH, MgH₂, AlH₃), their tetrahydroborates (LiBH₄, NaBH₄, KBH₄, Ca(BH₄)₂ and $Mg(BH_4)_2$), and tetrahydroaluminates (LiAlH₄, NaAlH₄, Ca(AlH₄)₂ and Mg(AlH₄)₂), as well as their hydride composites have high gravimetric hydrogen storage capacities, capable of fulfilling the minimum storage capacity requirements targeted by the DOE. The practical application of these materials, however, suffers from high operating temperatures, poor reversibility, slow kinetics, and low cyclic performance. To address these issues, large efforts have been devoted to tune hydrogen storage properties and recent research has justified that enhanced hydrogen storage can be achieved by nanostructuring and nanoconfining storage materials and incorporating catalysts. It has been found that small particle size and interaction between solid particles are vital elements for these catalysed reactions to enhance hydrogen

Effect of catalysts on the hydrogen absorption and desorption kinetics of RHCs^a Table 9

4,435		Isothe	Isothermal absorption	rption		Non-isoth. Des. ^b onset/peak	Isothermal desorption	mal ion			Cycles/ca _j retention	Cycles/capacity retention			$E_{ m a}^{\ b} ({ m des})$	
$ (Mi_2B) = 6.7 400 100 360 80/280 \qquad 4.5 370 vac 30 6.7 ^c 50 94 $ $ (Mi_2B) = 6.5 420 300 100 360 80/280 \qquad 4.5 275 vac 50 7.3 300 4 42 $ $ (5.5 420 33) 6.5 420 33 60 82, 138, 484/na. 1.7 420 1 60 n.a. n.a. n.a. n.a.$ $ (5.6 44) 300 300 n.a. 1.8 484/na. 1.7 420 1 60 n.a. n.a. n.a. n.a.$ $ (5.7 420 33) 300 n.a. n.a. n.a. n.a. n.a. n.a. n.a. n.a.$ $ (5.8 44) 350 300 300 n.a. 350 40 40 40 40 40 40 $ $ (5.9 44) 350 400 5 n.a. n.a. n.a. n.a. n.a. n.a. n.a. n.a.$ $ (5.9 44) 360 60 n.a. n.a. n.a. n.a. n.a. n.a.$ $ (5.9 44) 300 60 n.a. 39/n.a. n.a. n.a. n.a. n.a. n.a.$ $ (5.9 44) 300 60 n.a. 39/n.a. n.a. n.a. n.a. n.a.$ $ (5.9 44) 300 60 n.a. 39/n.a. n.a. n.a. n.a. n.a.$ $ (5.9 44) 300 60 n.a. 39/n.a. n.a. n.a. n.a. n.a.$ $ (5.9 44) 400 100 45 400 40 40 40 40 40 $	Catalyst (active form)	wt%	o.	bar	min	D₀/D₀	wt%	${\sf D}_{\circ}$	bar	min	wt%	၁့	No.	%	$k_1 \text{ mol}^{-1} \text{ H}_2$	Ref.
$ (Na_{1}B) = b.7 400 100 120 na_{1}/23B \qquad 7.0 300 vac 30 6.7 7.3 300 4.9 9.9 $ $ (Na_{1}B) = b.7 400 100 360 80/280 \qquad 4.5 275 vac 50 7.3 300 4 4 20 $ $ (a. 1) (a. 1) $	LiBH ₄ + KBH ₄	1								(I					;
	$\mathrm{NiCp_2/C}$ (40 wt%) ($\mathrm{Ni_2B}$) $\mathrm{LiBH_1} + \mathrm{Mc(BH_1)},$	6.7	400	100	120	n.a./238	7.0	300	vac	30	6.7	٠	20	94	101	273
	V_2C (20 wt%) (VH _{2.01})	n.a.	300	100	360	80/280	4.5	275	vac	20	7.3	300	4	42	118, 125	274
hand have the control of the contro							10.1	350	vac	20						
9.6 260 300 6.5 420 33 60 82,138,484/n.a. 1.7 420 1 60 n.a. n.a. n.a. n.a. n.a. n.a. n.a. n.a	${ m Ti}_2{ m C}$ (30 wt%) (Ti)	n.a.	400	100	480	124/198	6.5	200		300	9.6	260	4	37	106, 95, 122	277
6.5 420 33 60 82,138,484/n.a. 1.7 420 1 60 n.a. n.a. n.a. n.a. n.a. n.a. n.a. n.a	KBH, + 41.jAlH,						9.6	260		300						
6.4 400 30 n.a. n.a. n.a. 11.8 400 1 200 n.a. n.a. n.a. n.a. n.a. n.a. n.a. n.	no cat.	6.5	420	33	09	82, 138, 484/n.a.	1.7	420	1	09	n.a.	n.a.	n.a.	n.a.	153	278
6.4 400 30 300 n.a. 11.8 400 1 200 n.a. n.a. n.a. n.a. 1.8 400 1 200 n.a. n.a. n.a. n.a. n.a. 1.8 400 1 200 n.a. n.a. n.a. n.a. n.a. n.a. n.a. n.	$6\text{LiBH}_4 + \text{Mg}(\text{AlH}_4)_2$															
CoB) n.a. n.a. n.a. n.a. n.a. n.a. n.a. n.a	No cat. (Mg2Al3, Al)	6.4	400	30	300	n.a.	11.8	400	7	200	n.a.	n.a.	n.a.	n.a.	n.a.	279
CoB) n.a. n.a. n.a. n.a. n.a. n.a. n.a. n.a	$2\text{LiBH}_4 + \text{MgH}_2$ Ti $C \in \{1, 1, 1, 2, 3, 3, 4, 3, 4, 4, 4, 4, 4, 4, 4, 4, 4, 4, 4, 4, 4,$	5	0 110	100	u	ç	LI C	001	-	00		р	<u>-</u>	2	7	000
CoB) n.a. n.a. n.a. n.a. n.a. n.a. n.a. 5.5 380 4 360 9.4 400 10 96 9.4 350 75 5 236/342, 404, 435 9.0 400 2 60 8.3 420 50 8.4 350 60 n.a. n.a. n.a. n.a. n.a. n.a. n.a. n.a	11302 (3 WC%) (11D2)	7.4	000	100	c	11.4.	y.5	400	4	20	9.0		CT	26	114	700
9.4 350 75 5 236/342, 404, 435 9.0 400 2 600 8.9 d 20 93 8.4 350 40 120 221/n.a. 8.7 425 4 60 9.3 420 50 91 n.a. n.a. 70 n.a. 339/n.a. n.a. n.a. n.a. 11.6 450 80 0.3 320/a.a. 125/n.a. 13.8 3.50 40 1080 8.0 9.4 400 4 10.0 9.3 400 9.0 9.0 9.0 9.0 9.0 9.0 9.0 9.0 9.0 9	NiCo@NC (10 wt%) (MgNi ₃ B ₂ , CoB)	n.a.	n.a.	n.a.	n.a.	n.a.	5.5	380	4	360	9.4	400	10	96	n.a.	281
94 350 75 5 236/342, 404, 435 9.0 400 2 660 8.9 ^d 20 93 84 350 40 120 221/n.a. 8.7 425 4 60 9.3 420 50 91 85 9.3 350 60 n.a. n.a. 339/n.a. n.a. n.a. n.a. 1 n.a. 9.1 400 10 86 9.3 420 50 91 87 425 4 60 9.3 420 50 91 80 9.3 420 50 91 910 100							9.4	400	4	270						
84 350 40 120 221/n.a. 8.7 425 4 60 9.3 420 50 91 9.3 350 60 n.a. n.a. n.a. n.a. n.a. n.a. n.a. 1 n.a. 9.1 400 10 32 n.a. n.a. 70 n.a. n.a. n.a. n.a. n.a. n.a. 1 n.a. 9.1 400 10 32 11.6 450 80 960 n.a. 11.6 450 1.7 320 1 60 n.a. n.a. n.a. n.a. n.a. n.a. n.a. n.a	$\mathrm{Ti}_{3}\mathrm{CN}\left(5\ \mathrm{wt}\%\right)\left(\mathrm{TiB}_{2}\right)$	9.4	350	75	2	236/342, 404, 435	0.6	400	2	09	8.9	р	20	93	121, 119	282
9.3 350 60 n.a. 339/n.a. n.a. 9.23 400 4 120 9.3 d 100 100 n.a. n.a. 70 n.a. 339/n.a. n.a. 1 n.a. 9.1 400 10 32 11.6 450 n.a. n.a. n.a. 11.6 450 1 240 11.6 450 10 45 3.8 320 33 180 60/n.a. 1.7 320 1 60 n.a. n.a. n.a. n.a. n.a. 3.5 420 30 60 125/n.a. 3.0 420 1 60 n.a. n.a. n.a. n.a. n.a. n.a. 7.6 350 90 1080 320/339 6.9 320 vac 110 8.1 350 10 77	$TiS_2 (10 \text{ wt}\%) (MgS, TiB_2)$	8.4	350	40	120	221/n.a.	8.7	425	4	09	9.3	420	20	91	82, 101	283
n.a. n.a. 70 n.a. 339/n.a. n.a. n.a. 1 n.a. 9.1 400 10 32 11.6 450 n.a. n.a. n.a. 1 n.a. 9.1 400 10 45 11.6 450 n.a. 1 n.a. 1 450 1 61 61 61 3.8 320 33 180 60/n.a. 1 320 1 60 n.a. n.a. n.a. n.a. n.a. 3.5 420 30 60 125/n.a. 3.0 420 1 60 n.a. n.a. n.a. n.a. 7.6 350 90 1080 320/339 6.9 320 vac 110 8.1 350 10 77	$VB_2 (10 \text{ wt}\%) Ca(BH_4)_2 + MgH_2$	9.3	350	09	n.a.	n.a.	9.23	400	4	120	9.3	р	10	100	n.a.	284
n.a. n.a. n.a. n.a. n.a. 1 n.a. 9.1 400 10 45 11.6 450 80 960 n.a. 11.6 450 1 240 11.6 450 10 61 3.8 320 33 180 60/n.a. 1.7 320 1 60 n.a. n.a. n.a. n.a. n.a. 3.5 420 30 60 125/n.a. 3.0 420 1 60 n.a. n.a. n.a. n.a. n.a. 7.6 350 90 1080 320/339 6.9 320 vac 110 8.1 350 10 77	No cat.	n.a.	n.a.	20	n.a.	339/n.a.	n.a.	n.a.	1	n.a.	9.1	400	10	32	n.a.	285
11.6 450 80 960 n.a. 11.6 450 1 240 11.6 450 1 60 10 61 3.8 320 33 180 60/n.a. 1.7 320 1 60 n.a. n.a. n.a. n.a. n.a. 3.5 420 30 60 125/n.a. 3.0 420 1 60 n.a. n.a. n.a. n.a. 7.6 350 90 1080 320/339 6.9 320 vac 110 8.1 350 10 77	NbF_5 (2 mol%)	n.a.	n.a.	20	n.a.	n.a.	n.a.	n.a.	1	n.a.	9.1	400	10	45	n.a.	285
11.6 450 80 960 n.a. 11.6 450 1 240 11.6 450 10 61 3.8 320 33 180 60/n.a. 1.7 320 1 60 n.a. n.a. n.a. n.a. n.a. 3.5 420 30 60 125/n.a. 3.0 420 1 60 n.a. n.a. n.a. n.a. 7.6 350 90 1080 320/339 6.9 320 vac 110 8.1 350 10 77	$6LiBH_4 + CaH_2$															
3.8 320 33 180 60/n.a. 1.7 320 1 60 n.a. n.a. n.a. n.a. n.a. 3.5 420 30 60 125/n.a. 3.0 420 1 60 n.a. n.a. n.a. n.a. 7.6 350 90 1080 320/339 6.9 320 vac 110 8.1 350 10 77	$TiCl_3 (1 mol\%)$	11.6	450	80	096	n.a.	11.6	450	1	240	11.6	450	10	61	n.a.	286
3.8 320 33 180 60/n.a. 1.7 320 1 60 n.a. n.a. n.a. n.a. a.a. 3.5 420 30 60 125/n.a. 3.0 420 1 60 n.a. n.a. n.a. n.a. a.a. a.a. a.a. a.a	$2 \mathrm{Li}[\mathrm{AlH}_4] + \mathrm{Mg}[\mathrm{BH}_4]_2$															
	TiF_3 (5 wt%) (MgF ₂ , LIF, TiH ₂) 2NaAlH, + Ca(BH,)	3.8	320	33	180	60/n.a.	1.7	320	1	09	n.a.	n.a.	n.a.	n.a.	80, 109, 137	287
7.6 350 90 1080 320/339 6.9 320 vac 110 8.1 350 10 77	No cat.	3.5	420	30	09	125/n.a.	3.0	420	1	09	n.a.	n.a.	n.a.	n.a.	143, 147	288
7.6 350 90 1080 320/339 6.9 320 vac 110 8.1 350 10 77	$Ca(BH_4)_2 + 2LiBH_4 + 2MgH_2$															
	No cat. $(CaMgH_{3.72})$	2.6	350	90	1080	320/339	6.9	320	vac	110	8.1	350	10	77	n.a.	289

 $[^]a$ RT = room temperature, CNT = carbon nanotube, NC = nanoporous carbon, vac = vacuum, n.a. = not available. b Values for the first, second and third decomposition step are separated by comma. c Desorption at 300 $^\circ$ and absorption at 400 $^\circ$ C. d Desorption at 400 $^\circ$ C and absorption at 350 $^\circ$ C.

This article is licensed under a Creative Commons Attribution-NonCommercial 3.0 Unported Licence

Open Access Article. Published on 23 2025. Downloaded on 15-11-2025 3:35:14.

EES Catalysis

diffusion and mass transport, and preventing particle growth is a fundamental requirement for good cyclic performances. In addition, enhancement of storage properties is largely attributed to the *in situ* formation of active metal species or metal compounds during the synthesis and operation of storage material composites, as well as to high dispersion of catalytic species. It has become clear that multicomponent catalysts outperform conventional single catalyst systems due to their ability to address several steps of the multi-step processes of hydrogen release and absorption. Recent research has also highlighted that it is crucially important to prevent the crystallite growth and agglomeration, the separation of phases of storage components, and the redistribution of catalytic species or phases during hydrogen cycling. Incorporating additives for enhancing hydrogen and heat transport is also fundamentally important. All these requirements can only be fulfilled if the synergistic effect of multiple phases introduced into storage materials in situ and by mixing with additives is utilized.

Not all hydride and tetrahydroaluminate compounds are feasible targets for reversible hydrogen storage as AlH₃, LiAlH₄, $Ca(AlH_4)_2$ and $Mg(AlH_4)_2$ are metastable and their rehydrogenation is infeasible. They may serve as one-way hydrogen source media if their alternative economical synthesis is established. Their best performers can already operate with fast hydrogen release around and below 100 °C and could serve PEM fuel cells. Currently the Mg/MgH2 system is the best performer concerning reversibility, kinetics and cyclic properties. MgH₂ can be discharged and recharged with relatively fast kinetics, but only at high temperatures of 300-400 °C and pressures of 20-80 bar, respectively. In addition, a stable cycling for at least 1500 cycles has not been achieved yet. The required pressure for recharging discharged tetrahydroborates and their composites is even higher (30-120 bar at 300-400 °C). The challenge for NaAlH₄ is the same and if only partially discharged the storage capacity is insufficient for DOE targets. Currently, none of the discussed hydrogen storage systems can fulfill the requirements of close to ambient working conditions, namely below 10 bar pressure and 100 °C. The improvement for practical application, however, has seen extensive progress and recently developed catalysed and confined systems operate at much lower temperatures and pressures, exhibit faster kinetics and much lower capacity decay during cycling than their corresponding pristine derivatives. There is still room for improvement as for example modifying template materials by doping to alter thermodynamics and anionic tuning to enhance kinetics has hardly been utilized. The novel concept of light-driven reversible hydrogen storage is validated recently on binary hydrides, tetrahydroborates and tetrahydroaluminates, and opens a new direction for the development of storage systems. There are reasons for optimism when it comes to solving storage issues and future research is expected to focus on exploiting the advantage of synergistic effects of catalysis using multiple catalysts, nanoconfinement, nanostructuring, and host material doping. Understanding the mechanism of hydrogen release/absorption is crucial for storage material design; therefore future work is expected to shift stronger toward full understanding of catalytic mechanisms by using high-resolution operando techniques. Research in this field will gradually move from storage materials

toward developing engineered storage systems for real world applications. As current research is conducted at a small scale, scaling up for practical applications is expected to present new challenges especially in material and thermal transport.

Author contributions

Conceptualization and design: M. K.; acquisition of data: M. K. and T. P.; analysis and interpretation of data: M. K., T. P., S. S. and V. P. T.; writing - original draft: M. K. and T. P.; writing review and editing: M. K., T. P., S. S. and V. P. T.; final version of the manuscript is approved by M. K., T. P., S. S. and V. P. T.

Conflicts of interest

The authors declare no conflicts of interest.

Data availability

No primary research results, software or code have been included, and no new data were generated or analysed as part of this review.

Acknowledgements

This research was funded by the Australian Renewable Energy Agency, grant number 2023/TRAC733 (PRO-1050).

References

- 1 H. Ritchie and P. Rosado, Energy Mix, 2020, updated in 2024, https://ourworldindata.org/energy-mix (accessed on 9 March 2025).
- 2 L. Pang, L. Liu, X. Zhou, M. Hafeez, S. Ullah and M. T. Sohail, How does natural resource depletion affect energy security risk? New insights from major energy-consuming countries, Energy Strat. Rev., 2024, 54, 101460, DOI: 10.1016/j.esr.2024.101460.
- 3 P. Friedlingstein, et al., Global Carbon Budget 2021, Earth Syst. Sci. Data, 2022, 14, 1917-2005, DOI: 10.5194/essd-14-1917-2022.
- 4 International Energy Agency (IEA), 2023, Global Hydrogen Review 2023, https://www.iea.org/reports/global-hydrogenreview-2023 (accessed on 9 March 2025).
- 5 Hydrogen Europe 2025. Available on-line: https://hydroge neurope.eu/ (accessed on 9 March 2025).
- 6 Road Map to a US Hydrogen Economy. Available on-line: https://static1.squarespace.com/static/53ab1feee4b0bef0179 a1563/t/5e7ca9c03c2524311f3bef36/1585228227720/Road+ map+to+a+US+hydrogen+economy+Exec+Sum+Web+Final. pdf (accessed on 9 March 2025).
- 7 T. Li, W. Liu, et al., China's Green Hydrogen New Era: A 2030 Renewable Hydrogen 100 GW Roadmap, RMI, China Hydrogen Alliance Research Institute, 2022, https://rmi.org/wpcontent/uploads/dlm_uploads/2022/09/china_green_hydro gen_new_era_renewable_hydrogen_roadmap.pdf (accessed on 21 April 2025).

8 (a) N. Hyun-woo, Gov't unveils roadmap for hydrogen-powered economy, Korea Times, 2019. Available on-line: https://www.koreatimes.co.kr/www/tech/2019/01/419_262238. html; (b) K. Yoon-seung, Korea seeks to produce 6.2 million hydrogen cars by 2040, Yonhap News Agency, 2019, Available on-line: https://en.yna.co.kr/view/AEN2019 0117001400320?section=economy/economy (accessed on 9 March 2025).

- 9 E. W. Lemmon, I. H. Bell, M. L. Huber and M. O. McLinden, Thermophysical Properties of Fluid Systems, in NIST Chemistry WebBook, NIST Standard Reference Database Number 69, ed. P. J. Linstrom and W. G. Mallard, National Institute of Standards and Technology, Gaithersburg MD, 2025, p. 20899, DOI: 10.18434/t4d303 (accessed on 5 November, 2025).
- 10 DOE Technical Targets for Onboard Hydrogen Storage for Light-Duty Vehicles. https://www.energy.gov/eere/fuelcells/doe-technical-targets-onboard-hydrogen-storage-light-duty-vehicles (accessed on 9 March 2025).
- 11 J. C. Mankins, Technology readiness assessments: A retrospective, *Acta Astronaut.*, 2009, **65**, 1216–1223, DOI: **10.1016/j.actaastro.2009.03.058**.
- 12 J. A. Gómez and D. M. F. Santos, The Status of On-Board Hydrogen Storage in Fuel Cell Electric Vehicles, *Designs*, 2023, 7, 97, DOI: 10.3390/designs7040097.
- 13 J. Li, X. Chai, Y. Gu, P. Zhang, X. Yang, Y. Wen, Z. Xu, B. Jiang, J. Wang and G. Jin, et al., Small-Scale High-Pressure Hydrogen Storage Vessels: A Review, Materials, 2024, 17, 721, DOI: 10.3390/ma17030721.
- 14 J. Fesmire, A. Swanger, J. Jacobson and W. Notardonato, Energy efficient large-scale storage of liquid hydrogen, *IOP Conf. Series: Mater. Sci. Eng.*, 2022, 1240, 012088, DOI: 10.1088/1757-899X/1240/1/012088.
- 15 T. Zhang, J. Uratani, Y. Huang, L. Xu, S. Griffiths and Y. Ding, Hydrogen liquefaction and storage: Recent progress and perspectives, *Renewable Sustainable Energy Rev.*, 2023, 176, 113204, DOI: 10.1016/j.rser.2023.113204.
- 16 M. H. Hirscher, L. Zhang and H. Oh, Nanoporous adsorbents for hydrogen storage, *Appl. Phys. A: Mater. Sci. Process.*, 2023, 129, 112, DOI: 10.1007/s00339-023-06397-4.
- 17 M. D. Allendorf, Z. Hulvey, T. Gennett, A. Ahmed, T. Autrey, J. Camp, E. S. Cho, H. Furukawa, M. Haranczyk, M. Head-Gordon, S. Jeong, A. Karkamkar, D.-J. Liu, J. R. Long, K. R. Meihaus, I. H. Nayyar, R. Nazarov, D. J. Siegel, V. Stavila, J. J. Urban, S. Prasad Veccham and B. C. Wood, An assessment of strategies for the development of solid-state adsorbents for vehicular hydrogen storage, *Energy Environ. Sci.*, 2018, 11, 2784, DOI: 10.1039/c8ee01085d.
- 18 A. R. Yuvaraj, A. Jayarama, D. Sharma, S. S. Nagarkar, S. P. Duttagupta and R. Pinto, Role of metal-organic framework in hydrogen gas storage: A critical review, *Int. J. Hydren Energy*, 2024, 59, 1434–1458, DOI: 10.1016/j.ijhydene.2024.02.060.
- 19 D. W. Kim, Y. Chen, H. Kim, N. Kim, Y. H. Lee, H. Oh, Y. G. Chung and C. S. Hong, High Hydrogen Storage in Trigonal Prismatic Monomer-Based Highly Porous Aromatic

- Frameworks, *Adv. Mater.*, 2024, **36**, 2401739, DOI: **10.1002**/adma.202401739.
- 20 J. B. von Colbe, J.-R. Ares, J. Barale, M. Baricco, C. Buckley, G. Capurso, N. Gallandat, D. M. Grant, M. N. Guzik, I. Jacob, E. H. Jensen, T. Jensen, J. Jepsen, T. Klassen, M. V. Lototskyy, K. Manickam, A. Montone, J. Puszkiel, S. Sartori, D. A. Sheppard, A. Stuart, G. Walker, C. J. Webb, H. Yang, V. Yartys, A. Züttel and M. Dornheim, Application of hydrides in hydrogen storage and compression: Achievements, outlook and perspectives, *Int. J. Hydren Energy*, 2019, 44, 7780–7808, DOI: 10.1016/j.ijhydene.2019.01.104.
- 21 M. V. Lototskyy, B. P. Tarasov and V. A. Yartys, Gas-phase applications of metal hydrides, *J. Energy Storage*, 2023, 72, 108165, DOI: 10.1016/j.est.2023.108165.
- 22 A. Bishnoi, S. Pati and P. Sharma, Architectural design of metal hydrides to improve the hydrogen storage characteristics, *J. Power Sourc.*, 2024, 608, 234609, DOI: 10.1016/ j.jpowsour.2024.234609.
- 23 A. S. Mehr, A. D. Phillips, M. P. Brandon, M. T. Pryce and J. G. Carton, Recent challenges and development of technical and technoeconomic aspects for hydrogen storage, insights at different scales; A state of art review, *Int. J. Hydren Energy*, 2024, 70, 786–815, DOI: 10.1016/j.ijhydene.2024.05.182.
- 24 M. Niermann, A. Beckendorff, M. Kaltschmitt and K. Bonhoff, Liquid Organic Hydrogen Carrier (LOHC) – Assessment based on chemical and economic properties, *Int. J. Hydren Energy*, 2019, 44, 6631–6654, DOI: 10.1016/j.ijhydene.2019.01.199.
- 25 A. Lin and G. Bagnato, Revolutionising energy storage: The Latest Breakthrough in liquid organic hydrogen carriers, *Int. J. Hydren Energy*, 2024, 63, 315–329, DOI: 10.1016/ j.ijhydene.2024.03.146.
- 26 H. Li, X. Zhang, C. Zhang, Z. Ding and X. Jin, Application and Analysis of Liquid Organic Hydrogen Carrier (LOHC) Technology in Practical Projects, *Energies*, 2024, 17, 1940, DOI: 10.3390/en17081940.
- 27 M.-J. Zhou, Y. Miao, Y. Gu and Y. Xie, Recent Advances in Reversible Liquid Organic Hydrogen Carrier Systems: From Hydrogen Carriers to Catalysts, *Adv. Mater.*, 2024, 36, 2311355, DOI: 10.1002/adma.202311355.
- 28 AHEAD. World's first international transport of hydrogen Foreign-produced hydrogen has arrived in Japan for the first time from Brunei Darussalam. 2019. Available online: https://www.ahead.or.jp/en/pdf/20191218_ahead_press.pdf (accessed on 10 March 2025).
- 29 W. Liu, C. J. Webb and E. MacA, Gray, Review of hydrogen storage in AB₃ alloys targeting stationary fuel cell applications, *Int. J. Hydren Energy*, 2016, 41, 3485–3507, DOI: 10.1016/ j.ijhydene.2015.12.054.
- 30 G. Sandrock, A panoramic overview of hydrogen storage alloys from a gas reaction point of view, *J. Alloys Compd.*, 1999, 293– 295, 877–888, DOI: 10.1016/S0925-8388(99)00384-9.
- 31 M. V. Lototskyy, I. Tolj, M. W. Davids, Y. V. Klochko, A. Parsons, D. Swanepoel, R. Ehlers, G. Louw, B. van der Westhuizen, F. Smith, B. G. Pollet, C. Sita and V. Linkov, Metal hydride hydrogen storage and supply systems for electric forklift with low-temperature proton exchange

EES Catalysis

manufacture Collection and the fact of the form

membrane fuel cell power module, *Int. J. Hydren Energy*, 2016, **41**, 13831–13842, DOI: **10.1016/j.ijhydene.2016.01.148**.

- 32 T. Sawa, T. Aoki, I. Yamamoto, S. Tsukioka, H. Yoshida, T. Hyakudome, S. Ishibashi, T. Inada, T. Kabeno, R. Sasamoto and Y. Nasuno, Performance of the fuel cell underwater vehicle URASHIMA, Acoust. Sci. Tech., 2005, 26, 249–257, DOI: 10.1250/ ast.26.249.
- 33 A. I. Bevan, A. Züttel, D. Booka and I. R. Harris, Performance of a metal hydride store on the "Ross Barlow" hydrogen powered canal boat, *Faraday Discuss.*, 2011, 151, 353–367, DOI: 10.1039/C0FD00025F.
- 34 M. Jakubowski and C. PałczyŃski, Chapter 30 Beryllium, ed. G. F. Nordberg, B. A. Fowler and M. Nordberg, *Handbook on the Toxicology of Metals*, 4th edn, Academic Press, 2015, pp. 635–653, DOI: 10.1016/B978-0-444-59453-2.00030-5.
- 35 U. Wietelmann, M. Felderhoff and P. Rittmeyer, *Hydrides*. *Ullman's Encyclopedia in Industrial Chemistry*, Wiley-VCH Verlag GmbH & Co. KGaA, Weinheim, 2016, DOI: 10.1002/14356007.a13_199.pub2.
- 36 I. Dovgaliuk, D. A. Safin, N. A. Tumanov, F. Morelle, A. Moulai, R. Cerný, Z. Lodziana, M. Devillers and Y. Filinchuk, Solid Aluminum Borohydrides for Prospective Hydrogen Storage, *ChemSusChem*, 2017, 10, 4725–4734, DOI: 10.1002/ cssc.201701629.
- 37 D. Harrison and T. Thonhauser, Suppressing diborane production during the hydrogen release of metal borohydrides: The example of alloyed Al(BH₄)₃, *Int. J. Hydren Energy*, 2016, 41, 3571–3578, DOI: 10.1016/j.ijhydene.2015.12.159.
- 38 K. Miwa, N. Ohba, S. Towata, Y. Nakamori, A. Zuttel and S. Orimo, First-principles study on thermodynamical stability of metal borohydrides: Aluminum borohydride Al(BH₄)₃, *J. Alloys Compd.*, 2007, 446–447, 310–314, DOI: 10.1016/j.jallcom.2006.11.140.
- 39 T. Eggeman, Hydrides, Kirk-Othmer Encyclopedia of Chemical Technology, John Wiley & Sons, Inc., 2001, vol. 13, 607–631, DOI: 10.1002/0471238961.0825041819211212.a01.pub2.
- 40 N. Eisenreich, A. Keßler, A. Koleczko and V. Weiser, On the kinetics of AlH3 decomposition and the subsequent Al oxidation, *Int. J. Hydren Energy*, 2014, 39, 6286–6294, DOI: 10.1016/j.ijhydene.2014.01.167.
- 41 V. N. Konoplev and V. M. Bakulina, Some properties of magnesium borohydride, *Russ. Chem. Bull.*, 1971, **20**, 136–138, DOI: **10.1007/BF00849335**.
- 42 C. Comanescu, G. Capurso and A. Maddalena, Nanoconfinement in activated mesoporous carbon of calcium borohydride for improved reversible hydrogen storage, *Nanotechnology*, 2012, 23, 385401, DOI: 10.1088/0957-4484/23/38/385401.
- 43 S.-C. Chung and H. Morioka, Thermochemistry and crystal structures of lithium, sodium and potassium alanates as determined by *ab initio* simulations, *J. Alloys Compd.*, 2004, 372, 92–96, DOI: 10.1016/j.jallcom.2003.09.130.
- 44 M. Fichtner, J. Engel, O. Fuhr, A. Glöss, O. Rubner and R. Ahlrichs, The Structure of Magnesium Alanate, *Inorg. Chem.*, 2003, 42, 7060–7066, DOI: 10.1021/ic034160y.
- 45 A. Züttel, Materials for hydrogen storage, *Materialstoday*, 2003, **6**, 24–33, DOI: **10.1016/S1369-7021(03)00922-2**.

- 46 Q. Lai, M. Paskevicius, D. A. Sheppard, C. E. Buckley, A. W. Thornton, M. R. Hill, Q. Gu, J. Mao, Z. Huang, H. K. Liu, Z. Guo, A. Banerjee, S. Chakraborty, R. Ahuja and K.-F. Aguey-Zinsou, Hydrogen Storage Materials for Mobile and Stationary Applications: Current State of the Art, *Chem-SusChem*, 2015, 8, 2789–2825, DOI: 10.1002/cssc.201500231.
- 47 Y. T. Ge, Characterisation of pressure-concentration-temperature profiles for metal hydride hydrogen storage alloys with model development, *Energy Storage*, 2024, 6, e504, DOI: 10.1002/est2.504.
- 48 J. Huot, Metal hydrides, in *Handbook of Hydrogen Storage*, ed. M. Hirscher, Wiley-VCH Verlag GmbH & Co. KGaA, Weinheim, 2010, DOI: 10.1002/9783527629800.ch4.
- 49 S. Qian and D. O. Northwood, Hysteresis in metalhydrogen systems: a critical review of the experimental observations and theoretical models, *Int. J. Hydren Energy*, 1988, 13, 25–35, DOI: 10.1016/0360-3199(88)90006-7.
- 50 B. Bogdanovic, K. Bohmhammel, B. Christ, A. Reiser, K. Schlichte, R. Vehlen and U. Wolf, Thermodynamic investigation of the magnesium-hydrogen system, *J. Alloys Compd.*, 1999, 282, 84–92, DOI: 10.1016/S0925-8388(98)00829-9.
- 51 E. M. Dematteis, D. M. Dreistadt, G. Capurso, J. Jepsen, F. Cuevas and M. Latroche, Fundamental hydrogen storage properties of TiFe-alloy with partial substitution of Fe by Ti and Mn, *J. Alloys Compd.*, 2021, 874, 159925, DOI: 10.1016/j.jallcom.2021.159925.
- 52 R. M. R. Wellen and E. L. Canedo, On the Kissinger equation and the estimate of activation energies for non-isothermal cold crystallization of PET, *Polym. Test.*, 2014, **40**, 33–38, DOI: **10.1016/j.polymertesting.2014.08.008**.
- 53 S. Vyazovkin, Kissinger Method in Kinetics of Materials: Things to Beware and Be Aware of, *Molecules*, 2020, 25, 2813, DOI: 10.3390/molecules25122813.
- 54 J. M. Criado and A. Ortega, Non-Isothermal Transformation Kinetics: Remarks on the Kissinger Method, *J. Non-Cryst. Solids*, 1986, 87, 302–311, DOI: 10.1016/S0022-3093(86)80004-7.
- 55 S. Shriniwasan, H.-Y. Tien, M. Tanniru and S. S. V. Tatiparti, On the parameters of Johnson-Mehl-Avrami-Kolmogorov equation for the hydride growth mechanisms: A case of MgH2, *J. Alloys Compd.*, 2018, 742, 1002–1005, DOI: 10.1016/ j.jallcom.2017.12.283.
- 56 Y. Pang and Q. Li, A review on kinetic models and corresponding analysis methods for hydrogen storage materials, *Int. J. Hydren Energy*, 2016, 41, 18072–18087, DOI: 10.1016/j.ijhydene.2016.08.018.
- 57 M. T. Todinov, On Some Limitations of the Johnson–Mehl–Avrami–Kolmogorov Equation, *Acta Mater.*, 2000, **48**, 4217–4224, DOI: **10.1016/S1359-6454(00)00280-9**.
- 58 M. Fanfoni and M. Tomellini, The Johnson–Mehl–Avrami– Kolmogorov model: A brief review, *Nouv Cim D*, 1998, 20, 1171–1182, DOI: 10.1007/BF03185527.
- 59 T. Huang and C. Zhou, Surface Diffusion-Controlled Jonhson-Mehl-Avrami-Kolmogorov Model for Hydrogenation of Mg-based Alloys, *J. Phys. Chem. C*, 2023, 127, 13900–13910, DOI: 10.1021/acs.jpcc.3c02650.

60 M. J. Starink, Analysis of hydrogen desorption from linear heating experiments: Accuracy of activation energy determinations, *Int. J. Hydren Energy*, 2018, 43, 6632–6641, DOI: 10.1016/j.ijhydene.2018.02.064.

- 61 H. Cheng, C. Lu, J. Liu, Y. Yan, X. Han, H. Jin, Y. Wang, Y. Liu and C. Wu, Synchrotron radiation X-ray powder diffraction techniques applied in hydrogen storage materials A review, *Progr. Nat. Sci.: Mater. Int.*, 2017, 27, 66–73, DOI: 10.1016/j.pnsc.2016.12.007.
- 62 A. Fitch, Synchrotron radiation and powder diffraction, Synchrotron radiation and powder diffraction, in *International Tables for Crystallography*, vol. H, ch. 2.2, 2019, pp. 51–65, DOI: 10.1107/97809553602060000937.
- 63 X. Zhang, Y. Sun, G. Xia and X. Yu, Light-weight solid-state hydrogen storage materials characterized by neutron scattering, *J. Alloys Compd.*, 2022, 899, 163254, DOI: 10.1016/ j.jallcom.2021.163254.
- 64 A. Ramirez-Cuesta, R. B. Xicohtencatl and Y. Cheng, Inelastic neutron scattering: A unique tool to study hydrogen in materials, *J. Mater. Res.*, 2024, 39, 727–736, DOI: 10.1557/s43578-024-01284-x.
- 65 D. K. Ross, 6 Neutron scattering studies for analysing solid-state hydrogen storage, in *Woodhead Publishing Series* in *Electronic and Optical Materials*, *Solid-State Hydrogen Storage*, ed. G. Walker, Woodhead Publishing, 2008, pp. 135–173, DOI: 10.1533/9781845694944.2.135.
- 66 M. Schmidtmann, P. Coster, P. F. Henry, V. P. Ting, M. T. Wellere and C. C. Wilson, Determining hydrogen positions in crystal engineered organic molecular complexes by joint neutron powder and single crystal X-ray diffraction, CrystEngComm, 2014, 16, 1232–1236, DOI: 10.1039/C3CE42070A.
- 67 V. P. Ting, A. J. Ramirez-Cuesta, N. Bimbo, J. E. Sharpe, A. Noguera-Diaz, V. Presser, S. Rudic and T. J. Mays, Direct Evidence for Solid-like Hydrogen in a Nanoporous Carbon Hydrogen Storage Material at Supercritical Temperatures, ACS Nano, 2015, 9, 8249–8254, DOI: 10.1021/acsnano.5b02623.
- 68 D. Yang, S. Rochat, M. Krzystyniak, A. Kulak, J. Olivier, V. P. Ting and M. Tian, Investigation of the Dynamic Behaviour of H₂ and D₂ in a Kinetic Quantum Sieving System, ACS Appl. Mater. Interfaces, 2024, 16, 12467–12478, DOI: 10.1021/acsami.3c17965.
- 69 J. Matsuda, *In situ* TEM studies on hydrogen-related issues: hydrogen storage, hydrogen embrittlement, fuel cells and electrolysis, *Microscopy*, 2024, 73, 196–207, DOI: 10.1093/jmicro/dfad060.
- 70 J. Kim, J. O. Fadonougbo, J.-H. Bae, M. K. Cho, J. Hong, Y. W. Cho, J. W. Roh, G. H. Kim, J. H. Han, Y.-S. Lee, J. Y. Cho, K. H. Lee, J.-Y. Suh and D. W. Chun, Real-Time Monitoring of the Dehydrogenation Behavior of a Mg₂FeH₆-MgH₂ Composite by *In Situ* Transmission Electron Microscopy, *Adv. Funct. Mater.*, 2022, 32, 2204147, DOI: 10.1002/adfm.202204147.
- 71 F. Wu and N. Yao, In Situ Transmission Electron Microscopy Studies in Gas/Liquid Environment. *In Microscopy and Analysis*, ed. S. G. Stanciu, InTech, 2016, DOI: 10.5772/62551.

- 72 G. L. Soloveichik, Y. Gao, J. Rijssenbeek, M. Andrus, S. Kniajanski, R. C. Bowman, Jr., S.-J. Hwang and J.-C. Zhao, Magnesium borohydride as a hydrogen storage material: Properties and dehydrogenation pathway of unsolvated Mg(BH₄)₂, *Int. J. Hydren Energy*, 2009, 34, 916–928, DOI: 10.1016/j.ijhydene.2008.11.016.
- 73 L. Wang, M. Z. Quadir and K.-F. Aguey-Zinsou, Ni coated LiH nanoparticles for reversible hydrogen Storage, *Int. J. Hydren Energy*, 2016, 41, 6376–6386, DOI: 10.1016/ j.ijhydene.2016.01.173.
- 74 Y. Yang, X. Zhang, L. Zhang, W. Zhang, H. Liu, Z. Huang, L. Yang, C. Gu, W. Sun, M. Gao, Y. Liu and H. Pan, Recent advances in catalyst-modified Mg-based hydrogen storage materials, *J. Mat. Sci. Technol.*, 2023, 163, 182–211, DOI: 10.1016/j.jmst.2023.03.063.
- 75 K.-F. Aguey-Zinsou and J.-R. Ares-Fernández, Hydrogen in magnesium: new perspectives toward functional stores, *Energy Environ. Sci.*, 2010, 3, 526–543, DOI: 10.1039/b921645f.
- 76 Z. Han, M. L. Yeboah, R. Jiang, X. Li and S. Zhou, Hybrid activation mechanism of thermal annealing for hydrogen storage of magnesium based on experimental evidence and theoretical validation, *Appl. Surf. Sci.*, 2020, 504, 144491, DOI: 10.1016/j.apsusc.2019.144491.
- 77 H. Yun, H. Wang, J. Bai, X. Wang, X. Dai, X. Hou and Y. Xu, Activation and hydrogen storage properties of Mg-based composites synthesized by catalytic mechanochemical hydrogenation strategy, *Int. J. Hydren Energy*, 2024, 50, 1025–1039, DOI: 10.1016/j.ijhydene.2023.08.311.
- 78 Y. Kang, K. Zhang and X. Lin, Surface Modifications of Magnesium-Based Materials for Hydrogen Storage and Nickel-Metal Hydride Batteries: A Review, *Coatings*, 2023, 13, 1100, DOI: 10.3390/coatings13061100.
- 79 Y. Xu, Y. Li, Q. Hou, Y. Hao and Z. Ding, Ball Milling Innovations Advance Mg-Based Hydrogen Storage Materials Towards Practical Applications, *Materials*, 2024, 17, 2510, DOI: 10.3390/ma17112510.
- 80 G. Parry and R. J. Pulham, Rate of Reaction of Hydrogen with Liquid Lithium: Comparison with Sodium and Potassium, *J. Chem. Soc., Dalton Trans.*, 1975, 1915–1917, DOI: 10.1039/DT9750001915.
- 81 L. Wang, Md. Z. Quadir and K.-F. Aguey-Zinsou, Direct and reversible hydrogen storage of lithium hydride (LiH) nanoconfined in high surface area graphite, *Int. J. Hydren Energy*, 2016, 41, 18088–18094, DOI: 10.1016/j.ijhydene.2016.07.073.
- 82 R. T. Howie, O. Narygina, C. L. Guillaume, S. Evans and E. Gregoryanz, High-pressure synthesis of lithium hydride, *Phys. Rev. B: Condens. Matter Mater. Phys.*, 2012, **86**, 064108, DOI: **10.1103/PhysRevB.86.064108**.
- 83 R. C. Muduli, Z. Chen, F. Guo, A. Jain, H. Miyaoka, T. Ichikawa and P. Kale, Enhancing the solid-state hydrogen storage properties of lithium hydride through thermodynamic tuning with porous silicon nanowires, *Energy* Adv., 2024, 3, 2212–2219, DOI: 10.1039/d4ya00389f.
- 84 J. J. Vajo, F. Mertens, C. C. Ahn, R. C. Bowman, Jr. and B. Fultz, Altering Hydrogen Storage Properties by Hydride Destabilization through Alloy Formation: LiH and

MgH₂ Destabilized with Si, J. Phys. Chem. B, 2004, 108,

EES Catalysis

- 13977–13983, DOI: 10.1021/jp040060h.
 85 R. C. Muduli, Z. Chen, K. Shinzato, F. Guo, T. Ichikawa,
 A. Jain, H. Miyaoka and P. Kale, Thermodynamic improvement of lithium hydrides for hydrogen absorption and desorption by
- 86 J. Graetz and J. J. Reilly, Thermodynamics of the α , β and γ polymorphs of AlH₃, *J. Alloys Compd.*, 2006, **424**, 262–265, DOI: **10.1016/j.jalleom.2005.11.086**.

1094-1102, DOI: 10.1016/j.ijhydene.2023.09.015.

incorporation of porous silicon, Int. J. Hydren Energy, 2024, 50,

- 87 J. Graetz and J. J. Reilly, Decomposition Kinetics of the AlH₃ Polymorphs, *J. Phys. Chem. B*, 2005, **109**, 22181–22185, DOI: **10.1021/jp0546960**.
- 88 J. F. Fernandez and C. R. Sanchez, R ate determining step in the absorption and desorption of hydrogen by magnesium, *J. Alloys Compd.*, 2002, **340**, 189–198, DOI: **10.1016**/**S0925-8388(02)00120-2**.
- 89 A. S. Pedersen, J. Kjøller, B. Larsen, B. Vigeholm and J. A. Jensen, Long-Term Cycling of the Magnesium Hydrogen System, *Int. J. Hydren Energy*, 1984, **9**, 799–802, DOI: **10.1016**/0360-3199(84)90283-0.
- 90 J. Graetz, J. J. Reilly, V. A. Yartys, J. P. Maehlen, B. M. Bulychev, V. E. Antonov, B. P. Tarasov and I. E. Gabis, Aluminum hydride as a hydrogen and energy storage material: Past, present and future, *J. Alloys Compd.*, 2011, 509S, S517–S528, DOI: 10.1016/j.jallcom.2010.11.115.
- 91 G. Sandrock, J. Reilly, J. Graetz, W.-M. Zhou, J. Johnson and J. Wegrzyn, Accelerated thermal decomposition of AlH₃ for hydrogen-fueled vehicles, *Appl. Phys. A: Mater. Sci. Process.*, 2005, **80**, 687–690, DOI: **10.1007/s00339-004-3105-0**.
- 92 S. He, G. Li, Y. Wang, L. Liu, Z. Lu, L. Xu, P. Sheng, X. Wang, H. Chen, C. Huang, Z. Lan, W. Zhou, J. Guo and H. Liu, Achieving both high hydrogen capacity and low decomposition temperature of the metastable AlH₃ by proper ball milling with TiB₂, *Int. J. Hydren Energy*, 2023, 48, 3541–3551, DOI: 10.1016/j.ijhydene.2022.10.198.
- 93 H. Liu, L. Zhang, H. Ma, C. Lu, H. Luo, X. Wang, X. Huang, Z. Lan and J. Guo, Aluminum hydride for solid-state hydrogen storage: Structure, synthesis, thermodynamics, kinetics, and regeneration, *J. Energy Chem.*, 2021, 52, 428–440, DOI: 10.1016/j.jechem.2020.02.008.
- 94 Y. Nakagawa, C.-H. Lee, K. Matsui, K. Kousaka, S. Isobe, N. Hashimoto, S. Yamaguchi, H. Miyaoka, T. Ichikawa and Y. Kojima, Doping effect of Nb species on hydrogen desorption properties of AlH₃, *J. Alloys Compd.*, 2018, 734, 55–59, DOI: 10.1016/j.jallcom.2017.10.273.
- 95 L. Liang, Q. Yang, S. Zhao, L. Wang and F. Liang, Excellent catalytic effect of LaNi₅ on hydrogen storage properties for aluminium hydride at mild temperature, *Int. J. Hydrogen Energy*, 2021, 46, 38733–38740, DOI: 10.1016/j.ijhydene.2021.09.130.
- 96 H. Liu, S. He, G. Li, Y. Wang, L. Xu, P. Sheng, X. Wang, T. Jiang, C. Huang, Z. Lan, W. Zhou and J. Guo, Directed Stabilization by Air-Milling and Catalyzed Decomposition by Layered Titanium Carbide Toward Low-Temperature and High-Capacity Hydrogen Storage of Aluminum Hydride,

- ACS Appl. Mater. Interfaces, 2022, 14, 42102–42112, DOI: 10.1021/acsami.2c11805.
- 97 Y. Yang, F. Liang, Y. Cheng, D. Yin and L. Wang, Improvement of dehydrogenation performance by adding CeO₂ to α-AlH₃, *Int. J. Hydren Energy*, 2020, **45**, 2119–2126, DOI: **10.1016/j.ijhydene.2019.11.086**.
- 98 L. Liang, C. Wang, M. Ren, S. Li, Z. Wu, L. Wang and F. Liang, Unraveling the Synergistic Catalytic Effects of TiO₂ and Pr₆O₁₁ on Superior Dehydrogenation Performances of α-AlH₃, ACS Appl. Mater. Interfaces, 2021, 13, 26998–27005, DOI: 10.1021/acsami.1c04534.
- 99 Y. Zhao, Q. Wang, D. Yin, S. Li, C. Wang, L. Liang, S. Zhao, C. Zhang, L. Wang and Y. Cheng, Superior catalytic effect of Bi@C on dehydrogenation performance of α-AlH₃, *Int. J. Hydren Energy*, 2024, 50, 1164–1173, DOI: 10.1016/j.ijhydene.2023.09.049.
- 100 Y. Zhao, Q. Wang, D. Yin, X. Wang, S. Li, C. Wang, L. Liang, S. Zhao, L. Wang and Y. Cheng, Hollow structured Fe@C nanorods for boosting dehydrogenation properties of α-AlH₃, Nano Res., 2024, 17, 8184–8191, DOI: 10.1007/s12274-024-6867-z.
- 101 Y. Shanga, C. Pistiddaa, G. Gizer, T. Klassena and M. Dornheim, Mg-based materials for hydrogen storage, J. Magn. Alloys, 2021, 9, 1837–1860, DOI: 10.1016/j.jma. 2021.06.007.
- 102 Y. Li, Y. Zhang, H. Shang, Y. Qi, P. Li and D. Zhao, Investigation on structure and hydrogen storage performance of asmilled and cast Mg₉₀Al₁₀ alloys, *Int. J. Hydren Energy*, 2018, 43, 6642–6653, DOI: 10.1016/j.ijhydene.2018.02.086.
- 103 A. Andreasen, Hydrogenation properties of Mg-Al alloys, Int. J. Hydren Energy, 2008, 33, 7489-7497, DOI: 10.1016/ j.ijhydene.2008.09.095.
- 104 T. Liu, T. Zhang, X. Zhang and X. Li, Synthesis and hydrogen storage properties of ultrafine Mg–Zn particles, *Int. J. Hydren Energy*, 2011, 36, 3515–3520, DOI: 10.1016/ j.ijhydene.2010.12.049.
- 105 M. Pęska, A. Dębski, W. Gasior, S. Dyjak, W. Gierlotka, A. Baran, D. J. Zasada and M. Polanski, Hydrogenation Behavior of Mg-Li Alloys, ACS Appl. Energy Mater., 2025, 8, 1994-2002, DOI: 10.1021/acsaem.4c02396.
- 106 A. S. Pedersen, B. Vigeholm, J. Kjøller and B. Larsen, The effect of cycling in impure hydrogen on the hydrogen capacity of magnesium powder, *Int. J. Hydren Energy*, 1987, 12, 765–771, DOI: 10.1016/0360-3199(87)90092-9.
- 107 M. Krebsz, R. Y. Hodgetts, S. Johnston, C. K. Nguyen, Y. Hora, D. R. MacFarlane and A. N. Simonov, Reduction of dinitrogen to ammonium through a magnesium-based electrochemical process at close-to-ambient temperature, *Energy Environ. Sci.*, 2024, 17, 4481, DOI: 10.1039/d4ee01090f.
- 108 M. Krebsz, S. Johnston, C. K. Nguyen, Y. Hora, B. Roy, A. N. Simonov and D. R. MacFarlane, High-Performance Magnesium Electrochemical Cycling with Hybrid Mg—Li Electrolytes, ACS Appl. Mater. Interfaces, 2022, 14, 34552–34561, DOI: 10.1021/acsami.2c04073.
- 109 L. Ouyang, F. Liu, H. Wang, J. Liu, X.-S. Yang, L. Sun and M. Zhu, Magnesium-based hydrogen storage compounds:

A review, J. Alloys Compd., 2020, 832, 154865, DOI: 10.1016/j.jallcom.2020.154865.

- 110 Y. Liu, Y. Guo, Y. Jiang, L. Feng, Y. Sun and Y. Wang, Recent progress in thermodynamic and kinetics modification of magnesium hydride hydrogen storage materials, *Mater. Rep.: Energy*, 2024, 4, 100252, DOI: 10.1016/j.matre.2024.100252.
- 111 X. Yang, W. Li, J. Zhang and Q. Hou, Hydrogen Storage Performance of Mg/MgH₂ and Its Improvement Measures: Research Progress and Trends, *Materials*, 2023, **16**, 1587, DOI: 10.3390/ma16041587.
- 112 J. Zhang, M. Liu, J. Qi, N. Lei, S. Guo, J. Li, X. Xiao and L. Ouyang, Advanced Mg-based materials for energy storage: fundamental, progresses, challenges and perspectives, *Progr. Mater. Sci.*, 2025, 148, 101381, DOI: 10.1016/ j.pmatsci.2024.101381.
- 113 Z. Ding, Y. Li, H. Yang, Y. Lu, J. Tan, J. Li, Q. Li, Y. Chen, L. L. Shaw and F. Pan, Tailoring MgH2 for hydrogen storage through nanoengineering and Catalysis, *J. Magn. Alloys*, 2022, 10, 2946–2967, DOI: 10.1016/j.jma.2022.09.028.
- 114 Y. Zhang, F. Wu, S. Guemou, H. Yu, L. Zhang and Y. Wang, Constructing Mg₂Co-Mg₂CoH₅ nano hydrogen pumps from LiCoO₂ nanosheets for boosting the hydrogen storage property of MgH₂, *Dalton Trans.*, 2022, 51, 16195, DOI: 10.1039/d2dt02090d.
- 115 M. Dai, J. A. Bolarin, G. Lei, Z. Li, T. He, H. Cao and P. Chen, Potassium hydride reduced black TiO_{2-x} for boosting the hydrogenation of magnesium at room temperature, *J. Alloys Compd.*, 2022, **897**, 162750, DOI: **10.1016**/j.jallcom.2021.162750.
- 116 L. Ren, Y. Li, Z. Li, X. Lin, C. Lu, W. Ding and J. Zou, Boosting Hydrogen Storage Performance of MgH₂ by Oxygen Vacancy-Rich H-V₂O₅ Nanosheet as an Excited H-Pump, *Nano-Micro Lett.*, 2024, **16**, 160, DOI: **10.1007**/s40820-024-01375-8.
- 117 H. Liang, Z. Xie, R. Zhao, X. Wen, F. Hong, W. Shi, H. Chen, H. Liu, W. Zhou, J. Guo and Z. Lan, Facile synthesis of nickel-vanadium bimetallic oxide and its catalytic effects on the hydrogen storage properties of magnesium hydride, *Int J. Hydrogen Energy*, 2022, 47, 32969–32980, DOI: 10.1016/j.ijhydene.2022.07.012.
- 118 L. Zhang, Z. Cai, Z. Yao, L. Ji, Z. Sun, N. Yan, B. Zhang, B. Xiao, J. Du, X. Zhu and L. Chen, A striking catalytic effect of facile synthesized ZrMn₂ nanoparticles on the de/rehydrogenation properties of MgH₂, *J. Mater. Chem. A*, 2019, 7, 5626–5634, DOI: 10.1039/C9TA00120D.
- 119 J. Lu, Y. J. Choi, Z. Z. Fang, H. Y. Sohn and E. Rönnebro, Hydrogen Storage Properties of Nanosized MgH₂-0.1TiH₂ Prepared by Ultrahigh-Energy-High-Pressure Milling, *J. Am. Chem. Soc.*, 2009, 131, 15843-15852, DOI: 10.1021/ja906340u.
- 120 L. Zhang, L. Ji, Z. Yao, N. Yan, Z. Sun, X. Yang, X. Zhu, S. Hu and L. Chen, Facile synthesized Fe nanosheets as superior active catalyst for hydrogen storage in MgH₂, *Int. J. Hydren Energy*, 2019, 44, 21955–21964, DOI: 10.1016/j.ijhydene.2019.06.065.
- 121 S. Gao, X. Wang, H. Liu, T. He, Y. Wang, S. Li and M. Yan, CNTs decorated with CoFeB as a dopant to remarkably

- improve the dehydrogenation/rehydrogenation performance and cyclic stability of MgH₂, *Int. J. Hydren Energy*, 2020, **45**, 28964–28973, DOI: **10.1016/j.ijhydene.2020.07.148**.
- 122 X. Lu, L. Zhang, H. Yu, Z. Lu, J. He, J. Zheng, F. Wu and L. Chen, Achieving superior hydrogen storage properties of MgH₂ by the effect of TiFe and carbon nanotubes, *Chem. Eng. J.*, 2021, 422, 130101, DOI: 10.1016/j.cej.2021.130101.
- 123 Z.-Y. Dai, P. Wu, L.-R. Xiao, H. Kimura, C.-X. Hou, X.-Q. Sun, S.-J. Guo, W. Du and X.-B. Xie, Non-stoichiometric Ni₃ZnC_{0.7} carbide loading on melamine sponge-derived carbon for hydrogen storage performance improvement of MgH₂, *Rare Met.*, 2025, 44, 515–530, DOI: 10.1007/s12598-024-02943-y.
- 124 K. Nie, J. Li, H. Lu, R. Zhang, Y. Chen and F. Pan, Enhanced hydrogen storage properties of MgH₂ with alkalized Nb₂CT_x MXene: The role of enlarged interlayer spacing and optimized surface, *Sep. Purif. Technol.*, 2025, 354, 129069, DOI: 10.1016/j.seppur.2024.129069.
- 125 H. Wan, S. Zhou, D. Wei, J. Qiu, Z. Ding, Y. Chen, J. Wang and F. Pan, Enhancing hydrogen storage properties of MgH₂ *via* reaction-induced construction of Ti/Co/Mn-based multiphase catalytic system, *Sep. Purif. Technol.*, 2025, 355, 129776, DOI: 10.1016/j.seppur.2024.129776.
- 126 M. S. El-Eskandarany, F. Al-Ajmi, M. Banyan and A. Al-Duweesh, Synergetic effect of reactive ball milling and cold pressing on enhancing the hydrogen storage behavior of nanocomposite MgH₂/10 wt% TiMn₂ binary system, *Int. J. Hydrogen Energy*, 2019, 44, 26428–26443, DOI: 10.1016/j.ijhydene.2019.08.093.
- 127 C. Peng, Y. Li and Q. Zhang, Amorphous mixed transition metal oxides: A novel catalyst for boosting dehydrogenation of MgH₂, *Scr. Mater.*, 2024, **248**, 116149, DOI: **10.1016**/j.scriptamat.2024.116149.
- 128 H. Liu, X. Duan, Z. Wu, H. Luo, X. Wang, C. Huang, Z. Lan, W. Zhou, J. Guo and M. Ismail, Exfoliation of compact layered Ti₂VAlC₂ MAX to open layered Ti₂VC₂ MXene towards enhancing the hydrogen storage properties of MgH₂, *Chem. Eng. J.*, 2023, 468, 143688, DOI: 10.1016/j.cej.2023.143688.
- 129 W. Sun, H. Zhang, Q. He, R. Zhang, J. Wu, Y. Wang, Y. Bu, B. Li, L. Sun, F. Xu, Y. Lu, T. Yu, Z. Yang and L. Geng, Monolithic nickel-doped molybdenum nitride improves hydrogen storage properties of MgH₂, J. Alloys Compd., 2025, 1010, 177000, DOI: 10.1016/j.jallcom.2024.177000.
- 130 Y. Chen, B. Sun, G. Zhang, S. Ni, C. Li, J. Tian, Y. Zhang and X. Li, MOF-derived Ni₃Fe/Ni/NiFe₂O₄@C for enhanced hydrogen storage performance of MgH₂, *J. Energy Chem.*, 2025, 101, 333–344, DOI: 10.1016/j.jechem.2024.09.048.
- 131 C. Peng, X. Chen and Q. Zhang, Enhancing dehydrogenation kinetics of MgH₂ through doping with the Nb₂O₅-C/Ti₃C₂T_x catalyst synthesized by fast Joule heating, *J. Alloys Compd.*, 2025, **1014**, 178709, DOI: **10.1016/j.jallcom.2025.178709**.
- 132 H. Gao, M. Song, B. Zhao, J. Liu, R. Shi, Y. Liu, X. Hu and Y. Zhu, Assisting molybdenum trioxide catalysis by engineering oxygen vacancy for enhancing hydrogen storage performance of magnesium hydride, *J. Colloid Interface Sci.*, 2025, **678**, 343–352, DOI: **10.1016/j.jcis.2024.09.056**.

EES Catalysis

133 X. Lu, X. Yang, X. Liang, J. Su, J. Kong, Y. Pan and Q. Hou, MXene Ti₃C₂@NiO catalysts for improving the kinetic performance of MgH₂ hydrogen storage, *J. Alloys Compd.*, 2025, **1010**, 177963, DOI: **10.1016/j.jallcom.2024.177963**.

- 134 L. Wang, T. Zhong, F. Wu, D. Chen, Z. Yao, L. Chen and L. Zhang, Anions intercalated two-dimension high entropy layered metal oxides for enhanced hydrogen storage in magnesium hydride, *Chem. Eng. J.*, 2025, 505, 159591, DOI: 10.1016/j.cej.2025.159591.
- 135 X. Ou, J. Li, H. Lv, L. Wang and T. Yang, Effect of nanosized nickel diselenide on hydrogen storage properties of ball-milled magnesium hydride, *Int. J. Hydrogen Energy*, 2025, **101**, 594–604, DOI: **10.1016/j.ijhydene.2024.12.465**.
- 136 H. Chu, C. Yin, Y. Xia, Y. S. Chua, S. Qiu, F. Xu and L. Sun, Highly dispersed Ni nanoparticles decorated TiO₂ microspheres for enhancing hydrogen storage properties of magnesium hydride, *J. Alloys Compd.*, 2024, 997, 174927, DOI: 10.1016/j.jallcom.2024.174927.
- 137 H. Xiao, F. Qian, X. Zhang, H. Hu, R. Tang, C. Hu, W. Zhou, X. He, Z. Pu, C. Ma, R. Wang, L. Yi and Q. Chen, Effect of Ce_{0.6}Zr_{0.4}O₂ nanocrystals on boosting hydrogen storage performance of MgH₂, *Chem. Eng. J.*, 2024, **494**, 153203, DOI: **10.1016/j.cej.2024.153203**.
- 138 S. Long, Y. Qin, H. Fu, J. Hu, H. Xue, Y. Chen and F. Pan, Hydrogen storage properties of MgH₂ modified by efficient Co₃V₂O₈ catalyst, *Sep. Purif. Technol.*, 2024, **341**, 126901, DOI: **10.1016/j.seppur.2024.126901**.
- 139 K. Nie, J. Li, H. Lu, R. Zhang, Y. Chen and F. Pan, Cubic NaNbO₃ synthesized by alkali treatment of Nb₂C MXene for enhancing the hydrogen storage of MgH₂, *Sep. Purif. Technol.*, 2025, **359**, 130839, DOI: **10.1016/j.seppur.2024.130839**.
- 140 C. Ge, P. Wu, C. Ni, B. Wang, C. Hou, X. Sun, X. Yang, W. Du and X. Xie, Effect of Al₃V alloy on the hydrogen storage properties of MgH₂, *Int. J. Hydren Energy*, 2025, **97**, 738–747, DOI: **10.1016/j.ijhydene.2024.11.417**.
- 141 Z. Lu, H. Liu, H. Luo, Z. Wu, H. Ning, Y. Fan, X. Wang, X. Huang, C. Huang, Z. Lan, W. Zhou and J. Guo, Effect of Ti_{0.9}Zr_{0.1}Mn_{1.5}V_{0.3} alloy catalyst on hydrogen storage kinetics and cycling stability of magnesium hydride, *Chem. Eng. J.*, 2024, 479, 147893, DOI: 10.1016/j.cej.2023.147893.
- 142 X. Xie, L. Xiao, H. Kimura, P. Wu, W. Du and Y. Wu, Effects of layered walnut NiS@NTA on hydrogen storage performance of MgH₂, Sep. Purif. Technol., 2025, 359, 130837, DOI: 10.1016/j.seppur.2024.130837.
- 143 Q. Yuan, C. Peng, C. Yang, Y. Li, Q. Zhang, Y. Lv, G. Liu and D. Liu, Facilitated hydrogen storage properties of MgH₂ by Ni nanoparticles anchored on Mo₂C@C nanosheets, *Int. J. Hydren Energy*, 2024, 85, 12–19, DOI: 10.1016/j.ijhydene.2024.08.292.
- 144 T. Zhong, T. Xu, L. Zhang, F. Wu, Y. Jiang and X. Yu, Designing multivalent NiMn-based layered nanosheets with high specific surface area and abundant active sites for solid-state hydrogen storage in magnesium hydride, *J. Magn. Alloys*, 2025, 13, 148–160, DOI: 10.1016/j.jma.2024.04.027.
- 145 S. N. Nyamsi, M. V. Lototskyy, V. A. Yartys, G. Capurso, M. W. Davids and S. Pasupathi, 200 NL H2 hydrogen storage tank using MgH2-TiH2-C nanocomposite as H

- storage material, *Int. J. Hydren Energy*, 2021, **46**, 19046–19059, DOI: **10.1016/j.ijhydene**.2021.03.055.
- 146 X. Zhang, S. Ju, C. Li, J. Hao, Y. Sun, X. Hu, W. Chen, J. Chen, L. He, G. Xia, F. Fang, D. Sun and X. Yu, Atomic reconstruction for realizing stable solar-driven reversible hydrogen storage of magnesium hydride, *Nat. Commun.*, 2024, 15, 2815, DOI: 10.1038/s41467-024-47077-y.
- 147 Z. Cheng, Y. Guan, H. Wen, Z. Li, K. Cui, Q. Pei, S. Wang, C. Pistidda, J. Guo, H. Cao and P. Chen, Light-Driven De/Rehydrogenation of a LiH Surface under Ambient Conditions, *J. Phys. Chem. Lett.*, 2024, 15, 6662–6667, DOI: 10.1021/acs.jpclett.4c00874.
- 148 J. P. Weiler, Meridian Lightweight Technologies, Inc., Global Magnesium Market: Supply, Demand, and Future Outlook. Available online (assessed on 5 July 2025): https://www. lightmetalage.com/news/industry-news/magnesium/global-magnesium-market-supply-demand-and-future-outlook/.
- 149 U. Wietelmann, M. Felderhoff and P. Rittmeyer, *Hydrides. In Ullmann's Encyclopedia of Industrial Chemistry*, Wiley-VCH, 2016, DOI: 10.1002/14356007.a13 199.pub2.
- 150 H. Uesugi, T. Sugiyama, H. Nii, T. Ito and I. Nakatsugawa, Industrial production of MgH₂ and its application, *J. Alloys Compd.*, 2011, 509S, S650–S653, DOI: 10.1016/j.jallcom. 2010.11.047.
- 151 P. Yao, H. Zhao, M. Zhang, C. Xia, T. Yang and Q. Li, Synthesis of α-AlH3 by organic liquid reduction method and its hydrogen desorption performance, *Int. J. Hydrogen Energy*, 2023, **48**, 34132–34140, DOI: **10.1016/j.ijhydene.2023.05.170**.
- 152 M. J. Krause, F. Orlandi, A. T. Saurage and J. R. Zietz Jr., Aluminum Compounds, Organic. *In Ullmann's Encyclope-dia of Industrial Chemistry*, Wiley-VCH, 2020, DOI: 10.1002/14356007.a01 543.
- 153 L. Wang, A. Rawal, M. Z. Quadir and K.-F. Aguey-Zinsou, Formation of aluminium hydride (AlH₃) *via* the decomposition of organoaluminium and hydrogen storage properties, *Int. J. Hydren Energy*, 2018, **43**, 16749–16757, DOI: **10.1016/j.ijhydene.2017.12.052**.
- 154 P. Mauron, F. Buchter, O. Friedrichs, A. Remhof, M. Bielmann, C. N. Zwicky and A. Züttel, Stability and Reversibility of LiBH₄, *J. Phys. Chem. B*, 2008, 112, 906–910, DOI: 10.1021/jp077572r.
- 155 A. Züttel, P. Wenger, S. Rentsch, P. Sudan, P. Mauron and C. Emmenegger, LiBH₄ a new hydrogen storage material, *J. Power Sources*, 2003, 118, 1–7, DOI: 10.1016/S0378-7753(03)00054-5.
- 156 A. Züttel, A. Borgschulte and S. Orimo, Tetrahydroborates as new hydrogen storage materials, *Scripta Mater.*, 2007, 56, 823–828, DOI: 10.1016/j.scriptamat.2007.01.010.
- 157 P. Martelli, R. Caputo, A. Remhof, P. Mauron, A. Borgschulte and A. Züttel, Stability and Decomposition of NaBH₄, *J. Phys. Chem. C*, 2010, 114, 7173–7177, DOI: 10.1021/jp909341z.
- 158 S. Kumar, A. Jain, H. Miyaoka, T. Ichikawa and Y. Kojima, Study on the thermal decomposition of NaBH₄ catalyzed by ZrCl₄, *Int. J. Hydren Energy*, 2017, 42, 22432–22437, DOI: 10.1016/j.ijhydene.2017.02.060.
- 159 S. Kumar, Y. Kojima and G. Kumar Dey, Synergic effect of ZrCl₄ on thermal dehydrogenation kinetics of KBH₄,

- *J. Alloys Compd.*, 2017, **718**, 134–138, DOI: **10.1016**/i.iallcom.2017.05.118.
- 160 I. Saldan, Decomposition and formation of magnesium borohydride, *Int. J. Hydren Energy*, 2016, **41**, 11201–11224, DOI: **10.1016/j.ijhydene.2016.05.062**.
- 161 R. J. Newhouse, V. Stavila, S.-J. Hwang, L. E. Klebanoff and J. Z. Zhang, Reversibility and Improved Hydrogen Release of Magnesium Borohydride, *J. Phys. Chem. C*, 2010, 114, 5224–5232, DOI: 10.1021/jp9116744.
- 162 H.-W. Li, K. Kikuchi, Y. Nakamori, N. Ohba, K. Miwa, S. Towata and S. Orimo, Dehydriding and rehydriding processes of well-crystallized Mg(BH₄)₂ accompanying with formation of intermediate compounds, *Acta Mater.*, 2008, 56, 1342–1347, DOI: 10.1016/j.actamat.2007.11.023.
- 163 Y. Yan, D. Rentsch and A. Remhof, Controllable decomposition of Ca(BH₄)₂ for reversible hydrogen storage, *Phys. Chem. Chem. Phys.*, 2017, 19, 7788–7792, DOI: 10.1039/c7cp00448f.
- 164 C. J. Sahle, C. Sternemann, C. Giacobbe, Y. Yan, C. Weis, M. Harder, Y. Forov, G. Spiekermann, M. Tolan, M. Krischa and A. Remhof, Formation of CaB₆ in the thermal decomposition of the hydrogen storage material Ca(BH₄)₂, *Phys. Chem. Chem. Phys.*, 2016, **18**, 19866–19872, DOI: **10.1039/c6cp02495e**.
- 165 E. Rönnebro and E. H. Majzoub, Calcium Borohydride for Hydrogen Storage: Catalysis and Reversibility, *J. Phys. Chem. B*, 2007, **111**, 12045–12047, DOI: **10.1021/jp0764541**.
- 166 Y. Kim, D. Reed, Y.-S. Lee, J. Y. Lee, J.-H. Shim, D. Book and Y. W. Cho, Identification of the Dehydrogenated Product of Ca(BH₄)₂, *J. Phys. Chem. C*, 2009, 113, 5865–5871, DOI: 10.1021/jp8094038.
- 167 X. Yang, J. Su, X. Lu, J. Kong, D. Huo, Y. Pan and W. Li, Application and development of LiBH₄ hydrogen storage materials, *J. Alloys Compd.*, 2024, 1001, 175174, DOI: 10.1016/j.jallcom.2024.175174.
- 168 Y. Xu, Y. Zhou, Y. Li, M. Ashuri and Z. Ding, Engineering LiBH₄-Based Materials for Advanced Hydrogen Storage: A Critical Review of Catalysis, Nanoconfinement, and Composite Design, *Molecules*, 2024, 29, 5774, DOI: 10.3390/ molecules29235774.
- 169 S. Wang, Z. Li, M. Gao, Y. Liu and H. Pan, Low-temperature and reversible hydrogen storage advances of light metal borohydrides, *Renewable Sustainable Energy Rev.*, 2025, 208, 115000, DOI: 10.1016/j.rser.2024.115000.
- 170 X. Yang, J. Kong, X. Lu, J. Su, Q. Hou and W. Li, Hydrogen storage properties of metal borohydrides and their improvements: Research progress and trends, *Int. J. Hydren Energy*, 2024, **60**, 308–323, DOI: **10.1016/j.ijhydene.2024.02.097**.
- 171 E. M. Dematteis, M. B. Amdisen, T. Autrey, J. Barale, M. E. Bowden, C. E. Buckley, Y. W. Cho, S. Deledda, M. Dornheim, P. de Jongh, J. B. Grinderslev, G. Gizer, V. Gulino, B. C. Hauback, M. Heere, T. W. Heo, T. D. Humphries, T. R. Jensen, S. Y. Kang, Y.-S. Lee, H.-W. Li, S. Li, K. T. Møller, P. Ngene, S. Orimo, M. Paskevicius, M. Polanski, S. Takagi, L. Wan, B. C. Wood, M. Hirscher and M. Baricco, Hydrogen storage in complex hydrides: past activities and new trends, *Prog. Energy*, 2022, 4, 032009, DOI: 10.1088/2516-1083/ac7499.

- 172 S. Wang, Z. Li, M. Gao, Y. Liu and H. Pan, Low-temperature and reversible hydrogen storage advances of light metal borohydrides, *Renewable Sustainable Energy Rev.*, 2025, 208, 115000, DOI: 10.1016/j.rser.2024.115000.
- 173 A. Jain, S. Agarwal and T. Ichikawa, Catalytic Tuning of Sorption Kinetics of Lightweight Hydrides: A Review of the Materials and Mechanism, *Catalysts*, 2018, **8**, 651, DOI: **10**.3390/catal8120651.
- 174 C. J. Tomasso, A. L. Pham, T. M. Mattox and J. J. Urban, Using Additives to Control the Decomposition Temperature of Sodium Borohydride, *J. Energy Power Technol.*, 2020, 2, 009, DOI: 10.21926/jept.2002009.
- 175 T. D. Humphries, G. N. Kalantzopoulos, I. Llamas-Jansa, J. E. Olsen and B. C. Hauback, Reversible Hydrogenation Studies of NaBH₄ Milled with Ni-Containing Additives, *J. Phys. Chem. C*, 2013, 117, 6060–6065, DOI: 10.1021/jp312105w.
- 176 J. Mao and D. H. Gregory, Recent Advances in the Use of Sodium Borohydride as a Solid State Hydrogen Store, *Energies*, 2015, **8**, 430–453, DOI: 10.3390/en8010430.
- 177 C. Comanescu, Calcium Borohydride Ca(BH₄)₂: Fundamentals, Prediction and Probing for High-Capacity Energy Storage Applications, Organic Synthesis and Catalysis, *Energies*, 2023, **16**, 4536, DOI: **10.3390/en16114536**.
- 178 A. Schneemann, J. L. White, S. Y. Kang, S. Jeong, L. F. Wan, E. S. Cho, T. W. Heo, D. Prendergast, J. J. Urban, B. C. Wood, M. D. Allendorf and V. Stavila, Nanostructured Metal Hydrides for Hydrogen Storage, *Chem. Rev.*, 2018, 118, 10775–10839, DOI: 10.1021/acs.chemrev.8b00313.
- 179 X. Yang, J. Su, X. Lu, J. Kong, D. Huo, Y. Pan and W. Li, Application and development of LiBH₄ hydrogen storage materials, *J. Alloys Compd.*, 2024, 1001, 175174, DOI: 10.1016/j.jallcom.2024.175174.
- 180 M. A. Wahab, I. Urooj, M. Sohail, M. R. Karim, I. A. Alnaser, A. Abdala and R. Haque, Advancing Catalysts by Nanoconfinement and Catalysis for Enhanced Hydrogen Production from Magnesium Borohydride: A Review, *Chem. – Asian J.*, 2024, 19, e202400174, DOI: 10.1002/asia.202400174.
- 181 Y. Lv, Y. Jing, B. Zhang, Y. Li, G. Xia, X. Yu, P. Huang, H. Huang, B. Liu, J. Yuan and Y. Wu, 2D transition metal carbides trigger enhanced dehydrogenation and reversibility properties in Mg(BH₄)₂, *Chem. Eng. J.*, 2023, 478, 147387, DOI: 10.1016/j.cej.2023.147387.
- 182 I. L. Jansa, G. N. Kalantzopoulos, K. Nordholm and B. C. Hauback, Destabilization of NaBH₄ by Transition Metal Fluorides, *Molecules*, 2020, 25, 780, DOI: 10.3390/molecules25040780.
- 183 A. Nale, F. Pendolino, A. Maddalena and P. Colombo, Enhanced hydrogen release of metal borohydrides M(BH₄)n (M = Li, Na, Mg, Ca) mixed with reduced graphene oxide, *Int. J. Hydrogen Energy*, 2016, 41, 11225–11231, DOI: 10.1016/j.ijhydene.2016.04.191.
- 184 M. Au and A. Jurgensen, Modified Lithium Borohydrides for Reversible Hydrogen Storage, *J. Phys. Chem. B*, 2006, **110**, 7062–7067, DOI: **10.1021/jp056240o**.
- 185 Z. Li, K. Xian, H. Chen, M. Gao, S. Qu, M. Wu, Y. Yang, W. Sun, C. Gao, Y. Liu, X. Zhang and H. Pan, Enhanced

EES Catalysis

reversible hydrogen storage properties of wrinkled graphene microflowers confined LiBH₄ system with high volumetric hydrogen storage capacity, *Mater. Rep.: Energy*, 2024, 4, 100249, DOI: 10.1016/j.matre.2024.100249.

- 186 Y. Jia, P. Zhou, X. Xiao, X. Wang, B. Han, J. Wang, F. Xu, L. Sun and L. Chen, Synergetic action of 0D/2D/3D N-doped carbon nanocages and NbB₂ nanocatalyst on reversible hydrogen storage performance of lithium borohydride, *Chem. Eng. J.*, 2024, 485, 150090, DOI: 10.1016/j.cej.2024.150090.
- 187 K. Xian, B. Nie, Z. Li, M. Gao, Z. Li, C. Shang, Y. Liu, Z. Guo and H. Pan, TiO₂ decorated porous carbonaceous network structures offer confinement, catalysis and thermal conductivity for effective hydrogen storage of LiBH₄, Chem. Eng. J., 2021, 407, 127156, DOI: 10.1016/j.cej.2020.127156.
- 188 S. Wang, M. H. Wu, Y. Y. Zhu, Z. L. Li, Y. X. Yang, Y. Z. Li, H. F. Liu and M. X. Gao, Reactive destabilization and bidirectional catalyzation for reversible hydrogen storage of LiBH₄ by novel waxberry-like nano-additive assembled from ultrafine Fe₃O₄ particles, *J. Mater. Sci. Technol.*, 2024, 173, 63–71, DOI: 10.1016/j.jmst.2023.07.020.
- 189 W. Zhang, L. Zhou, X. Zhang, L. Zhang, Z. Lou, B. Guo, Z. Hong, M. Gao, W. Sun, Y. Liu and H. Pan, From nanorods to nanoparticles: Morphological engineering enables remarkable hydrogen storage by lithium borohydride, *Nano Energy*, 2024, 130, 110128, DOI: 10.1016/j.nanoen.2024.110128.
- 190 G. Na, W.-G. Cui, H. Shi, Z. Li, F. Gao, X. Wang, K. Wang, Y. Gao, Y. Yang, Z. Shen, Y. Liu, J. Miao and H. Pan, *In Situ* Generation and Stabilization of Multiple Catalysts by Introducing a Graphene-Supported FeF₂/FeO_X Additive for Enhancing the Hydrogen Storage of LiBH₄, *ACS Appl. Energy Mater.*, 2025, 8, 3802–3811, DOI: 10.1021/acsaem.4c02891.
- 191 Y. Liu, W. Chen, S. Ju, X. Yu and G. Xia, Stable hydrogen storage of lithium borohydrides *via* the catalytic effect of Ni₂B induced by thermodynamic destabilization reaction, *J. Mat. Sci. Technol.*, 2024, 202, 192–200, DOI: 10.1016/j.jmst.2024.03.035.
- 192 X. Zhang, L. Zhang, W. Zhang, Z. Ren, Z. Huang, J. Hu, M. Gao, H. Pan and Y. Liu, Nano-synergy enables highly reversible storage of 9.2 wt% hydrogen at mild conditions with lithium borohydride, *Nano Energy*, 2021, 83, 105839, DOI: 10.1016/j.nanoen.2021.105839.
- 193 Y. Ding, C. Li, X. Zhang, W. Chen, X. Yu and G. Xia, Spatial Confinement of Lithium Borohydride in Bimetallic ConiDoped Hollow Carbon Frameworks for Stable Hydrogen Storage, *ACS Appl. Mater. Interfaces*, 2024, **16**, 50717–50725, DOI: **10.1021/acsami.4c09512**.
- 194 Z. Li, M. Gao, J. Gu, K. Xian, Z. Yao, C. Shang, Y. Liu, Z. Guo and H. Pan, *In Situ* Introduction of Li₃BO₃ and NbH Leads to Superior Cyclic Stability and Kinetics of a LiBH₄-Based Hydrogen Storage System, *ACS Appl. Mater. Interfaces*, 2020, 12, 893–903, DOI: 10.1021/acsami.9b19287.
- 195 J. Xu, Y. Li, J. Cao, R. Meng, W. Wang and Z. Chen, Preparation of graphene-supported highly dispersed nickel nanoparticles for the improved generation of hydrogen

- from ball-milled LiBH₄, *Catal. Sci. Technol.*, 2015, 5, 1821–1828, DOI: 10.1039/C4CY01276C.
- 196 L. Chong, J. Zou, X. Zengab and W. Ding, Effects of LnF3 on reversible and cyclic hydrogen sorption behaviors in NaBH₄: electronic nature of Ln versus crystallographic factors, *J. Mater. Chem. A*, 2015, 3, 4493–4500, DOI: 10.1039/c4ta06556e.
- 197 W. Chen, S. Ju, Y. Sun, T. Zhang, J. Wang, J. Ye, G. Xia and X. Yu, Thermodynamically favored stable hydrogen storage reversibility of NaBH₄ inside of bimetallic nanoporous carbon nanosheets, *J. Mater. Chem. A*, 2022, 10, 7122–7129, DOI: 10.1039/d1ta10361j.
- 198 M. S. Salman, M. Zubair, Y. Yang, N. M. Bedford and K.-F. Aguey-Zinsou, Doping and Structure-Promoted Destabilization of NaBH₄ Nanocubes for Hydrogen Storage, ACS Appl. Nano Mater., 2023, 6, 4178–4189, DOI: 10.1021/acsanm.2c05209.
- 199 S. Kumar, Y. Kojima and G. K. Dey, Synergic effect of ZrCl₄ on thermal dehydrogenation kinetics of KBH₄, *J. Alloys Compd.*, 2017, 718, 134–138, DOI: 10.1016/j.jallcom.2017.05.118.
- 200 H. Zhang, G. Xia, J. Zhang, D. Sun, Z. Guo and X. Yu, Graphene-Tailored Thermodynamics and Kinetics to Fabricate Metal Borohydride Nanoparticles with High Purity and Enhanced Reversibility, *Adv. Energy Mater.*, 2018, 8, 1702975, DOI: 10.1002/aenm.201702975.
- 201 Z. Zhang, D. Gao, J. Zheng, A. Xia, Q. Zhang, L. Wang and L. Zhang, Heterostructured VF₄@Ti₃C₂ catalyst improving reversible hydrogen storage properties of Mg(BH₄)₂, *Chem. Eng. J.*, 2023, 460, 141690, DOI: 10.1016/j.cej.2023.141690.
- 202 X. Wang, X. Xiao, J. Zheng, X. Huang, M. Chen and L. Chen, *In-situ* synthesis of amorphous Mg(BH₄)₂ and chloride composite modified by NbF₅ for superior reversible hydrogen storage properties, *Int. J. Hydren Energy*, 2020, 45, 2044–2053, DOI: 10.1016/j.ijhydene.2019.11.023.
- 203 J. Zheng, X. Wang, X. Xiao, H. Cheng, L. Zhang and L. Chen, Improved reversible dehydrogenation properties of Mg(BH₄)₂ catalyzed by dual-cation transition metal fluorides K₂TiF₆ and K₂NbF₇, *Chem. Eng. J.*, 2021, 412, 128738, DOI: 10.1016/j.cej.2021.128738.
- 204 X. Wang, X. Xiao, J. Zheng, Z. Hang, W. Lin, Z. Yao, M. Zhang and L. Chen, The dehydrogenation kinetics and reversibility improvements of Mg(BH₄)₂ doped with Ti nanoparticles under mild conditions, *Int. J. Hydren Energy*, 2021, 46, 23737–23747, DOI: 10.1016/j.ijhydene.2021.04.149.
- 205 J. Yuan, H. Huang, Z. Jiang, Y. Lv, B. Liu, B. Zhang, Y. Yan and Y. Wu, Ni-Doped Carbon Nanotube-Mg(BH₄)₂ Composites for Hydrogen Storage, ACS Appl. Nano Mater., 2021, 4, 1604–1612, DOI: 10.1021/acsanm.0c02738.
- 206 A. Xia, J. Zheng, Q. Zhang, M. Lv, Z. Ma and C. Su, Mxene-supported NbVH nanoparticles as efficient catalysts for reversible hydrogen storage in magnesium borohydride, *Chem. Eng. J.*, 2024, 496, 154381, DOI: 10.1016/j.cej.2024.154381.
- 207 J. Gu, M. Gao, H. Pan, Y. Liu, B. Li, Y. Yang, C. Liang, H. Fua and Z. Guo, Improved hydrogen storage performance of Ca(BH₄)₂: a synergetic effect of porous morphology and *in situ* formed TiO₂, *Energy Environ. Sci.*, 2013, 6, 847–858, DOI: 10.1039/C2EE24121H.

208 Q. Lai, C. Milanese and K.-F. Aguey-Zinsou, Stabilization of Nanosized Borohydrides for Hydrogen Storage: Suppressing the Melting with TiCl₃ Doping, ACS Appl. Energy Mater., 2018, 1, 421-430, DOI: 10.1021/acsaem.7b00082.

- 209 L. Feng, Y. Liu, Y. Jiang, Y. Guo, Y. Sun and Y. Wang, Lightdriven rapid dehydrogenation of LiBH₄-TiF₃-TiO₂ hydrogen storage composite, J. Alloys Compd., 2025, 1010, 176848, DOI: 10.1016/j.jallcom.2024.176848.
- 210 X. Zhang, C. Li, J. Ye, X. Hu, W. Chen, F. Fang, D. Sun, Y. Liu, X. Yu and G. Xia, Light-Enabled Reversible Hydrogen Storage of Borohydrides Activated by Photogenerated Vacancies, J. Am. Chem. Soc., 2025, 147, 2786-2796, DOI: 10.1021/jacs.4c15744.
- 211 V. N. Konoplev and V. M. Bakulina, Some properties of magnesium borohydride, Russ. Chem. Bull., 1971, 20, 136-138, DOI: 10.1007/BF00849335.
- 212 Global Sodium Borohydride Market to Hit Sales of USD 2606 Million by 2032, at 5.89% CAGR Growth: Astute Analytica. https://www.globenewswire.com/news-release/2024/03/25/ 2851764/0/en/Global-Sodium-Borohydride-Market-to-Hit-Sales-of-USD-2-606-Million-by-2032-at-5-89-CAGR-Growth-Astute-Analytica.html (accessed on 5 July 2025).
- 213 H. Hagemann and R. Cerny, Synthetic approaches to inorganic borohydrides, Dalton Trans., 2010, 39, 6006-6012, DOI: 10.1039/b927002g.
- 214 H. C. Brown, Y. M. Choi and S. Narasimhan, Convenient procedure for the conversion of sodium borohydride into lithium borohydride in simple ether solvents, *Inorg. Chem.*, 1981, 20(12), 4454-4456, DOI: 10.1021/ic50226a091.
- 215 K. Chłopek, C. Frommen, A. Leon, O. Zabara and M. Fichtner, Synthesis and properties of magnesium tetrahydroborate, Mg(BH₄)₂, J. Mater. Chem., 2007, 17, 3496-3503, DOI: 10.1039/b702723k.
- 216 Y. J. Cho, S. Li, J. L. Snider, M. A. T. Marple, N. A. Strange, J. D. Sugar, F. El Gabaly, A. Schneemann, S. Kang, M. Kang, H. Park, J. Park, L. F. Wan, H. E. Mason, M. D. Allendorf, B. C. Wood, E. S. Cho and V. Stavila, Reversing the Irreversible: Thermodynamic Stabilization of LiAlH₄ Nanoconfined Within a Nitrogen-Doped Carbon Host, ACS Nano, 2021, 15, 10163-10174, DOI: 10.1021/acsnano.1c02079.
- 217 I. P. Jain, P. Jain and A. Jain, Novel hydrogen storage materials: A review of lightweight complex hydrides, J. Alloys Compd., 2010, 503, 303-339, DOI: 10.1016/j.jallcom.2010.04.250.
- 218 J.-W. Jang, J.-H. Shim, Y. W. Cho and B.-J. Lee, Thermodynamic calculation of LiH \leftrightarrow Li₃AlH₆ \leftrightarrow LiAlH₄ reactions, J. Alloys Compd., 2006, 420, 286-290, DOI: 10.1016/ j.jallcom.2005.10.040.
- 219 F. Habermann, A. Wirth, K. Burkmann, J. Kraus, B. Störr, H. Stöcker, J. Seidel, J. Kortus, R. Gumeniuk, K. Bohmhammel and F. Mertens, Thermodynamic and kinetic study of the effect of LiCl and NaCl on the thermal dehydrogenation of $Ca(AlH_4)_2$, RSC Mechanochem., 2025, 2, 603-615, DOI: 10.1039/D4mr00140k.
- 220 F. Habermann, A. Wirth, K. Burkmann, B. Störr, J. Seidel, R. Gumeniuk, K. Bohmhammel and F. Mertens, Heat Capacity Function, Enthalpy of Formation and Absolute

- Entropy of Mg(AlH₄)₂, ChemPhysChem, 2024, 25, e202300748, DOI: 10.1002/cphc.202300748.
- 221 Rafi-ud-din, L. Zhang, L. Ping and Q. Xuanhui, Catalytic effects of nano-sized TiC additions on the hydrogen storage properties of LiAlH₄, J. Alloys Compd., 2010, 508, 119-128, DOI: 10.1016/j.jallcom.2010.08.008.
- 222 J. Wang, A. D. Ebner and J. A. Ritter, Physiochemical Pathway for Cyclic Dehydrogenation and Rehydrogenation of LiAlH₄, J. Am. Chem. Soc., 2006, 128, 5949-5954, DOI: 10.1021/ja060045l.
- 223 N. A. M. Y. Omar, Z. Omar, M. Ismail and N. S. M. Mustafa, Enhancing the dehydrogenation properties of LiAlH₄ through the addition of ZrF₄ for solid-state hydrogen storage, J. Alloys Compd., 2025, 1010, 177250, DOI: 10.1016/ i.jallcom.2024.177250.
- 224 Y. Xia, H. Zhang, Y. Sun, L. Sun, F. Xu, S. Sun, G. Zhang, P. Huang, Y. Du, J. Wang, S. P. Verevkin and A. A. Pimerzin, Dehybridization effect in improved dehydrogenation of LiAlH₄ by doping with two-dimensional Ti₃C₂, Mater. Today Nano, 2019, 8, 100054, DOI: 10.1016/j.mtnano.2019.100054.
- 225 L. Zang, J. Cai, L. Zhao, W. Gao, J. Liu and Y. Wang, Improved hydrogen storage properties of LiAlH₄ by mechanical milling with TiF3, J. Alloys Compd., 2015, 647, 756-762, DOI: 10.1016/j.jallcom.2015.06.036.
- 226 S.-S. Liu, Z.-B. Li, C.-L. Jiao, X.-L. Si, L.-N. Yang, J. Zhang, H.-Y. Zhou, F.-L. Huang, Z. Gabelica, C. Schick, L.-X. Sun and F. Xu, Improved reversible hydrogen storage of LiAlH₄ by nano-sized TiH2, Int. J. Hydren Energy, 2013, 38, 2770-2777, DOI: 10.1016/j.ijhydene.2012.11.042.
- 227 S.-S. Liu, L.-X. Sun, Y. Zhang, F. Xu, J. Zhang, H.-L. Chu, M.-Q. Fan, T. Zhang, X.-Y. Song and J. P. Grolier, Effect of ball milling time on the hydrogen storage properties of TiF₃-doped LiAlH₄, Int. J. Hydren Energy, 2009, 34, 8079-8085, DOI: 10.1016/j.ijhydene.2009.07.090.
- 228 B. Bogdanovic and M. Schwickardi, Ti-doped alkali metal aluminium hydrides as potential novel reversible hydrogen storage materials, J. Alloys Compd., 1997, 253-254, 1-9, DOI: 10.1016/S0925-8388(96)03049-6.
- 229 N. A. Ali and M. Ismail, Modification of NaAlH₄ properties using catalysts for solid-state hydrogen storage: A review, Int. J. Hydren Energy, 2021, 46, 766-782, DOI: 10.1016/ j.ijhydene.2020.10.011.
- 230 J. Khan and I. P. Jain, Chloride catalytic effect on hydrogen desorption in NaAlH₄, Int. J. Hydren Energy, 2016, 41, 8271-8276, DOI: 10.1016/j.ijhydene.2015.11.116.
- 231 J. Khan and I. P. Jain, Catalytic effect of Nb₂O₅ on dehydrogenation kinetics of NaAlH4, Int. J. Hydren Energy, 2016, 41, 8264-8270, DOI: 10.1016/j.ijhydene.2015.11.072.
- 232 Q. Wan, P. Li, Z. Li, K. Zhao, Z. Liu, L. Wang, F. Zhai, X. Qu and A. A. Volinsky, NaAlH₄ dehydrogenation properties enhanced by MnFe₂O₄ nanoparticles, J. Power Sourc., 2014, 248, 388-395, DOI: 10.1016/j.jpowsour.2013.09.093.
- 233 Y. Huang, P. Li, Q. Wan, J. Zhang, Y. Li, R. Li, X. Dong and X. Qu, Improved dehydrogenation performance of NaAlH₄ using NiFe₂O₄ nanoparticles, J. Alloys Compd., 2017, 709, 850-856, DOI: 10.1016/j.jallcom.2017.03.182.

- 234 N. S. Mustafa, N. A. Sazelee, N. A. Ali, N. N. Sulaiman and M. Ismail, Enhancement of hydrogen storage properties of NaAlH₄ catalyzed by CuFe₂O₄, *Int. J. Hydren Energy*, 2023, 48, 35197–35205, DOI: 10.1016/j.ijhydene.2023.05.277.
- 235 T. K. Nielsen, M. Polanski, D. Zasada, P. Javadian, F. Besenbacher, J. Bystrzycki, J. Skibsted and T. R. Jensen, Improved Hydrogen Storage Kinetics of Nanoconfined NaAlH4 Catalyzed with TiCl₃ Nanoparticles, ACS Nano, 2011, 5, 4056–4064, DOI: 10.1021/nn200643b.
- 236 M. Paskevicius, U. Fils, F. Karimi, J. Puszkiel, P. K. Pranzas, C. Pistidda, A. Hoell, E. Welter, A. Schreyer, T. Klassen, M. Dornheim and T. R. Jensen, Cyclic stability and structure of nanoconfined Ti-doped NaAlH₄, *Int. J. Hydren Energy*, 2016, 41, 4159–4167, DOI: 10.1016/j.ijhydene.2015.12.185.
- 237 D. Pukazhselvan, B. K. Gupta, A. Srivastava and O. N. Srivastava, Investigations on hydrogen storage behavior of CNT doped NaAlH₄, *J. Alloys Compd.*, 2005, 403, 312–317, DOI: 10.1016/j.jallcom.2005.05.008.
- 238 B. Bogdanovic, M. Felderhoff, A. Pommerin, F. Schüth and N. Spielkamp, Advanced Hydrogen-Storage Materials Based on Sc-, Ce-, and Pr-Doped NaAlH₄, *Adv. Mater.*, 2006, **18**, 1198–1201, DOI: **10.1002/adma.200501367**.
- 239 Y. Kima, E.-K. Lee, J.-H. Shima, Y. W. Cho and K. B. Yoon, Mechanochemical synthesis and thermal decomposition of Mg(AlH₄)₂, *J. Alloys Compd.*, 2006, **422**, 283–287, DOI: **10.1016/j.jallcom.2005.11.063**.
- 240 V. Iosub, T. Matsunaga, K. Tange and M. Ishikiriyama, Direct synthesis of Mg(AlH₄)₂ and CaAlH₅ crystalline compounds by ball milling and their potential as hydrogen storage materials, *Int. J. Hydren Energy*, 2009, 34, 906–912, DOI: 10.1016/j.ijhydene.2008.11.013.
- 241 J. Wang, A. D. Ebner and J. A. Ritter, On the Reversibility of Hydrogen Storage in Novel Complex Hydrides, *Adsorption*, 2005, **11**, 811–816, DOI: **10.1007/s10450-005-6028-y**.
- 242 N. Morisaku, K. Komiya, L. Yuzhan, H. Yukawa, M. Morinaga, K. Ikeda and S. Orimo, Synthesis and Decomposition of Pure Ca(AlH4)2, *Adv. Mat. Res.*, 2007, 26–28, 869–872, DOI: 10.4028/www.scientific.net/AMR.26-28.869.
- 243 C. Li, X. Xiao, P. Ge, J. Xue, S. Li, H. Ge and L. Chen, Investigation on synthesis, structure and catalytic modification of Ca(AlH₄)₂ complex hydride, *Int. J. Hydren Energy*, 2012, 37, 936–941, DOI: 10.1016/j.ijhydene.2011.03.151.
- 244 N. A. Sazelee, N. A. Ali, H. Liu and M. Ismail, Improving the desorption properties of LiAlH₄ by the addition of Ni_{0.6}Zn_{0.4}O, *Int. J. Hydren Energy*, 2024, **56**, 543–551, DOI: **10.1016/j.ijhydene.2023.12.181**.
- 245 Y. Bu, L. Sun, F. Xu, Y. Luo, C. Zhang, S. Wei, G. Zhang, H. Pan, J. Zeng and Z. Cao, Improved dehydrogenation of LiAlH₄ by hollow 3D flower-like bimetallic composites M-NC@TiO₂ (M=Ni, Co, Fe, Cu), *Ceram. Int.*, 2024, **50**, 34251–34263, DOI: **10.1016/j.ceramint.2024.06.244**.
- 246 X. Li, X. Zheng, Q. Ma, B. Xu, Y. Wang and Y. Li, Effect of Co-B on the hydrogen storage properties of LiAlH₄, *Chem. Phys. Lett.*, 2025, **859**, 141764, DOI: **10.1016/j.cplett.2024.141764**.
- 247 R. Cheng, Z. Liu, P. Manasa, Z. Zhao, H. Pan, F. Xu, L. Sun and F. Rosei, Nanoflower-engineered Co₃O₄@CoNi-LDO

- bimetallic oxide: A catalyst for revolutionizing hydrogen storage in LiAlH₄, *Int. J. Hydrogen Energy*, 2025, **102**, 375–385, DOI: **10.1016/j.ijhydene.2025.01.085**.
- 248 J. Wang, A. D. Ebner and J. A. Ritter, On the Reversibility of Hydrogen Storage in Novel Complex Hydrides, *Adsorption*, 2005, **11**, 811–816, DOI: **10.1007/s10450-005-6028-y**.
- 249 Y. Liu, Y. Pang, X. Zhang, Y. Zhou, M. Gao and H. Pan, Synthesis and hydrogen storage thermodynamics and kinetics of Mg(AlH₄)₂ submicron rods, *Int. J. Hydren Energy*, 2012, 37, 18148–18154, DOI: 10.1016/j.ijhydene.2012.09.081.
- 250 X. Fan, X. Xiao, L. Chen, L. Zhang, J. Shao, S. Li, H. Ge and Q. Wang, Significantly improved hydrogen storage properties of NaAlH₄ catalyzed by Ce-based nanoparticles, *J. Mater. Chem. A*, 2013, 1, 9752–9759, DOI: 10.1039/ c3ta11860f.
- 251 J. Chen, C. Li, W. Chen, X. Zhang, X. Yu and G. Xia, Tailoring reversible hydrogen storage performance of NaAlH₄ through NiTiO₃ nanorods, *J. Alloys Compd.*, 2024, 971, 172689, DOI: 10.1016/j.jallcom.2023.172689.
- 252 Z. Yuan, Y. Fan, Y. Chen, X. Liu, B. Liu and S. Han, Two-dimensional C@TiO₂/Ti₃C₂ composite with superior catalytic performance for NaAlH₄, *Int. J. Hydren Energy*, 2020, 45, 21666–21675, DOI: 10.1016/j.ijhydene.2020.05.243.
- 253 R. Wu, H. Du, Z. Wang, M. Gao, H. Pan and Y. Liu, Remarkably improved hydrogen storage properties of NaAlH₄ doped with 2D titanium carbide, *J. Power Sourc.*, 2016, 327, 519–525, DOI: 10.1016/j.jpowsour.2016.07.095.
- 254 N. A. Ali, M. Ismail, M. M. Nasef and A. A. Jalil, Enhanced hydrogen storage properties of NaAlH4 with the addition of CoTiO₃ synthesised *via* a solid-state method, *J. Alloys Compd.*, 2023, **934**, 167932, DOI: **10.1016/j.jallcom.2022.167932**.
- 255 C. Pratthana and K.-F. Aguey-Zinsou, Tuning the hydrogen thermodynamics of NaAlH₄ by encapsulation within a titanium shell, *Int. J. Hydren Energy*, 2023, **48**, 29240–29255, DOI: **10.1016/j.ijhydene.2023.04.028**.
- 256 Y. Sun, X. Zhang, W. Chen, J. Ye, S. Ju, K.-F. Aguey-Zinsou, G. Xia, D. Sun and X. Yu, Light-Driven Reversible Hydrogen Storage in Light-Weight Metal Hydrides Enabled by Photothermal Effect, *Small*, 2022, 18, 2202978, DOI: 10.1002/smll.202202978.
- 257 D. A. Mosher, S. Arsenault, X. Tang and D. L. Anton, Design, fabrication and testing of NaAlH₄ based hydrogen storage systems, *J. Alloys Compd.*, 2007, 446–447, 707–712, DOI: 10.1016/j.jallcom.2007.01.042.
- 258 J. Graetz, J. Wegrzyn and J. J. Reilly, Regeneration of Lithium Aluminum Hydride, *J. Am. Chem. Soc.*, 2008, 130, 17790–17794, DOI: 10.1021/ja805353w.
- 259 T. D. Humphries, D. Birkmire, G. S. McGrady, B. C. Hauback and C. M. Jensen, Regeneration of LiAlH₄ at sub-ambient temperatures studied by multinuclear NMR Spectroscopy, *J. Alloys Compd.*, 2017, 723, 1150–1154, DOI: 10.1016/ j.jallcom.2017.06.300.
- 260 X. Liu, G. S. McGrady, H. W. Langmi and C. M. Jensen, Facile Cycling of Ti-Doped LiAlH₄ for High Performance Hydrogen Storage, *J. Am. Chem. Soc.*, 2009, 131(14), 5032–5033, DOI: 10.1021/ja809917g.

261 I. Utz, M. Linder, N. Schmidt, J. J. Hu, M. Fichtner and A. Wörner, Experimental study of powder bed behavior of sodium alanate in a lab-scale H₂ storage tank with flow-through mode, *Int. J. Hydren Energy*, 2012, 37, 7645–7653, DOI: 10.1016/j.ijhydene.2012.02.016.

- 262 J. M. Bellosta von Colbe, O. Metz, G. A. Lozano, P. K. Pranzas, H. W. Schmitz, F. Beckmann, A. Schreyer, T. Klassen and M. Dornheim, Behavior of scaled-up sodium alanate hydrogen storage tanks during sorption, *Int. J. Hydren Energy*, 2012, 37, 2807–2811, DOI: 10.1016/j.ijhydene.2011.03.153.
- 263 N. A. Ali, N. A. Sazelee and M. Ismail, An overview of reactive hydride composite (RHC) for solid-state hydrogen storage materials, *Int. J. Hydrogen Energy*, 2021, 46, 31674–31698, DOI: 10.1016/j.ijhydene.2021.07.058.
- 264 C. Abetz, P. Georgopanos, C. Pistidda, T. Klassen and V. Abetz, Reactive Hydride Composite Confined in a Polymer Matrix: New Insights into the Desorption and Absorption of Hydrogen in a Storage Material with High Cycling Stability, Adv. Mater. Technol., 2022, 7, 2101584, DOI: 10.1002/admt.202101584.
- 265 Z.-Z. Fang, X.-D. Kang, P. Wang, H.-W. Li and S.-I. Orimo, Unexpected dehydrogenation behavior of LiBH₄/Mg(BH₄)₂ mixture associated with the *in situ* formation of dualcation borohydride, *J. Alloys Compd.*, 2010, **491**, L1–L4, DOI: **10.1016/j.jallcom.2009.10.149**.
- 266 J. Huang, M. Gao, Z. Li, X. Cheng, J. Gu, Y. Liu and H. Pan, Destabilization of combined Ca(BH₄)₂ and Mg(AlH₄)₂ for improved hydrogen storage properties, *J. Alloys Compd.*, 2016, **670**, 135–143, DOI: **10.1016/j.jallcom.2016.02.035**.
- 267 N. N. Sulaiman, M. Ismail, S. N. Timmiati and K. L. Lim, Improved hydrogen storage performances of LiAlH₄ + Mg(BH₄)₂ composite with TiF₃ addition, *Int. J. Energy Res.*, 2020, 1–17, DOI: 10.1002/er.5984.
- 268 H. Xiao, H. Leng, Z. Yu, Q. Li and K.-C. Chou, Improved Hydrogen Storage Properties of Mg(BH₄)₂-Mg(AlH₄)₂ Combined Systems, ed. J. S. Carpenter, *et al.*, *Characterization of Minerals, Metals, and Materials*, Springer, Cham, 2015, DOI: 10.1007/978-3-319-48191-3_49.
- 269 J. J. Vajo, S. L. Skeith and F. Mertens, Reversible Storage of Hydrogen in Destabilized LiBH₄, *J. Phys. Chem. B*, 2005, **109**, 3719–3722, DOI: **10.1021/jp040769o**.
- 270 N. A. Ali and M. Ismail, Advanced hydrogen storage of the Mg-Na-Al system: A review, *J. Magnesium Alloys*, 2021, 9, 1111–1122, DOI: 10.1016/j.jma.2021.03.031.
- 271 Y.-J. Kwak, M.-Y. Song and K.-T. Lee, Improvement in the Hydrogen Storage Properties of MgH₂ by Adding NaAlH₄, *Metals*, 2024, **14**, 227, DOI: **10**.3390/met14020227.
- 272 M. Ismail, Study on the hydrogen storage properties and reaction mechanism of NaAlH₄-MgH₂-LiBH₄ ternary-hydride system, *Int. J. Hydren Energy*, 2014, **39**, 8340–8346, DOI: **10.1016/j.ijhydene.2014.03.166**.
- 273 S. Qu, Y. Yang, C. Yan, M. Gao, M. Wu, Z. Li, S. Wang, Y. Liu, W. Sun, C. Liang, X. Zhang and H. Pan, Catalyzed eutectic LiBH₄–KBH₄ system nanoconfined at low temperature for superior hydrogen storage reversibility, *J. Mater. Chem. A*, 2025, **13**, 2757–2768, DOI: **10.1039/d4ta06500j.**

- 274 Q. Zhang, J. Zheng, A. Xia, M. Lv, Z. Ma and M. Liu, Enhanced reversible hydrogen storage in LiBH₄-Mg(BH₄)₂ composite with V₂C-Mxene, *Chem. Eng. J.*, 2024, 487, 150629, DOI: 10.1016/j.cej.2024.150629.
- 275 F. Karimi, P. K. Pranzas, J. A. Puszkiel, M. V. C. Riglos, C. Milanese, U. Vainio, C. Pistidda, G. Gizer, T. Klassen, A. Schreyer and M. Dornheim, A comprehensive study on lithium-based reactive hydride composite (Li-RHC) as a reversible solid-state hydrogen storage system toward potential mobile applications, *RSC Adv.*, 2021, 11, 23122, DOI: 10.1039/d1ra03246a.
- 276 M. Ismail and N. S. Mustafa, Improved hydrogen storage properties of NaAlH₄-MgH₂-LiBH₄ ternary-hydride system catalyzed by TiF₃, *Int. J. Hydren Energy*, 2016, **41**, 18107–18113, DOI: **10.1016/j.ijhydene.2016.07.090**.
- 277 Y. Lv, B. Zhang, H. Huang, X. Yu, T. Xu, J. Chen, B. Liu, J. Yuan, G. Xia and Y. Wu, Excellent low-temperature dehydrogenation performance and reversibility of 0.55LiBH₄-0.45Mg(BH₄)₂ composite catalyzed by few-layer Ti₂C, *J. Alloys Compd.*, 2024, 972, 172896, DOI: 10.1016/j.jallcom.2023.172896.
- 278 N. A. Sazelee, N. A. Ali, S. Suwarno, S.-U. Rather and M. Ismail, Reaction mechanism and absorption/desorption kinetics performance of the destabilised KBH₄-LiAlH₄ system, *Int. J. Hydren Energy*, 2025, 109, 520–527, DOI: 10.1016/ j.ijhydene.2025.02.104.
- 279 D. Liu, Q. Liu, T. Si, Q. Zhang, F. Fang, D. Sun, L. Ouyangc and M. Zhu, Superior hydrogen storage properties of LiBH₄ catalyzed by Mg(AlH₄)₂, *Chem. Commun.*, 2011, 47, 5741–5743, DOI: 10.1039/C1CC11238D.
- 280 K. Xian, M. Gao, Z. Li, J. Gu, Y. Shen, S. Wang, Z. Yao, Y. Liu and H. Pan, Superior Kinetic and Cyclic Performance of a 2D Titanium Carbide Incorporated 2LiH + MgB₂ Composite toward Highly Reversible Hydrogen Storage, ACS Appl. Energy Mater., 2019, 2, 4853–4864, DOI: 10.1021/acsaem.9b00557.
- 281 W. Chen, Y. Sun, T. Xu, J. Ye, G. Xia, D. Sun and X. Yu, Reversible Hydrogen Storage Performance of 2LiBH₄-MgH₂ Enabled by Dual Metal Borides, *ACS Appl. Energy Mater.*, 2022, 5, 10501–10508, DOI: 10.1021/acsaem.2c01142.
- 282 H. Luo, Y. Yang, L. Lu, G. Li, X. Wang, X. Huang, X. Tao, C. Huang, Z. Lan, W. Zhou, J. Guo and H. Liu, Highly-dispersed nano-TiB₂ derived from the two-dimensional Ti₃CN MXene for tailoring the kinetics and reversibility of the Li-Mg-B-H hydrogen storage material, *Appl. Surf. Sci.*, 2023, **610**, 155581, DOI: **10.1016/j.apsusc.2022.155581**.
- 283 Z. Ma, J. Zang, W. Hu, Q. Wang, Z. Sun, F. Fang, Y. Song and D. Sun, From Back to Stage: Superior Cycling Stability of 2LiBH₄-MgH₂ Enabled by Anion Tuning, *Adv. Energy Mater.*, 2024, 14, 2401156, DOI: 10.1002/aenm.202401156.
- 284 Y.-K. Liu, Y.-C. Pang, C.-Q. Li, X.-Y. Zhang, X.-C. Hu, W. Chen, X.-B. Yu and G.-L. Xia, Amorphous VB2 nanoparticles for stable hydrogen storage of 2LiBH₄-MgH₂, *Rare Met.*, 2025, 44, 5544–5553, DOI: 10.1007/s12598-025-03327-6.
- 285 Y. Li, P. Li, Q. Tan, Z. Zhang, Q. Wan, Z. Liu, A. Subramanian and X. Qu, Thermal properties and cycling performance of Ca(BH₄)₂/MgH₂ composite for energy

storage, *Chem. Phys. Lett.*, 2018, **700**, 44–49, DOI: **10.1016**/j.cplett.2018.04.011.

286 Y. Li, P. Li and X. Qu, Investigation on LiBH₄-CaH₂ composite and its potential for thermal energy storage, *Sci. Rep.*, 2017, 7, 41754, DOI: 10.1038/srep41754.

EES Catalysis

- 287 N. N. Sulaiman, M. Ismail, S. N. Timmiati and K. L. Lim, Improved hydrogen storage performances of LiAlH⁴⁺ $Mg(BH_4)_2$ composite with TiF₃ addition, *Int. J. Energy Res.*, 2021, 45, 2882–2898, DOI: 10.1002/er.5984.
- 288 N. S. Mustafa, F. A. Halim Yap, M. S. Yahya and M. Ismail, The hydrogen storage properties and reaction mechanism of the

- NaAlH₄ + Ca(BH₄)₂ composite system, *Int. J. Hydren Energy*, 2018, **43**, 11132.e11140, DOI: **10.1016/j.ijhydene.2018.04.234**.
- 289 M. Gao, J. Gu, H. Pan, Y. Wang, Y. Liu, C. Liang and Z. Guo, Ca(BH₄)₂-LiBH₄-MgH₂: a novel ternary hydrogen storage system with superior long-term cycling performance, *J. Mater. Chem. A*, 2013, 1, 12285, DOI: 10.1039/c3ta12472j.
- 290 O. Jin, Y. Shang, X. Huang, D. V. Szabó, T. T. Le, S. Wagner, T. Klassen, C. Kübel, C. Pistidda and A. Pundt, Transformation Kinetics of LiBH₄-MgH₂ for Hydrogen Storage, *Molecules*, 2022, 27, 7005, DOI: 10.3390/molecules 27207005.